DNAZYMES AS INTRACELLULAR SENSORS FOR METAL ION IMAGING AND THEIR STRUCTURAL CHARACTERIZATION

BY

PEIWEN WU

DISSERTATION

Submitted in partial fulfillment of the requirements
for the degree of Doctor of Philosophy in Biochemistry
in the Graduate College of the
University of Illinois at Urbana-Champaign, 2015

Urbana, Illinois

Doctoral Committee:

Professor Yi Lu, Chair
Associate Professor Raven Huang
Professor Susan Martinis
Assistant Professor Andrew Smith

ABSTRACT

Metal ions are essential for numerous biological processes and their regulation is crucial for maintaining normal functions. To gain a better fundamental understanding of how metal ions are regulated and where the potential molecular targets are for toxic metal ions, tools that can monitor localization and concentration of metal ions in living cells are required. Toward this goal, tremendous effort has been applied towards the development of intracellular metal ion sensors. Among them, both small molecular sensors and genetically encoded protein sensors have enjoyed the most success in intracellular metal ion sensing. A large number of sensors have been successfully used to detect metal ions that have important biological functions, such as calcium, zinc, copper and iron. At the same time, there is also emerging development in intracellular sensors for toxic metal ions, such as mercury, cadmium and lead. Despite the advances made over the previous years, it remains a significant challenge to rationally design sensors for metal ions of interest with both high sensitivity and selectivity.

To meet this challenge and design sensors for a much broader range of metal ions, we and others have taken advantage of an emerging field of metalloenzymes called deoxyribozymes (DNAzymes), i.e., DNA molecules with enzymatic activities. Unlike small molecule or protein-based sensors, DNAzymes with high specificity for a specific metal ion of interest can be obtained from a combinatorial process, starting from a large DNA library containing up to 10^{15} different sequences. Because of such high metal ion selectivity, these DNAzymes have been converted into sensors for many metal ions, such as Pb^{2+}, UO_2^{2+}, Hg^{2+} and Cu^{2+}, based on fluorescence, colorimetry, or electrochemistry. The development of these sensors has significantly expanded the range of metal ions that can be detected. The biggest advantages of

this type of sensor are that it does not require advanced knowledge in order to construct a metal-binding site, and the binding affinity and selectivity toward metal ions can be fine-tuned by introducing different levels of stringency during the selection process. Moreover, it is relatively simple to synthesize DNA and many different modifications and functional groups can be easily introduced into the DNA during synthesis. Furthermore, DNA is naturally water soluble and biocompatible. All of these properties make DNAzyme sensors an attractive candidate for intracellular sensing of metal ions. However, even though DNAzymes have first been demonstrated as metal ion sensors over 10 years ago and many sensors have been reported since then, all of these sensors are limited to detecting metal ions in extracellular environments.

In this dissertation, I present 1) the design, synthesis, and application of a DNAzyme-gold nanoparticle probe for uranyl detection in living HeLa cells; 2) Na^+ imaging in living cells using a photocaged Na^+-specific DNAzyme; and 3) fluorescent iron sensors based on Fe(II) and Fe(III) DNAzymes for iron detection in mammalian and bacterial cells. These studies demonstrated that DNAzymes, a new type of intracellular sensors, could be used as a general platform for imaging a wide range of metal ions in living organisms.

Despite numerous practical applications, the mechanism of metallo-DNAzymes' reaction and the role of metal ion in their structure and function are not yet fully understood. It remains unclear how DNA can carry out catalysis with simpler building blocks, fewer functional groups and less diverse structures than ribozymes and proteins. Similarly, the spatial arrangement of the DNAzyme enabling its superior selectivity for one metal ion over others also remains a mystery. To address these questions, an atomic resolution structure of a DNAzyme is highly desired and would greatly improve our understanding about the role of metal ion and nucleotide bases in the

catalysis. However, unlike the mature fields of ribozyme and protein crystallization, DNA crystallization, especially of molecules with non-canonical structures, remains very challenging. In the last part of this dissertation, effort towards obtaining the first crystal structure of a DNAzyme in its active form is described and future directions are discussed.

To all the people who were with me in this journey

ACKNOWLEDGMENTS

This thesis would not have been possible without the support of many people. I acknowledge, with gratitude, my debt of thanks to my advisor, Dr. Yi Lu, for your support during the five and a half years. I still clearly remember the day when I failed my first qualification exam, you told me firmly that I should not give up easily. Looking back, I am very grateful for your trust, encouragement and advice during the most stressful days in graduate school. I never regretted of taking this road, along which I became more mature and independent as a scientist. I would like to thank my qualification committee, Dr. Lin-Feng Chen, Dr. Rutilio Fratti, and Dr. Colin Wright, for discussing projects with me and giving me constructive feedbacks. Thank you all for letting me face one of the toughest decisions in my life, and making me think about what I really want to do in the next five years. I would also like to thank my thesis committee, Dr. Raven Huang, Dr. Susan Martinis, and Dr. Andrew Smith, for your insightful suggestions for my projects.

I want to thank my first mentor in graduate school, Dr. Tian Lan, for your kindness in welcoming me to the Lu group and your patience in teaching me every basic technique I need. I wish to thank Dr. Marjorie Cepeda, Dr. Yu Xiang, Dr. Le-Le Li, Dr. Hui Wei, Hannah Ihms, Dr. Eric Null, Dr. Zidong Wang, Dr. Ying He, Dr. Brian Wong, Dr. Hang Xing, Dr. Seyed-Fakhreddin Torabi and Dr. Li Huey Tan for being great seniors in the DNA subgroup. You have always been my idols to look up to. I hope to thank Dr. Yang Yu, Dr. Seyed-Fakhreddin Torabi, Shiliang Tian, Igor Petrik, Dr. Nan Zheng from Dr. Jianjun Cheng's lab, and Dr. Sibo Jiang from Dr. Zhen Huang's lab at Geogia State University, for being great collaborators. Thank you all for your generous and professional help for my projects. Thank Mr. Yi Gui Gao at the X-ray facility

and Dr. Sandra McMasters at cell media facility on campus, for generously sharing their facilities with me and offering help for my projects. I hope to express my special thanks to Dr. Parisa Hosseinzadeh and Kevin Hwang, for being excellent colleagues who taught me how to think, write and present professionally and handle impossible tasks with a can-do attitude. I want to thank all the girls in the Lu group, Dr. Ying He, Hannah Ihms, Dr. Panshu Song, Dr. Jiangjiexing Wu, Dr. Yuan Yue, Dr. Chunmei Gu, Dr. Li Huey Tan, Dr. Parisa Hosseinzadeh, Claire McGhee, Chang Cui, Ambika Bhagi, Nitya sai Reddy and Lu Chen, for all the potlucks, gym time and girls' nights we had together. You made Lu group feel like a warm family. Thank all the Lu group members I have met and worked with. I feel lucky and proud of being surrounded by you.

I want to thank my dear friends at UIUC. You made life in graduate school memorable with lots of joy. Thank Dr. Yue Hao, Chang Sun, Dr. Pei Wang, Hanchao Zhao, Xinying Zong for all the hot pots we had together in cold and dark winter days. Thank Dr. Qian Yin and Dr. Qingzhou Luo for always being there whenever I need help. Thank Dr. Shipeng Shu and Sai Zhang for the wonderful Christmas trip. Thank Jake Reynolds for all the laughter and technical discussions we had together.

Last but not least, I want to thank my parents for their unconditional love and support that never ends. I know you are always with me, no matter where I am. You are always my source of courage to take new challenges and move forward.

TABLE OF CONTENTS

LIST OF FIGURES

LIST OF TABLES

1 Chapter 1. Introduction

1.1 DNAzymes

Nucleic acids, which include deoxyribonucleic acid (DNA) and ribonucleic acid (RNA), are known as genetic material of all forms of life. Nucleic acids were first discovered by a young Swiss doctor, Friedrich Miescher, who noticed an unknown precipitation in his samples while working on analyzing chemical composition of leukocytes.[1] He found that the precipitated molecules were mainly composed of phosphorous, and they were resistant to protease digestion. He named these molecules as "nuclein" since they were isolated from cell nuclei. These molecules, later found out to be DNA and RNA, are one of the major types of biomolecules for all living organisms.

The building blocks of nucleic acids are nucleotides. Nucleotides connect to each other through phosphodiester bonds to form long linear polymer chains, which encode the genetic information of organisms. All nucleotides share the common structure, which contains a nitrogenous base, a sugar moiety, and one or more phosphate groups (Figure 1). There are five different types of nucleotides found in nucleic acids, differing in the nitrogenous base. If categorized by the type of bases, nucleotides can be divided into two groups. One group contains purine bases, including adenine (A) and guanine (G). The other group contains pyrimidine bases, such as cytosine (C), thymine (T), and uracil (U). In nature, A forms base pair with T in DNA or U in RNA through two hydrogen bonds, while C pairs with G via three hydrogen bonds. Base pairing and base stacking effects further lead to the formation of the double helical structure of DNA, which remained a mystery until X-ray diffractograms of DNA crystals were recorded by

Rosalind Franklin and the double-helix model was proposed by Watson and Crick in 1953.

For a long time, DNA and RNA were considered solely as the template for protein synthesis in organisms. With the discoveries of various types of RNA molecules with distinct functions, such as ribozyme, ribosome, transfer RNA, small interfering RNA, people started to realize that nucleic acids not only serve as the template for protein expression, but also can be regulatory molecules and have enzymatic activities.

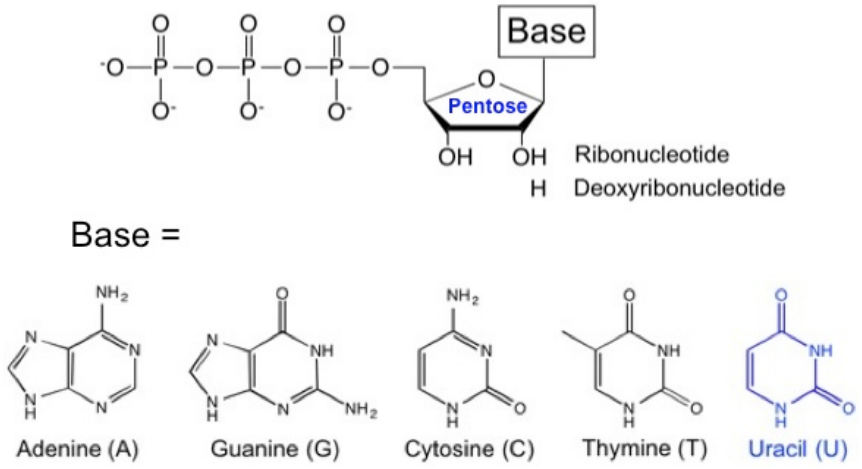

Figure 1.1 Nucleotide structures.

1.1.1 Discovery of DNAzymes

The discovery of ribozymes,[2,3] which are RNA molecules with enzymatic functions, gave researchers inspirations to find DNA molecules with catalytic activities. Since DNA shares many similarities with RNA in terms of structure and chemical property, it is reasonable to make the hypothesis that DNA might be able to carry out enzymatic reactions as well. Compared with protein enzymes, DNA molecules share several features that would potentially make them good

candidates to carry out reactions. First of all, DNA has the ability to recognize its complementary strand with high specificity, which is a prerequisite of a good enzyme. In addition, single-stranded DNA is able to form secondary and tertiary structures, such as wobble base pairs, hairpin loops, and quadruplexes. Moreover, DNA has good stability and is known to bind metal ions that might be able to serve as cofactors.

The first successful attempt of finding DNA enzymes was made by Breaker and Joyce in 1994.[4] They developed a general method to rapidly select DNA molecules with desired catalytic functions from a pool of random sequences. As the first trial, they looked at a reaction that was commonly performed by many naturally occurring ribozymes, which was the hydrolytic cleavage of an RNA phosphodiester bond. It had been shown at that time that ribozymes with Pb^{2+}-dependent RNA phosphoesterase activity could be obtained from a randomized library of RNA molecules. Based on the similarity between DNA and RNA, Breaker and Joyce incorporated an RNA nucleotide into an otherwise all DNA sequence, and intentionally randomized 50 nucleotides in the sequence to allow diversity in the starting selection pool. They performed selective amplification on this population of DNA molecules, and selected out a DNA enzyme that was able to use Pb^{2+} as a cofactor to promote the cleavage reaction at the phosphodiester bond of the ribonucleotide.

The rate of the selected DNA enzyme was found to be ~ 10^4 times faster than the spontaneous rate of phosphodiester bond cleavage under the same condition. This DNA enzyme was further converted into a *trans* construct, which could do multiple turnovers in an intermolecular context. The kinetics of the reaction also obeyed Michaelis-Menten kinetics. This was the first demonstration of the catalytic potential of DNA. It was also a proof-of-concept

example that DNA can adopt similar properties as protein enzymes.

1.1.2 Types of DNAzymes

Although no natural DNA catalysts have yet been reported, many artificial DNA enzymes have been reported since the first discovery in 1994. Up to now, it has been shown that DNA molecules can perform various types of reactions, such as RNA cleavage, RNA ligation, DNA cleavage, DNA ligation, Diels-Alder reaction, etc. (Table 1.1)

Table 1.1 Different types of DNAzymes and their cofactors.

Reaction	Cofactor	k_{max} (min^{-1})	Ref.
RNA cleavage	Pb^{2+}	1	4
	Mg^{2+}	0.01	5
	Ca^{2+}	0.1	6,7
	Mg^{2+}	10	7
	None	0.006	8
	L-histidine	0.2	9
	Zn^{2+}	~40	10
	Zn^{2+} [a]	~4	11
	Mg^{2+}	1.7	12
	None [b]	0.044 - 0.1	13-15
	Co^{2+}	7	16
	Cd^{2+}, Mn^{2+}, Ni^{2+}	~1	17
	UO_2^{2+}	~1.2	18
	Ce^{3+} [c]		19
	Na^{+}		20
DNA cleavage	Cu^{2+}	0.2	21
	Zn^{2+}	1	22
	Mn^{2+} and Zn^{2+}	0.045	23
RNA ligation	Mn^{2+}	~2.2	24
	Mg^{2+}	0.5	25
	Mg^{2+}	0.013	26
	Mg^{2+}	0.1	27
	Zn^{2+}	0.5	28
DNA ligation	Cu^{2+} or Zn^{2+}	0.07	29
	Mn^{2+}	4-Oct	30
DNA phosphorylation	Ca^{2+}	0.01	31
DNA depurination	IO_4^{-}		32
DNA adenylation	Cu^{2+}	0.003	33
Thymine dimer cleavage	None	4.5	34
Phosphoramidate bond cleavage	Mg^{2+}	$\sim 5\times10^{-4}$	35
N-glycosylation	Ca^{2+}	0.5	36
Porphyrin metallation	None	1.3	37
Carbon-carbon bond formation	Ca^{2+}	3	38
Reductive amination	Ni^{2+} and IO_4^{-}	0.006	39
Peptide-DNA conjugation	Zn^{2+}	0.007	40
Hydrolysis of amides	Zn^{2+} and Mn^{2+}	0.05	41
Tyrosine phosphorylation	Zn^{2+} and Mn^{2+}	0.004	42
Tyrosine and serine dephosphorylation	Zn^{2+}	0.7	43

1.1.3 RNA-cleaving DNAzymes

Among different types of DNAzymes, RNA-cleaving DNAzymes using metal ion cofactors are of our particular interest, due to their fast reaction rate and ease of practical application into metal ion sensors. The general strategy to obtain RNA-cleaving DNAzymes is through *in vitro* selection process, which was proposed by Breaker and Joyce in their initial proof-of-principle study.[4]

1.1.3.1 *In vitro* selection

In vitro selection is a combinatorial screening technique that has been demonstrated by several groups including our own.[44,45] To select an RNA-cleaving DNAzyme that uses a specific metal ion as its cofactor, a library containing $10^{14\text{-}15}$ random sequences is normally used as the starting pool for selection. Each individual sequence is composed of all deoxyribonucleotides except one ribonucleotide serving as the cleavage site. To allow diversity in the selection pool, 25 to 50 nucleotides in the sequence are intentionally randomized (Figure 1.2). The pool is then subject to incubation with the metal ion solution. Sequences that show activity in the presence of the metal ion of interest are collected and further amplified by PCR. These sequences are used to seed the next round of selection. In order to select out the most active and selective sequences, such process is repeated several rounds with more stringent conditions, such as lower concentrations of metal ion, shorter reaction time, and negative selection against other competing metal ions. In the end, the selection product is cloned and sequenced, and individual sequences are tested in terms of their activity and selectivity.

Following this *in vitro* selection strategy, our group as well as other groups has

successfully obtained DNAzymes for different metal ion cofactors, such as Mg,[5,7] Ca,[6,7] Zn^{2+},[10,11] UO_2^{2+},[46] Pb^{2+},[4] Na^{+},[20] Fe^{2+}, and Fe^{3+}.

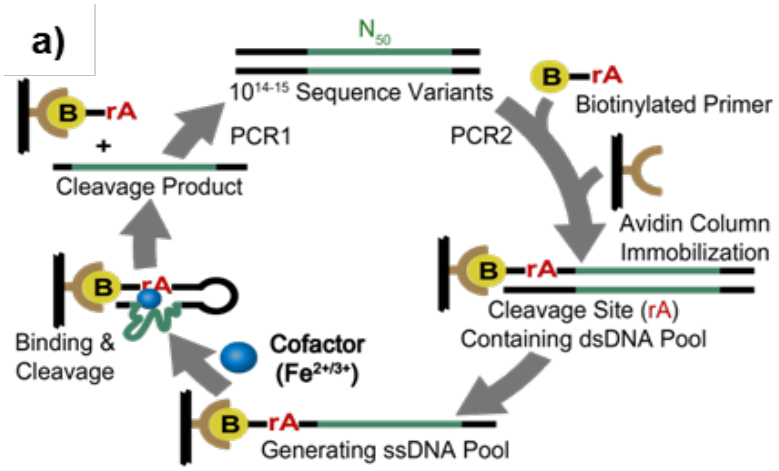

Figure 1.2 *In vitro* selection process.

1.1.3.2 Role of metal ions in DNAzymes

Although it has been over 20 years since the first RNA-cleaving DNAzyme was discovered, the role of metal ions in the cleavage reaction performed by DNAzymes is still a mystery. Despite the fact that biochemical studies have provided us with some insights on the mechanistic basis of the reaction, a detailed mechanism is still unknown due to lack of three-dimensional structure of any active DNAzyme. Based on observations from ribozyme-catalyzed reactions, possible catalytic functions of metal ions can be summarized as follows[47] (Figure 1.3): 1) the metal ion acts as a Lewis acid and coordinating directly with the 2′-oxygen of the ribonucleotide at cleavage site to accelerate the deprotonation of 2′-OH (Figure 1.3a), or the metal ion acts as a Lewis acid catalyst by directly coordinating with the 5′-oxygen leaving group (Figure 1.3b); 2) the metal-coordinated hydroxide acting as a general base by abstracting the

proton from the 2′-OH (Figure 1.3c), or metal-bound water molecule acts as a general acid to stabilize the developing negative charge on the 5′-oxygen leaving group (Figure 1.3d); 3) the metal ion directly coordinates to the non-bridging oxygen, which renders the phosphorus center more susceptible to nucleophilic attack (Figure 1.3e), or the metal-bound water molecule forms hydrogen bonding with the non-bridging oxygen to stabilize the charged transition state (Figure 1.3f).

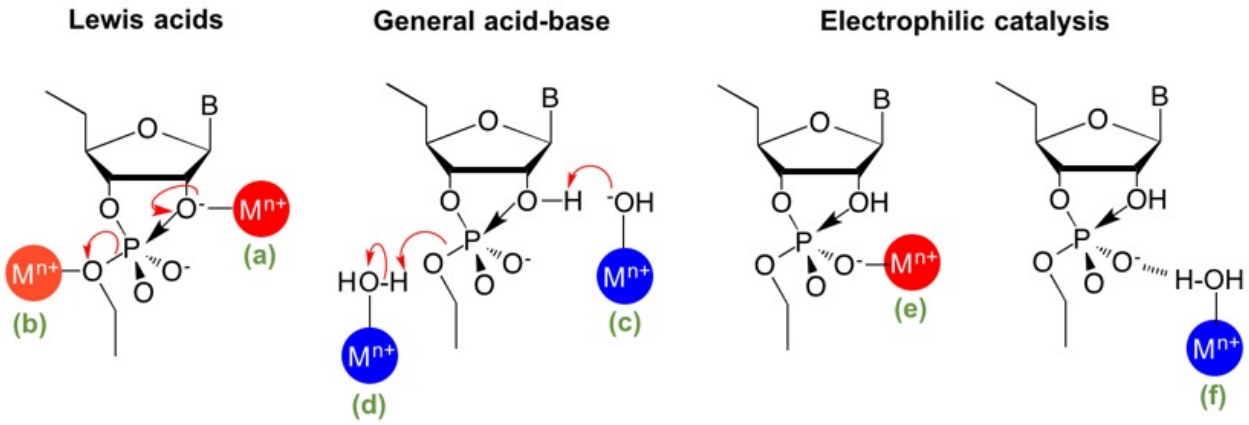

Figure 1.3 Possible roles of metal ions in the cleavage reaction performed by DNAzymes.

Although the knowledge of how metal ion is involved in the cleavage reaction is limited, the cleavage steps can be derived from the intermediates and final products of the reaction based on results obtained from matrix-assisted laser desorption/ionization mass spectroscopy (MALDI-MS). It is known that for the cleavage of the phosphodiester bond, large ribozymes, including group I and II introns and the catalytic domain of RNase P, can accept external nucleophiles such as the 2′-OH of an internal adenosine. Small ribozymes, such as hammerheads, hairpins and HDV ribozymes, usually utilize an internal nucleophile, which is normally the 2′-OH of the ribonucleotide at the cleavage site. In contrast to ribozymes, DNAzymes is small in size and lack

external 2′-OH. Therefore, the 2′-OH at the cleavage site is most likely to serve as the nucleophile to attack the phosphorus center. Cleavage product analysis shows that the final products of 8-17 DNAzyme contain a 2′,3′-cyclic phosphate at the 3′-terminus and a 5′-hydroxyl at the 5′-terminus. When the metal cofactor is Pb^{2+}, the 2′,3′-cyclic phosphate further hydrolyzed into a monophosphate (Figure 4). Similar phenomenon was observed in a leadzyme (ribozyme) and several protein ribonucleases.

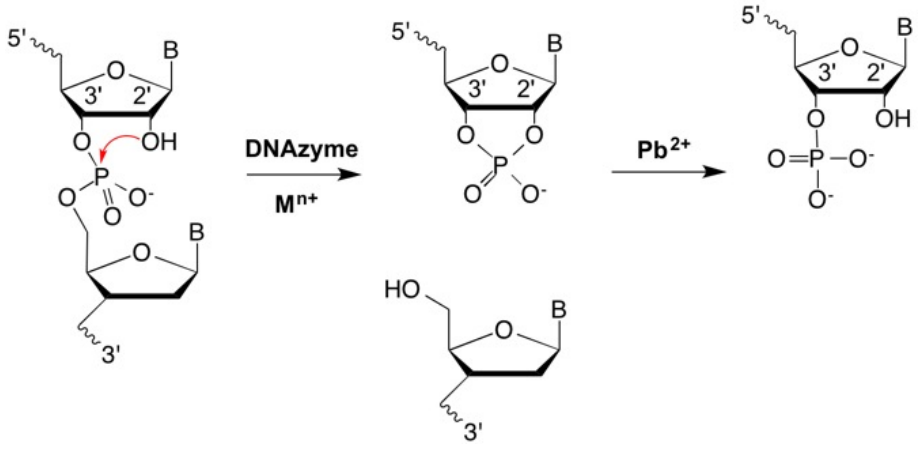

Figure 1.4 Cleavage steps of 8-17 DNAzyme based on MALDI-MS data.

1.1.3.3 Characterization methods

DNAzyme, the newest member in the enzyme family after protein enzymes and ribozymes, has attracted a lot of attention from researchers, as they were purely selected by *in vitro* selection and yet not found in nature. Their small size, simple building blocks, fast reaction rate, and high selectivity have made them popular to be engineered for many applications. Our current knowledge about how DNAzymes work largely relies on biochemical and biophysical characterizations. Methods that have been successfully applied for protein enzyme and ribozyme

characterization can be adapted for DNAzyme characterization.

In terms of biochemical characterization, conserved sequence analysis, use of modified bases, footprinting, determination of steady-state kinetic parameters, metal ion dependence analysis, pH-dependence analysis, and reaction intermediates and product analysis are the most common strategies to understand the mechanistic basis of DNAzyme-catalyzed reactions. Conserved sequence can be obtained by performing sequence alignment of selected DNAzyme candidates and mutagenesis to pinpoint positions that are critical for activity. Modified bases with different pK_a can be used to elucidate the role of a chemical moiety in a specific nucleotide base in the catalytic reaction. Kinetic parameters, such as $k_{obs,}$ K_{cat}, K_M, and K_d, can tell us the reaction rate and metal ion binding affinity of the DNAzyme. Selectivity of a DNAzyme can be evaluated by subjecting the DNAzyme to different metal ions and monitoring the cleavage product. pH-dependence analysis can not only provide information about the working pH range of DNAzymes, but also reveal the potential reaction mechanism. A slope of 1 for log k_{obs} vs. pH is an indication that a single deprotonation occurs during the rate-limiting step, which has been observed for both hammerhead ribozymes,[48] 10-23 DNAzyme,[49] and 8-17[10] DNAzyme. Reaction intermediates and product analysis can provide insights on the potential cleavage mechanism, as discussed in Section 1.1.3.2.

While biochemical studies tell us how DNAzymes work from a mechanistic perspective, biophysical studies usually focus more on the structural side. Spectroscopy, NMR, crystallography, and computational modeling are the most common approaches for studying ligand coordination and overall structures of DNAzymes. However, due to the complexity of spectral interpretation and the high cost of isotope labeling, NMR has been extremely difficult to

use for elucidating DNAzyme structures. Without solid knowledge basis of non-canonical DNA structures and DNA-metal interaction, computational modeling is also challenge and has been limited to only the metal binding site. Crystallography of DNAzymes has turned out to be more difficult than expected, largely due to the small and flexible structure of DNAzymes. Up to now, there is only one crystal structure available, which is for 10-23 DNAzyme in its inactive form.[50] Spectroscopic approaches, such as electron paramagnetic resonance (EPR) and extended X-ray absorption fine structure (EXAFS), are the most common techniques for studying geometry and ligand coordination of metal binding site in metalloproteins and metallo-ribozymes. So far, there is still no report on using EPR and EXAFS to study the metal binding site in DNAzymes, mostly because the majority of metal ion cofactors for existing DNAzymes are non-paramagnetic and spectroscopically silent, making it impossible to use the above techniques. The only EXAFS study that is related to DNAzyme-metal interaction was from Ravel *et al*., in which they characterized the interaction between Hg^{2+} and T-T mismatch in a double-stranded DNA.[51] In addition to characterization of the metal binding sites, small-angel X-ray scattering (SAXS) has shown to be a powerful tool for studying the overall three-dimensional structure and folding intermediates when high-resolution crystal or NMR structure is not available. Current progress on using SAXS to characterize nucleic acids has been limited to RNA, such as ribozymes,[52,53], riboswitches,[54,55] and aptamers.[56-59] Since DNAzymes share much in common with them, it will be interesting to see if SAXS can tell conformational changes of DNAzymes in the presence of metal ions.

1.2 Metal ion sensing

1.2.1 Metal ions in biology and existing sensors

Metal ions are the smallest components of biological systems, but they are essential for sustaining all forms of life. Metal ion homeostasis and signaling have attracted increasing attention in recent years, when people start to realize that metal ions are not only cofactors for metalloproteins, but also critical signaling molecules involved in numerous pathways. Organisms have evolved to use different strategies to strictly regulate metal ions, and alterations in their homeostasis are often linked with diseases, such as cancer, diabetes, and neurodegenerative diseases.

To probe physiological and pathological roles of metal ions with spatial and temporal fidelity, fluorescent sensors based on small molecules and proteins have been developed for different metal ions of interest, such as Ca^{2+}, Zn^{2+}, Cu^{+}, Fe^{2+}, Fe^{3+}, etc. Invention of these fluorescent metal ion sensors enabled us to track the concentration and distribution of metal ions in living organisms, and largely enriched our knowledge about metal ions in biology. In the meanwhile, it has been great challenge to develop sensitive and selective metal ion sensors for different uses in the biological systems. Ideally, fluorescent metal ion sensors should have high selectivity for their target metal ions to reduce false positive signals, proper dissociation constant (K_d) to match metal-ligand association equilibrium in the cellular environment, and high optical brightness to achieve better signal-to-noise ratio and less disturbance to native systems. In addition to these properties, turn-on sensors are preferred to prevent false positive signals, and sensors with visible- or near infrared (NIR)-light excitation and emission wavelength are desirable to minimize damage to samples and autofluorescence. All these requirements make it

challenging to design sensors for metal ions. It is often a trial and error process to rationally design metal binding site in both small molecule and protein based sensors, and it is not easy to generalize the existing designs into making new sensors since different metal ions have different chemical properties and different preferences for binding geometry. Small molecule-based fluorescent sensors also suffer from water solubility issues. For fluorescent sensors based on protein scaffold, design of these sensors also largely depends on our existing knowledge about protein motifs that would undergo conformational change in the presence of metal ions.

1.2.2 DNAzyme-based metal ion sensors

To circumvent the above challenges of developing metal ion sensors by rational design, we utilize RNA-cleavage DNAzymes as a new platform for metal ion detection. Compared with small molecule- or protein-based sensors, DNAzyme-based metal ion sensors have the following advantages. Firstly, DNAzymes with high specificity for a specific metal ion of interest can be obtained from *in vitro* selection, and this process does not require existing knowledge about metal ion binding sites. Secondly, selected DNAzymes usually can be easily truncated and converted from *cis* to *trans* form (Figure 1.5a), and further engineered into fluorescent sensors by attaching fluorophores and quenchers on the two ends (Figure 1.5b). As shown in Figure 1.5b, the enzyme strand (green) is hybridized to the substrate strand (black) in buffer when there is no target metal ion. The fluorophore is quenched by a nearby quencher as well as another quencher at the opposite end, resulting in minimal fluorescence background. With the addition of target metal ions, substrate strand will be cleaved by the enzyme strand at the ribonucleotide site, resulting in two shorter pieces of cleaved products. Since the melting temperature of the shorter cleavage product is much lower than the intact substrate we start with, these cleavage product

will be released from the substrate due to dehybridization, resulting in increased fluorescence since the quencher no longer quench the fluorescence of the fluorophore.

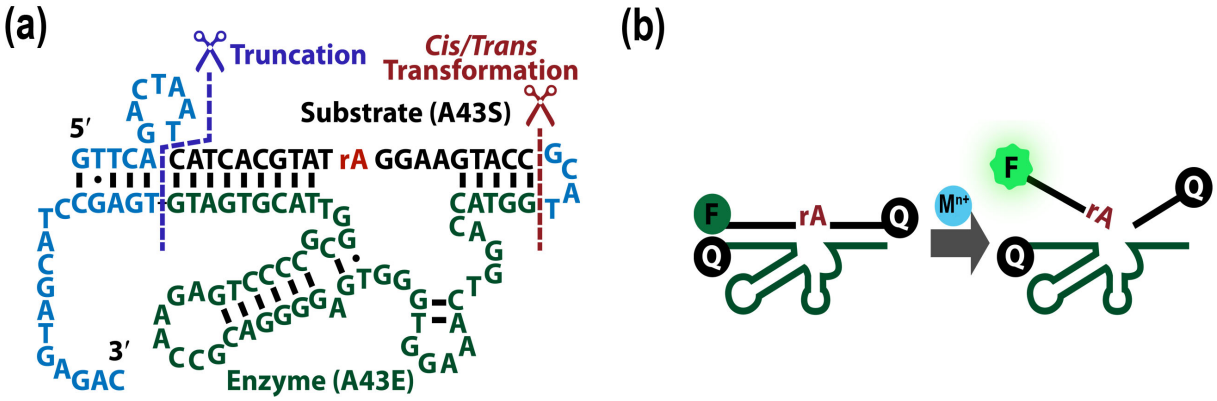

Figure 1.5 a) Truncation and *cis*-to-*trans* transformation of DNAzyme; b) design of turn-on fluorescent sensors based on DNAzymes.

Based on this strategy, many of the selected DNAzymes have been converted into metal ion sensors for different metal ions, such as Pb^{2+},[17,44,60,61] UO_2^{2+},[18] Hg^{2+},[62,63] Cu^{2+},[64] Zn^{2+}, and Na^{+}.[20] Different designs based on various readouts, such as fluorescence, colorimetry, or electrochemistry, have been developed for desired sensitivity, reaction time and specific application purposes. Some of these sensors can achieve high selectivity and sensitivity that surpass U.S. EPA limit or even instrumental analysis. For example, the 8-17 DNAzyme can detect Pb^{2+} as low as 10 nM, which is below the maximal contamination level for drinking water defined by U.S. Environment Protection Agency (EPA). The UO_2^{2+}-specific DNAzyme (39E) has a detection limit of 45 pM in solution, which is lower than the detection limit of ICP-MS (420 pM) as well as toxic level of UO_2^{2+} in drinking water defined by EPA (130 nM).

However, all the previous success has been limited to environmental sensing, and it was a

question whether we could engineer DNAzyme-based sensors for intracellular metal ion detection. Potential advantages of this type of sensors are that 1) it would be a general platform that allows us to easily obtain metal ion sensors with high sensitivity and selectivity; 2) it would be easy to tune the fluorescence of the sensors to avoid spectral overlap by incorporating different fluorophores; 3) it inherits the intrinsic properties of being water soluble and biocompatible from DNA. In the meanwhile, there are also many unknowns about applying this sensing system in biological systems.

1.2.3 Challenges of developing DNAzyme-based intracellular sensors

There were several challenges that we had to address before we can make DNAzyme into a new category of intracellular sensor. First of all, unlike most of the small molecules, DNAzymes cannot diffuse into living cells easily by its own due to its size and charge, and thus an efficient delivery method is required to allow sufficient loading of DNAzymes sensors with minimal disturbance to cells. Secondly, there are different endonucleases and exonucleases inside cells that would degrade foreign DNA or RNA. Therefore, methods that can improve the stability of DNAzymes inside cells would be preferred. Moreover, a triggered activation strategy is highly desired for using DNAzyme-based sensors in biological systems. Since the cleavage reaction is irreversible, cleavage of the sensors by extracellular metal ions during delivery process needs to be avoided to achieve maximal turn-on signal. In addition, most of the existing DNAzymes were selected for environmental sensing purposes and their working conditions can be quite different from physiological conditions. A careful survey and activity tests under physiological conditions are needed to decide the best candidates that can be used for the first proof-of-concept demonstration. New selections and re-selections need to be carried out in order

to obtain better DNAzyme candidates that suit biological applications.

1.3 Research focus

The focus of this dissertation includes development of DNAzyme-based sensors for intracellular metal ion detection and attempts to obtain a crystal structure of the 8-17 DNAzyme.

The first part (Chapter 2) is focused on developing the DNAzyme-gold nanoparticle conjugates as intracellular sensors for UO_2^{2+} ion detection in living cells, whereas the second part (Chapter 3) focuses on utilizing a newly selected Na^+-specific DNAzyme and a photocaging protection strategy to image Na^+ fluctuation inside cells. The third part (Chapter 4) covers the progresses towards developing DNAzyme-based sensors for Fe^{2+} and Fe^{3+} detection in both bacterial and mammalian cells. The last part (Chapter 5) focuses on the efforts towards obtaining a crystal structure of 8-17 DNAzyme.

1.4 References

1. Dahm R, Discovering DNA: Friedrich Miescher and the early years of nucleic acid research. *Hum. Genet.* **2008** *122*, 565-581.

2. Bass BL, Cech TR, Specific interaction between the self-splicing RNA of Tetrahymena and its guanosine substrate: implications for biological catalysis by RNA. *Nature* **1984** *308*, 820-826.

3. Cech TR, Bass BL, Biological catalysis by RNA. *Annu. Rev. Biochem.* **1986** *55*, 599-629.

4. Breaker RR, Joyce GF, A DNA enzyme that cleaves RNA. *Chem. Biol.* **1994** *1*, 223-229.

5. Breaker RR, Joyce GF, A DNA enzyme with Mg2+-dependent RNA phosphoesterase activity. *Chem. Biol.* **1995** *2*, 655-660.

6. Faulhammer D, Famulok M, Characterization and divalent metal-ion dependence of in vitro selected deoxyribozymes which cleave DNA/RNA chimeric oligonucleotides. *J. Mol. Biol.* **1997** *269*, 188-202.

7. Santoro SW, Joyce GF, A general purpose RNA-cleaving DNA enzyme. *Proc. Natl. Acad. Sci. U. S. A.* **1997** *94*, 4262-4266.

8. Geyer CR, Sen D, Evidence for the metal-cofactor independence of an RNA phosphodiester-cleaving DNA enzyme. *Chem. Biol.* **1997** *4*, 579-593.

9. Roth A, Breaker RR, An amino acid as a cofactor for a catalytic polynucleotide. *Proc. Natl. Acad. Sci. U. S. A.* **1998** *95*, 6027-6031.

10. Li J, Zheng W, Kwon AH, Lu Y, In vitro selection and characterization of a highly efficient Zn(II)-dependent RNA-cleaving deoxyribozyme. *Nucleic Acids Res.* **2000** *28*, 481-488.

11. Santoro SW, Joyce GF, Sakthivel K, Gramatikova S, Barbas CF, RNA cleavage by a DNA enzyme with extended chemical functionality. *J. Am. Chem. Soc.* **2000** *122*, 2433-2439.

12. Feldman AR, Sen D, A new and efficient DNA enzyme for the sequence-specific cleavage of RNA. *J. Mol. Biol.* **2001** *313*, 283-294.

13. Ting R, Thomas JM, Lermer L, Perrin DM, Substrate specificity and kinetic framework of a DNAzyme with an expanded chemical repertoire: a putative RNaseA mimic that catalyzes RNA hydrolysis independent of a divalent metal cation. *Nucleic Acids Res.* **2004** *32*, 6660-6672.

14. Hollenstein M, Hipolito CJ, Lam CH, Perrin DM, A DNAzyme with Three Protein-Like Functional Groups: Enhancing Catalytic Efficiency of M2+-Independent RNA Cleavage. *ChemBioChem* **2009** *10*, 1988-1992.

15. Hollenstein M, Hipolito CJ, Lam CH, Perrin DM, Toward the Combinatorial Selection of Chemically Modified DNAzyme RNase A Mimics Active Against all-RNA Substrates. *Acs Combinatorial Science* **2013** *15*, 174-182.

16. Mei SHJ, Liu ZJ, Brennan JD, Li YF, An efficient RNA-cleaving DNA enzyme that synchronizes

catalysis with fluorescence signaling. *J. Am. Chem. Soc.* **2003** *125*, 412-420.

17. Liu JW, Lu Y, A colorimetric lead biosensor using DNAzyme-directed assembly of gold nanoparticles. *J. Am. Chem. Soc.* **2003** *125*, 6642-6643.

18. Liu J, Brown AK, Meng X, Cropek DM, Istok JD, Watson DB, Lu Y, A catalytic beacon sensor for uranium with parts-per-trillion sensitivity and millionfold selectivity. *Proc. Natl. Acad. Sci. U. S. A.* **2007** *104*, 2056-2061.

19. Huang PJJ, Vazin M, Liu JW, In Vitro Selection of a New Lanthanide-Dependent DNAzyme for Ratiometric Sensing Lanthanides. *Anal. Chem.* **2014** *86*, 9993-9999.

20. Torabi S-F, Wu P, McGhee CE, Chen L, Hwang K, Zheng N, Cheng J, Lu Y, In vitro selection of a sodium-specific DNAzyme and its application in intracellular sensing. *Proc. Natl. Acad. Sci. U. S. A.* **2015** *112*, 5903-5908.

21. Carmi N, Balkhi SR, Breaker RR, Cleaving DNA with DNA. *Proc. Natl. Acad. Sci. U. S. A.* **1998** *95*, 2233-2237.

22. Gu HZ, Furukawa K, Weinberg Z, Berenson DF, Breaker RR, Small, Highly Active DNAs That Hydrolyze DNA. *J. Am. Chem. Soc.* **2013** *135*, 9121-9129.

23. Chandra M, Sachdeva A, Silverman SK, DNA-catalyzed sequence-specific hydrolysis of DNA. *Nat. Chem. Biol.* **2009** *5*, 718-720.

24. Wang YM, Silverman SK, Deoxyribozymes that synthesize branched and lariat RNA. *J. Am. Chem. Soc.* **2003** *125*, 6880-6881.

25. Coppins RL, Silverman SK, A DNA enzyme that mimics the first step of RNA splicing. *Nat. Struct. Mol. Biol.* **2004** *11*, 270-274.

26. Flynn-Charlebois A, Prior TK, Hoadley KA, Silverman SK, In vitro evolution of an RNA-cleaving DNA enzyme into an RNA ligase switches the selectivity from 3 '-5 ' to 2 '-5 '. *J. Am. Chem. Soc.* **2003** *125*, 5346-5350.

27. Flynn-Charlebois A, Wang YM, Prior TK, Rashid I, Hoadley KA, Coppins RL, Wolf AC, Silverman SK, Deoxyribozymes with 2 '-5 ' RNA ligase activity. *J. Am. Chem. Soc.* **2003** *125*, 2444-2454.

28. Hoadley KA, Purtha WE, Wolf AC, Flynn-Charlebois A, Silverman SK, Zn2+-dependent deoxyribozymes that form natural and unnatural RNA linkages. *Biochemistry* **2005** *44*, 9217-9231.

29. Cuenoud B, Szostak JW, A DNA Metalloenzyme with DNA-Ligase Activity. *Nature* **1995** *375*, 611-614.

30. Sreedhara A, Li YF, Breaker RR, Ligating DNA with DNA. *J. Am. Chem. Soc.* **2004** *126*, 3454-3460.

31. Li YF, Breaker RR, Phosphorylating DNA with DNA. *Proc. Natl. Acad. Sci. U. S. A.* **1999** *96*, 2746-2751.

32. Hobartner C, Pradeepkumar PI, Silverman SK, Site-selective depurination by a periodate-

dependent deoxyribozyme. *Chem. Commun.* **2007**, 2255-2257.

33. Li YF, Liu Y, Breaker RR, Capping DNA with DNA. *Biochemistry* **2000** *39*, 3106-3114.

34. Chinnapen DJF, Sen D, A deoxyribozyme that harnesses light to repair thymine dimers in DNA. *Proc. Natl. Acad. Sci. U. S. A.* **2004** *101*, 65-69.

35. Burmeister J, vonKiedrowski G, Ellington AD, Cofactor-assisted self-cleavage in DNA libraries with a 3'-5'-phosphoramidate bond. *Angew. Chem., Int. Ed.* **1997** *36*, 1321-1324.

36. Sheppard TL, Ordoukhanian P, Joyce GF, A DNA enzyme with N-glycosylase activity. *Proc. Natl. Acad. Sci. U. S. A.* **2000** *97*, 7802-7807.

37. Li YF, Sen D, A catalytic DNA for porphyrin metallation. *Nat. Struct. Biol.* **1996** *3*, 743-747.

38. Chandra M, Silverman SK, DNA and RNA can be equally efficient catalysts for carbon-carbon bond formation. *J. Am. Chem. Soc.* **2008** *130*, 2936-2937.

39. Wong OY, Mulcrone AE, Silverman SK, DNA-Catalyzed Reductive Amination. *Angew. Chem., Int. Ed.* **2011** *50*, 11679-11684.

40. Chu CC, Wong OY, Silverman SK, A Generalizable DNA-Catalyzed Approach to Peptide-Nucleic Acid Conjugation. *ChemBioChem* **2014** *15*, 1905-1910.

41. Brandsen BM, Hesser AR, Castner MA, Chandra M, Silverman SK, DNA-Catalyzed Hydrolysis of Esters and Aromatic Amides. *J. Am. Chem. Soc.* **2013** *135*, 16014-16017.

42. Walsh SM, Sachdeva A, Silverman SK, DNA Catalysts with Tyrosine Kinase Activity. *J. Am. Chem. Soc.* **2013** *135*, 14928-14931.

43. Chandrasekar J, Silverman SK, Catalytic DNA with phosphatase activity. *Abstr. Pap. Am. Chem. Soc.* **2013** *246*.

44. Li J, Lu Y, A highly sensitive and selective catalytic DNA biosensor for lead ions. *J. Am. Chem. Soc.* **2000** *122*, 10466-10467.

45. Szurdoki F, Ren D, Walt DR, A Combinatorial Approach To Discover New Chelators for Optical Metal Ion Sensing. *Anal. Chem.* **2000** *72*, 5250-5257.

46. Liu JW, Brown AK, Meng XL, Cropek DM, Istok JD, Watson DB, Lu Y, A catalytic beacon sensor for uranium with parts-per-trillion sensitivity and millionfold selectivity. *Proc. Natl. Acad. Sci. U. S. A.* **2007** *104*, 2056-2061.

47. Takagi Y, Warashina M, Stec WJ, Yoshinari K, Taira K, Recent advances in the elucidation of the mechanisms of action of ribozymes. *Nucleic Acids Res.* **2001** *29*, 1815-1834.

48. Dahm SC, Derrick WB, Uhlenbeck OC, Evidence for the role of solvated metal hydroxide in the hammerhead cleavage mechanism. *Biochemistry* **1993** *32*, 13040-13045.

49. Santoro SW, Joyce GF, Mechanism and utility of an RNA-cleaving DNA enzyme. *Biochemistry*

1998 *37*, 13330-13342.

50. Nowakowski J, Shim PJ, Prasad GS, Stout CD, Joyce GF, Crystal structure of an 82-nucleotide RNA-DNA complex formed by the 10-23 DNA enzyme. *Nat. Struct. Biol.* **1999** *6*, 151-156.

51. Ravel B, Slimmer SC, Meng X, Wong GCL, Lu Y, EXAFS studies of catalytic DNA sensors for mercury contamination of water. *Radiat. Phys. Chem.* **2009** *78*, S75-S79.

52. Russell R, Millett IS, Doniach S, Herschlag D, Small angle X-ray scattering reveals a compact intermediate in RNA folding. *Nat. Struct. Biol.* **2000** *7*, 367-370.

53. Lipfert J, Ouellet J, Norman DG, Doniach S, Lilley DMJ, The complete VS ribozyme in solution studied by small-angle X-ray scattering. *Structure* **2008** *16*, 1357-1367.

54. Stoddard CD, Montange RK, Hennelly SP, Rambo RP, Sanbonmatsu KY, Batey RT, Free state conformational sampling of the SAM-I riboswitch aptamer domain. *Structure* **2010** *18*, 787-797.

55. Chen B, Zuo X, Wang YX, Dayie TK, Multiple conformations of SAM-II riboswitch detected with SAXS and NMR spectroscopy. *Nucleic Acids Res.* **2012** *40*, 3117-3130.

56. Werner A, Konarev PV, Svergun DI, Hahn U, Characterization of a fluorophore binding RNA aptamer by fluorescence correlation spectroscopy and small angle X-ray scattering. *Anal. Biochem.* **2009** *389*, 52-62.

57. Anthony PC, Perez CF, Garcia-Garcia C, Block SM, Folding energy landscape of the thiamine pyrophosphate riboswitch aptamer. *Proc. Natl. Acad. Sci. U. S. A.* **2012** *109*, 1485-1489.

58. Reinstein O, Yoo M, Han C, Palmo T, Beckham SA, Wilce MC, Johnson PE, Quinine binding by the cocaine-binding aptamer. Thermodynamic and hydrodynamic analysis of high-affinity binding of an off-target ligand. *Biochemistry* **2013** *52*, 8652-8662.

59. Baird N, Ferré-D'Amaré A. Analysis of Riboswitch Structure and Ligand Binding Using Small-Angle X-ray Scattering (SAXS). In: Lafontaine D, Dubé A, editors. Therapeutic Applications of Ribozymes and Riboswitches: Humana Press; 2014. p. 211-225.

60. Liu JW, Lu Y, Optimization of a Pb2+-directed gold nanoparticle/DNAzyme assembly and its application as a colorimetric biosensor for Pb2+. *Chem. Mater.* **2004** *16*, 3231-3238.

61. Liu J, Lu Y, Accelerated color change of gold nanoparticles assembled by DNAzymes for simple and fast colorimetric Pb2+ detection. *J. Am. Chem. Soc.* **2004** *126*, 12298-12305.

62. Liu J, Lu Y, Rational design of "Turn-On" allosteric DNAzyme catalytic beacons for aqueous mercury ions with ultrahigh sensitivity and selectivity. *Angew. Chem., Int. Ed.* **2007** *46*, 7587-7590.

63. Torabi SF, Lu Y, Small-molecule diagnostics based on functional DNA nanotechnology: a dipstick test for mercury. *Faraday Discuss.* **2011** *149*, 125-135.

64. Liu J, Lu Y, A DNAzyme catalytic beacon sensor for paramagnetic Cu2+ ions in aqueous solution with high sensitivity and selectivity. *J. Am. Chem. Soc.* **2007** *129*, 9838-9839.

2 Chapter 2. A DNAzyme-based probe for intracellular UO_2^{2+} detection[1]

2.1 Introduction

Metal ions are essential for numerous biological processes and their regulation is crucial for maintaining normal functions. However, the beneficial features of many metal ions are often counterbalanced by their toxic effects when the metal ions are in excess, or by the presence of other toxic metal ions in the environment. To gain a better fundamental understanding of how metal ions are regulated and where the potential molecular targets are for toxic metal ions, tools that can monitor localization and concentration of metal ions in living cells are required.[1,2] Toward this goal, tremendous effort has been applied towards the development of intracellular metal ion sensors. Among them, both small molecular sensors and genetically encoded protein sensors have enjoyed the most success in intracellular metal ion sensing.[3] A large number of sensors have been successfully used to detect metal ions that have important biological functions, such as calcium,[4] zinc,[5-7] copper,[8-10] and iron.[11-16] At the same time, there is also emerging development in intracellular sensors for toxic metal ions, such as mercury,[17] cadmium[18], nickel,[19], cobalt,[20] and lead.[21,22] Despite the advances made over the previous years, it remains a significant challenge to rationally design sensors for metal ions of interest with both high sensitivity and selectivity.

To meet this challenge and design sensors for a much broader range of metal ions, we and others have taken advantage of DNAzymes. Unlike small molecule or protein-based sensors,

[1] Reprinted, with permission, from Wu P, Hwang K, Lan T, Lu Y, "A DNAzyme-gold nanoparticle probe for uranyl ion in living cells," *J. Am. Chem. Soc.* **2013** *135*, 5254-5257.

DNAzymes with high specificity for a specific metal ion of interest can be obtained from a combinatorial process, starting from a large DNA library containing up to 10^{15} different sequences.[23] Because of such high metal ion selectivity, these DNAzymes have been converted into sensors for many metal ions, such as Pb^{2+},[24] UO_2^{2+},[25] Hg^{2+},[26] and Cu^{2+},[27] based on fluorescence, colorimetry, or electrochemistry. The development of these sensors has significantly expanded the range of metal ions that can be detected. The biggest advantages of this type of sensor are that it does not require existing knowledge in order to construct a metal-binding site, and the binding affinity and selectivity toward metal ions can be fine-tuned by introducing different levels of stringency during the selection process. Moreover, it is relatively simple to synthesize DNA and many different modifications and functional groups can be easily introduced into the DNA during synthesis. Furthermore, DNA is naturally water soluble and biocompatible. All of these properties make DNAzyme sensors an attractive candidate for intracellular sensing of metal ions. However, even though DNAzymes have first been demonstrated as metal ion sensors over 10 years ago and many sensors have been reported since then, all of these sensors are limited to detecting metal ions in extracellular environments.

In this chapter, I present the design, synthesis, and application of a DNAzyme-gold nanoparticle probe for metal ions in living cells. As an initial demonstration, the 39E DNAzyme was chosen because of it exceptional selectivity (more than 1 million-fold over other competing metal ions) and sensitivity (45 pM detection limit) for the uranyl ion (UO_2^{2+}).[25] Uranium has been used in nuclear power and nuclear weapons. However, there is also growing concern about adverse health effects associated with uranium exposure.[28,29] Uranium is known as a highly toxic carcinogen.[28,30] High doses of uranium can cause kidney damage,[30] and may lead to urinary

system disease and lung cancer.[31] Chronic low-dose exposure to uranium has been shown to exert negative impacts on many different stages of animal development.[32] Uranium can also cross the blood brain barrier and accumulate in regions of the brain, resulting in alterations in behavior.[33] Uranyl is the water-soluble form of uranium, and due to its bioavailability, is the form that poses the greatest risk to human health. However, despite its high toxicity, no intracellular sensor for uranyl has been reported.

Based on our previously reported *in vitro* selection of the uranyl-specific 39E DNAzyme, this DNAzyme has been converted into uranyl sensors with many different methods for signal transduction.[25] However, all work to date involves detection outside of cells, and the sensors as designed are not suitable for detection within live cells, in part due to difficulty in delivering the DNAzyme into cells. To overcome this limitation, I chose gold nanoparticles (AuNPs) for cellular delivery of the DNAzyme, as the AuNP-DNA conjugate has many desirable properties, including stability in serum, ability to enter cells without use of transfection agents, much larger DNA loading efficiency than conventional transfection methods, and increased resistance to enzymatic degradation.[34]

2.2 Materials and Methods

2.2.1 Sequences

Table 2.1 Sequences of DNAzymes used in this study.

Name	Sequence of Oligonucleotide (5' to 3')
39E-SH	C*A*CGTCCATCTCTGCAGTCGGGTAGTTAAACCGACCTTCAGACAT AGTGAGTAGCAAAAAAAAAA*A*A-SH
39S	Cy3-A*C*TCACTAT (rA) GGAAGAGATGGACG*T*G-BHQ-2
Cy3-39S	Cy3-A*C*TCACTAT (rA) GGAAGAGATGGACG*T*G
FAM-39S	FAM-A*C*TCACTAT (rA) GGAAGAGATGGACG*T*G
Inactive 39S	Cy3-A*C*TCACTAT (A) GGAAGAGATGGACG*T*G-BHQ-2
dsDNA-1	C*A*CGTCCATCTCTTCCTATAGTGAGTAGC-AAAAAAAAAA*A*A-SH
dsDNA-2	G*C*TACTCACTATAGGAAGAGATGGACG*T*G-Cy3

* represents phosphorothioate modification; rA represents the ribonucleotide cleavage site in the substrate strand.

FAM-39S strand was only used for selectivity test and stability test because of the limitation of excitation wavelength (450 nm) of the optical scanner. Cy3-39S was only used for determining the loading of 39S on AuNPs. dsDNA-1 and dsDNA-2 hybridize to each other and were used for co-localization study. Chemical structures of the Cy3 and BHQ-2 modification of 39S are shown in Figure 2.1.

39S:

5'- (Cy3)-A*C*TCACTAT(rA)GGAAGAGATGGACG*T*G-(BHQ-2)-3'

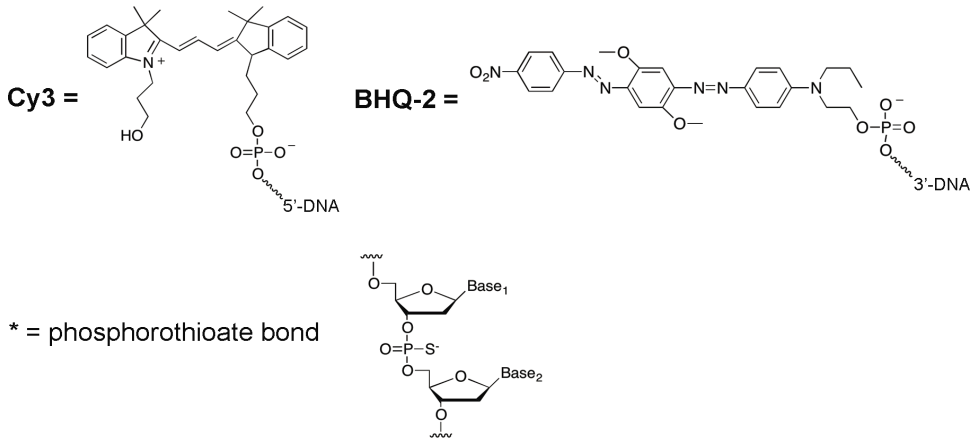

Figure 2.1 Structures of fluorophore and quencher on the substrate strand.

2.2.2 Synthesis of gold nanoparticles

- **REAGENTS**

Hydrogen tetrachloroaurate (III) ($HAuCl_4$) solution (50 mM) (Aldrich); Trisodium citrate dehydrate (38.8 mM) (Aldrich); Millipore water.

- **EQUIPMENT**

250 ml two-neck round-bottom flask with a magnetic stir bar, a stopper and a condenser; hot plate with oil bath; UV-visible spectrophotometer (Hewlett-Packard 8453); quartz UV-visible cell (Hellma); transmission and scanning transmission electron microscopy (TEM) (JEOL 2100 Cryo TEM, Frederick Seitz Materials Research Laboratory at UIUC).

- **METHODS**

13 nm AuNPs were synthesized following a previously reported protocol.[35] Before starting the synthesis, all the glassware, magnetic stir bar, stopper and condenser were soaked with freshly prepared aqua regia (3:1 concentrated HCl:HNO3) for at least 15 min. All of them were rinsed with deionized water for 20 times followed by Millipore water for another 20 times. Then 98 ml of Millipore water and 2 ml of 50 mM $HAuCl_4$ solution were mixed in the clean 200 ml two-neck flask equipped with the reflux condenser and stopper. The flask was heated to reflux, whereupon 10 ml of 38.8 mM sodium citrate was quickly added to the reaction mixture. The color of the solution was observed to change to deep red in 1 min. The system was refluxed for a further 20 min, and then allowed to cool to room temperature while stirring. The size and shape of resulting nanoparticles were characterized using TEM at 200 kV. The diameter of the nanoparticles is ~13 nm (Figure 2.2). In a typical reaction, the concentration of the final AuNP solution is ~13 nM. The extinction coefficient of this type of AuNPs at 520 nm is 1.85×10^8 M^{-1} cm^{-1}. The AuNP solution was stored in a clean glass bottle for long-term storage at room temperature.

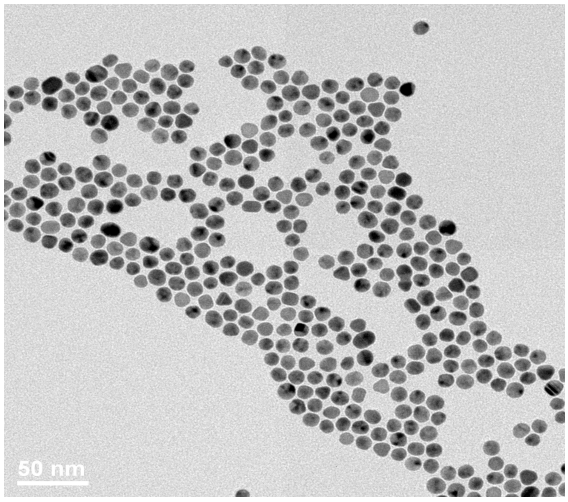

Figure 2.2 TEM image of the obtained 13 nm gold nanoparticles.

2.2.3 Functionalization of AuNP with DNAzymes

- **REAGENTS**

Freshly prepared Tris-(2-carboxymethyl)phosphine hydrochloride (TCEP) (10 mM) (Sigma®); Ultrapure Tris-(hydroxymethyl) aminomethane (Tris) (Aldrich®); Glacier acetic acid (Fisher®); Tris acetate buffer (500 mM, pH 8.2); Acetate buffer (500 mM sodium acetate, pH adjusted to 5.2 by acetic acid); NaOH (12 M); NaCl (1M); KCN (2 mM); Buffer A (25 mM Tris acetate, 100 mM NaCl, pH 8.2); Buffer B (20 mM MOPS, 100 mM NaCl, pH 7.0)

- **EQUIPMENT**

Two disposable scintillation vials (20 ml); 1.7 ml MaxyClear Snaplock Microcentrifuge tube (Axygen®, Product # MCT-175-C); Benchtop centrifuge (Eppendorf 5418); Fluorometer (Jobin Yvon FluoroMax-P); pH meter (Fisher Scientific Accumet AB15).

- **METHODS**

To reduce the disulfide linkage of the thiol-modified DNAzyme strand (39E-SH), 9 μl of 1 mM 39E-SH was mixed with 1.5 μl of 10 mM TCEP in 500 mM acetate buffer (pH 5.2). After one hour, the reduced 39E-SH was added to 3 ml of AuNP solution in a clean glass vial while gently shaking by hand to form 39E-AuNP conjugates through gold-thiol bonds. The vial was stored in the dark for a day. On the second day, 30 μl of 500 mM Tris acetate (pH 8.2) buffer and 300 μl of 1 M NaCl were added dropwise while gently shaking. The vial was stored in the dark for at least another day before use.

To transfer 39E-AuNPs from functionalization buffer to reaction buffer, 500 μl of 39E-

AuNP was transferred to a 1.7 ml microcentrifuge tube and centrifuged at 16,100*g* for 18 min. The supernatant containing free DNAzyme was removed. Particles were washed two more times with 200 μl of buffer A, then dispersed in 200 μL of buffer B. It is important to use the specific brand of microcentrifuge tubes (mentioned in the equipment section) to prevent adhesion of AuNPs to the wall of tubes. The supernatants obtained from all washes were combined and the absorbance at 260 nm measured. The number of 39E-SH strands per AuNP was estimated by subtracting the amount of 39E-SH in the supernatant mixture from the total amount of 39E-SH added into AuNP solution. The extinction coefficient of AuNP is 1.85×10^8 $M^{-1}cm^{-1}$ at 520 nm.

To anneal the substrate strands with the enzyme strands on gold nanoparticles to form 39ES-AuNPs, 39S was added to a 39E-AuNP solution to a final ratio of 1.5:1 39S to 39E. The solution was heated at 65°C for 5 min, and cooled down at room temperature for 1 h. The solution was stored at 4°C overnight to allow full hybridization. After overnight incubation, excess 39S was removed by centrifugation and washing with 3 × 200 μl buffer B. Finally, 39ES-AuNP was dispersed in 200 μl buffer B for further use.

Another way to determine the loading of 39S on AuNP is based on etching away AuNPs and measuring the fluorescence from fluorophore-labeled 39S. The AuNP core of 39ES-AuNP was removed with 2 mM KCN and the concentration of Cy3-39S was determined by measurement of Cy3 fluorescence and comparison to a standard curve.

2.2.4 Activity and selectivity

- **REAGENTS**

Buffer C (20 mM MOPS, 100 mM NaCl, 2 mM $MgCl_2$, pH 7.0); Freshly prepared uranyl citrate (1 volume of 100 mM uranyl nitrate mixed with 1 volume of 100 mM); Freshly prepared uranyl bicarbonate (1 volume of 100 mM uranyl citrate with 5 volume of 100 mM sodium bicarbonate); 10× TBE buffer ; Premixed acrylamide solution (acrylamide: Bis-acrylamide ratio of 29:1, Bio-Rad); 10% Polyacrylamide gel stock; 20% Polyacrylamide gel stock; 25% (w/w) Ammonium persulfate (APS) (Bio-Rad); TEMED (Bio-Rad); Stop solution with dyes (8 M urea, 50 mM EDTA in 1× TBE buffer, 0.05 % xylene cyanol and 0.05 % bromophenol blue); Stop solution without dyes (8 M urea, 50 mM EDTA in 1× TBE buffer).

- **EQUIPMENT**

Phosphorimager (STORM 840 optical scanner); Fluorometer (Jobin Yvon FluoroMax-P); Electrophoresis power supply

- **METHODS**

39ES-AuNP was diluted to a concentration of 1 nM in buffer C. Fluorescence intensity of samples was measured using a fluorometer at 548 nm excitation and 568 nm emission over 30 min. Fluorescence spectra were collected in the same fluorometer from 555 nm to 700 nm using 545 nm excitation. To start the reaction, a 100× stock solution of uranyl citrate or uranyl bicarbonate was added into 39ES-AuNP solution while stirring.

To test the selectivity of the probe for UO_2^{2+}, 39ES-AuNP (FAM-39S was used in this case) was concentrated to 60 nM in buffer C. 24× stock solutions of different metal salts were freshly prepared. All the reactions were tested in buffer C for 2 hours. Stop solution containing 8 M urea and 50 mM EDTA was added into reaction samples to a volume ratio of 1:1 to fully stop

reaction before samples were loaded into 20% polyacrylamide gel. Polyacrylamide gel electrophoresis was used to separate cleaved 39S strand from intact strand based on the different lengths of the two strands. After running at 26 Watts for one hour and a half, the gel was scanned using STORM 840 optical scanner with excited fluorescence at 450 nm to visualize FAM-labeled 39S strand.

2.2.5 Cell lysate

The following protocol of making cell lysate was adapted from the work by Mei, Q *et al.,* in which they tested the stability of DNA origami in cell lysate.[36] The lysis solution contains 50 mM Tris-HCl, 150 mM NaCl, 0.1% SDS, 0.5% deoxycholic acid and protease inhibitor at the ratio of 1:100. HeLa cells were washed with PBS and detached from the flask with 0.25% trypsin. After trypsin treatment, cells were centrifuged at 900 rpm for 3 minutes and resuspended in 1 mL of 1× PBS. Cells were lysed in 500 μL of the lysis solution and incubated on ice for 20 min on a shaker. The lysates were then centrifuged at 17000 × g at 4 °C for 30 min. Finally, the supernatant was removed and stored at -20 °C for later experiments.

2.2.6 Stability of 39ES-AuNPs

- **REAGENTS**

  Bovine serum (Atlanta Biologicals®); Cell lysate (See Section 2.2.5)

- **EQUIPMENT**

  Phosphorimager (STORM 840 optical scanner); Electrophoresis power supply.

- **METHODS**

39ES-AuNP with FAM-39S was incubated in 80% bovine serum, cell lysate or buffer for 3 hours at 37°C. As a control, uranyl citrate was added into 39ES-AuNP at final concentration of 50 μM. After 3-hour incubation, stop solution containing 8 M urea and 50 mM EDTA was added into each reaction with the volume ratio of 1:1 to fully denature DNAzyme and stop reactions. Polyacrylamide gel electrophoresis was used to separate stands with different lengths.

2.2.7 Uranyl uptake in HeLa cells

- **REAGENTS**

Freshly prepared uranyl citrate (1 volume of 200 mM uranyl nitrate with 5 volumes of 400 mM sodium citrate); Freshly prepared uranyl bicarbonate (1 volume of 200 mM uranyl nitrate with 5 volumes of 400 mM sodium bicarbonate); PBS solution; Dulbecco's modification of Eagle's medium (DMEM); Fetal Bovine Serum (FBS); penicillin; streptomycin; trypsin-EDTA (0.25%).

- **EQUIPMENT**

ICP-MS instrument (PerkinElmer-SCIEX ELAN DRCe); 35 mm glass-bottom dishes (MatTek); 25 cm^2 culture flasks; Cell incubator

- **METHODS**

HeLa cells were cultured in Dulbecco's modification of Eagle's medium (DMEM) supplemented with 10% Fetal Bovine Serum (FBS), 100 U/mL penicillin, and 100 μg/mL streptomycin, on 25 cm^2 culture flasks at 37°C in a humidified 5% CO2 incubator. Prior to

imaging, cells were plated on 35 mm glass-bottom dishes (MatTek) and grown to 70-90% confluence before imaging.

After cells reached ~50% confluency in culture flasks, the cell media was replaced with 5 mL fresh cell culture medium containing 750 μM uranyl citrate. Cells were incubated with uranyl for 12 hours to allow sufficient uptake. To determine the cellular concentration of uranyl, cells were thoroughly washed with PBS 6 times and incubated with fresh medium for 20 min to further reduce membrane-bound uranyl. Then cells were detached using 0.25% trypsin-EDTA and collected by centrifugation. The total number of cells was counted using hemocytometer. Cells were then treated with ultrapure nitric acid at 60°C overnight and the amount of uranyl was measured by inductively coupled plasma mass spectrometry (ICP-MS) in the Microanalysis Laboratory at UIUC. It was estimated that the cellular concentration of uranyl was ~100 μM (Assuming 2,000 μm^3 as the volume of a HeLa cell).

The amount of uranium in culture medium during two-hour incubation was measured in order to ensure no significant leakage of uranyl during the time frame of experiment. After incubation with uranyl for 12 hours, we thoroughly washed cells with PBS and added fresh medium without uranyl. After a two-hour incubation at 37°C, we collected the medium and digested it with ultrapure nitric acid. The amount of uranium in the extracellular medium was undetectable by ICP-MS.

2.2.8 Cell viability

- **REAGENTS**

Freshly prepared uranyl citrate (1 volume of 200 mM uranyl nitrate with 5 volumes of

400 mM sodium citrate); Freshly prepared uranyl bicarbonate (1 volume of 200 mM uranyl nitrate with 5 volumes of 400 mM sodium bicarbonate); PBS solution; Dulbecco's modification of Eagle's medium (DMEM); Fetal Bovine Serum (FBS); penicillin; streptomycin; trypsin-EDTA (0.25%); 3-(4,5-dimethylthiazol-2-yl)-2,5-diphenyltetrazolium bromide (MTT, 12 mM in PBS); Dimethyl sufoxide (DMSO, Fisher®).

- **EQUIPMENT**

96-well plate; Microplate reader (SpectraMax M2 Multi-detection reader, Metabolomics Center at UIUC);

- **METHODS**

HeLa cells were seeded in 96-well plate at a concentration of 1×10^5 cells/well. After one day, uranyl citrate or uranyl bicarbonate was introduced into the culture media at concentrations ranging from 0 - 1000 μM. Cells were grown in uranyl-containing media for another 12 hours before removing extracellular uranyl by washing. MTT was added to each well at a final concentration of 1.2 mM. After five hours the MTT-containing media was removed, cells were washed, and 100 μL of DMSO was added to each well to dissolve the formazan. The absorbance at 540 nm was measured using a microplate reader.

2.2.9 39ES-AuNP uptake and imaging

- **REAGENTS**

Freshly prepared uranyl citrate (1 volume of 200 mM uranyl nitrate with 5 volumes of 400 mM sodium citrate); Freshly prepared uranyl bicarbonate (1 volume of 200 mM uranyl

nitrate with 5 volumes of 400 mM sodium bicarbonate); PBS solution; Dulbecco's modification of Eagle's medium (DMEM); Opti-MEM (gibco®); Fetal Bovine Serum (FBS); penicillin; streptomycin; trypsin-EDTA (0.05%); 3-(4,5-dimethylthiazol-2-yl)-2,5-diphenyltetrazolium bromide (MTT, 12 mM in PBS); Dimethyl sufoxide (DMSO) (Fisher®); Hoechst 33258 (2.5 μg/ml, Invitrogen®); 4% w/w paraformaldehyde in PBS; Lysotracker Green (Invitrogen®);

- **EQUIPMENT**

96-well plate; Zeiss LSM 710 NLO confocal microscope (IGB imaging center at UIUC);

- **METHODS**

After incubating HeLa cells with uranyl citrate and thoroughly washing with PBS, 2 mL of Opti-MEM containing 3 nM 39ES-AuNP was added to each glass-bottom dish. After 2 hours, cells were washed with PBS three times and fresh DMEM was added. Cells were further stained for 20 minutes with Hoechst 33258 at a final concentration of 2.5 ng/mL. Images were obtained using a Zeiss LSM 710 NLO confocal microscope at 63x magnification equipped with a Mai-Tai Ti-Sapphire laser. Fluorescence emission was measured over 450-520 nm and 575-620 nm ranges, with excitation at 401 nm and 561 nm, respectively. The pinhole and gain settings were kept constant throughout the whole imaging process. Z-stack images were also obtained to confirm that the fluorescent signal was inside cells. For colocalization studies, Lysotracker Green was added to cells for 30 minutes after Hoechst staining, at a final concentration of 50 nM. Cells were fixed with 4% paraformaldehyde and the fluorescence emission was measured over 510-570 nm, with excitation at 488 nm.

To estimate the amount of AuNP per cell, cells were washed with PBS 6 times after

incubation with 3 nM 39ES-AuNP. Then cells were detached by 0.25% trypsin-EDTA and collected by centrifugation. The total number of cells was counted. Cells were further treated with neat nitric acid at 60°C overnight and the amount of Au was measured by ICP-MS. It was estimated that there was ~1×10^6 AuNPs/cell (Assuming 6.78×10^4 atoms/particle[37]).

2.2.10 Flow cytometry

HeLa cells were grown with or without uranyl citrate in culture media for 12 hours. After washing cells thoroughly with PBS for five times, Opti-MEM containing 3 nM active or inactive 39ES-AuNP was added to cells. After two-hour incubation, cells were washed with PBS and detached from the culture plate by trypsin. The suspended cell solution was centrifuged at 2,000 g for 5 min and washed with PBS three times. Flow cytometry was performed using a BD FACSCanto system under 488 nm excitation. Control cells without any treatment were used to set the gating. Each set of measurement was performed in triplicate and averaged, and each measurement used 10,000 cells. The standard deviation of mean fluorescence was used as the error bar.

2.3 Results and Discussion

2.3.1 Activity of 39ES-AuNPs

As shown in Figure 2.3, the DNAzyme-AuNP cellular sensor (39ES-AuNP) consists of a 13 nm AuNP, 39E enzyme strand, and its substrate strand (39S). The 3′ end of the enzyme strand is functionalized with a thiol group (SH) for immobilization onto the AuNP. In addition, a poly-A spacer is added between the thiol moiety and the enzyme strand to avoid loss of activity due to steric interference of the AuNP. The substrate strand is labeled with a fluorophore (Cy3) at the 5′ end and a quencher (BHQ-2) at the 3′ end (Figure 2.1 and 2.3). Upon immobilization of enzyme strands onto the AuNP, the substrate strands were hybridized with enzyme strands by heating and annealing. When hybridized, the fluorescence signal from Cy3 should be quenched by the AuNP, as AuNP is known to quench fluorophores. However, the poly-A spacer between the enzyme strand and AuNP surface were found to weaken the quenching effect of AuNP, since quenching of a dye's fluorescence is strongly dependent on the spatial separation of the dye from the nanoparticle surface. Figure 2.4(a) shows that when 39S was modified with Cy3 fluorophore but without BHQ-2 quencher, the turn-on signal was not strong. To ensure complete quenching, we added a quencher (Black Hole Quencher-2, BHQ-2) at the 3′ end of 39S, resulting in increased S/N ratio (Figure 2.4(b)). In the presence of uranyl, the substrate strand is cleaved, resulting in a shorter DNA strand with corresponding lower melting temperature (21°C) than the original full-length substrate strand (60°C). The shorter DNA strand containing Cy3 fluorophore is released. The Cy3 is separated from both the AuNP and BHQ-2 quencher, and the fluorescent signal is enhanced.

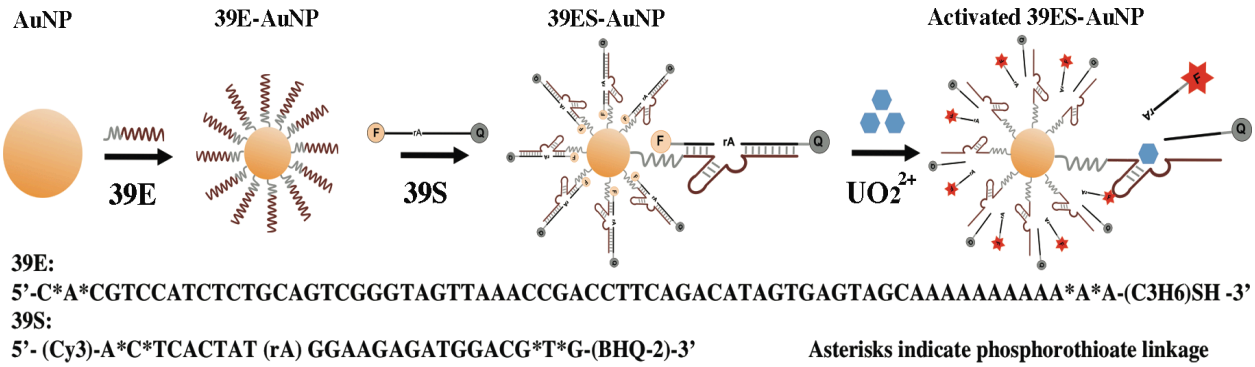

Figure 2.3 Design of a fluorescent DNAzyme immobilized onto gold nanoparticles as selective probe of uranyl inside live cells.

Quantification of the DNAzyme on the AuNP surface by UV absorption and fluorescence showed that there were about 70 copies of 39E on each AuNP, and the same number of 39S strands hybridized to the enzyme strands. Such a dense loading of DNAzymes and efficient hybridization between the DNAzyme and their substrate strand allows for efficient cellular uptake of many DNAzymes per AuNP and thus maximum dynamic range.

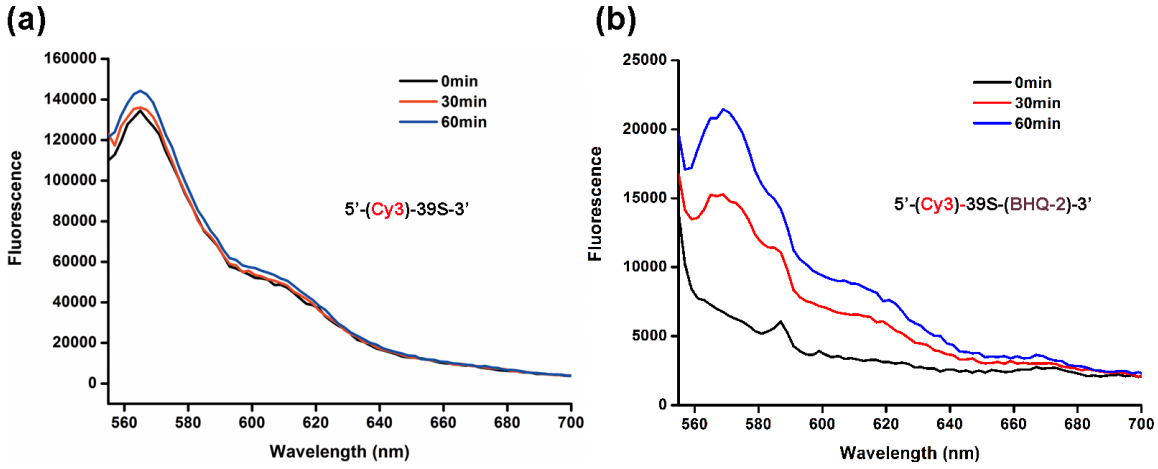

Figure 2.4 An additional BHQ-2 quencher at 3′ end of 39S is necessary for better S/N ratio.

The performance of the 39ES-AuNP cellular sensor was first evaluated in a buffer (20 mM MOPS, 100 mM NaCl, 2 mM $MgCl_2$, pH 7.0) (Figure 2.5). Uranyl citrate and uranyl bicarbonate are two major uranyl species at physiological conditions.[28,30-32] To test the response of 39ES-AuNP on both uranyl species, the increase of fluorescent signal with increasing concentrations of both species were measured. Since 39E performs best at pH 5.5, we tested the activity of 39ES-AuNP at both pH 7.0 and pH 5.0. The conjugates showed faster reaction rate at pH 5.0 compare to pH 7.0 (Figure 2.6). Improved sensitivity for uranyl at pH 5.0 also makes the sensor suitable for working in acidic organelles. During the time course of 30 min, 2-4 fold of fluorescence increase was observed for both pH conditions with 20 μM to 100 μM uranyl (Figure 2.5 and 2.6). The rate for fluorescence increase reached plateaus at higher concentration of uranyl citrate, while the rate for fluorescence decreased if the concentration of uranyl bicarbonate was more than 10 μM (Figure 2.7). We attribute the different response to different solubility of the two uranyl species in buffer. Because 39ES-AuNP has a wider dynamic range in the presence of uranyl citrate than uranyl bicarbonate, we chose uranyl citrate in our later studies.

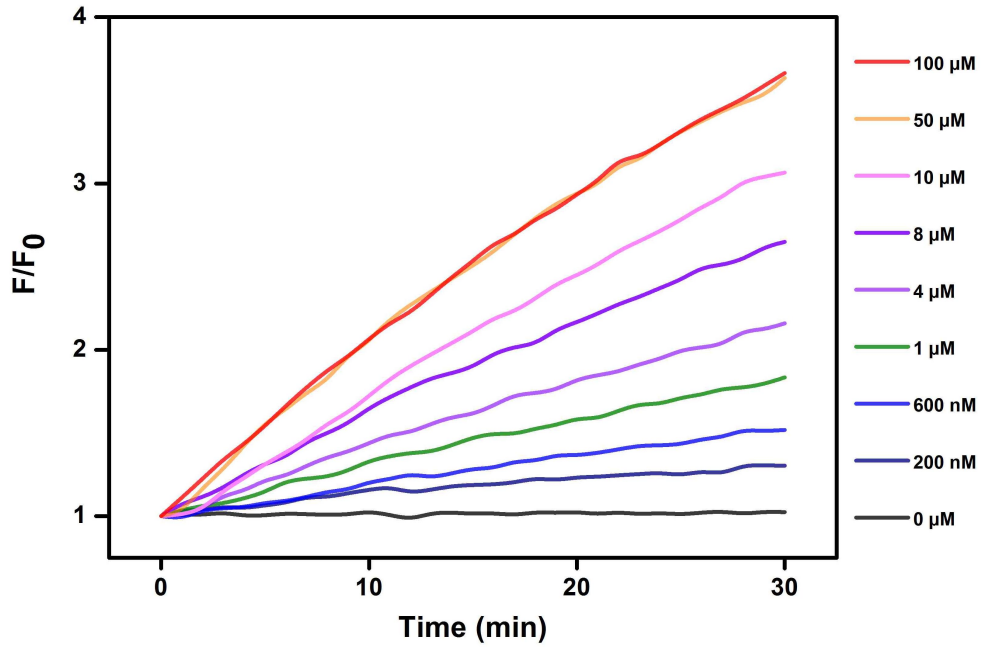

Figure 2.5 Turn-on response of 39ES-AuNP to different concentrations of uranyl citrate over time at pH 7.0.

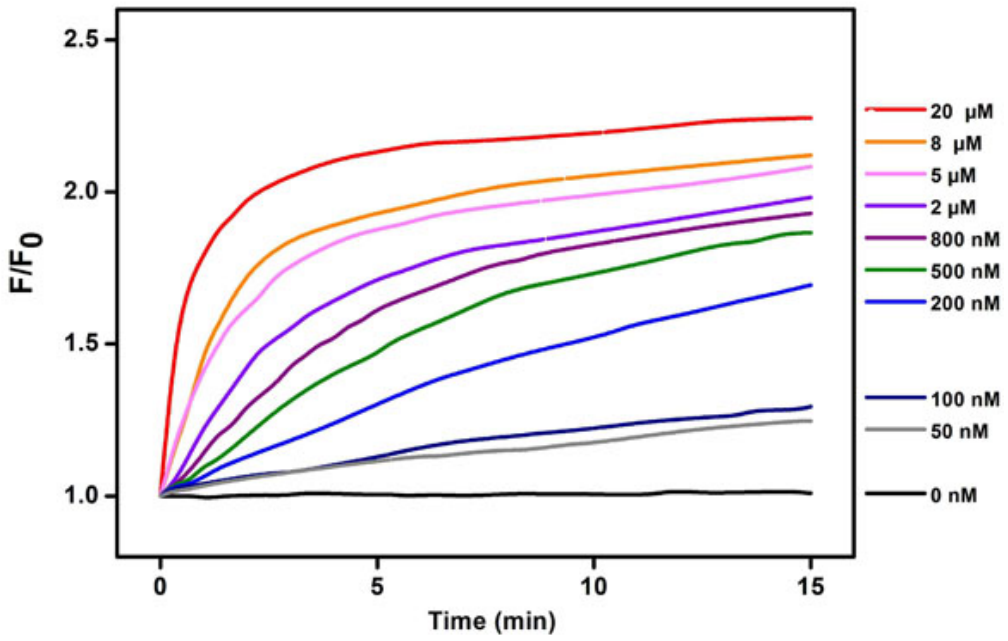

Figure 2.6 Turn-on response of 39ES-AuNP to different concentrations of uranyl citrate over time at pH 5.0.

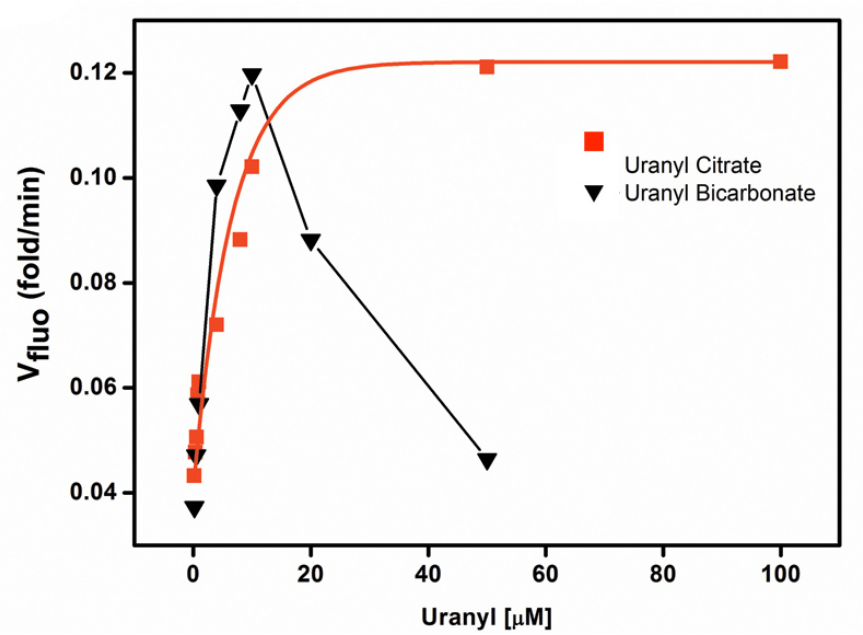

Figure 2.7 Rate of turn-on fluorescence increase at different concentrations of uranyl citrate or uranyl bicarbonate.

2.3.2 Selectivity of 39ES-AuNPs

Selectivity of 39ES-AuNP was tested in the presence of other common physiological metal ions, such as Mg^{2+}, Ca^{2+}, Zn^{2+}, *etc.* The concentrations of these metal ions were chosen based on their physiological concentrations (100 mM for K^{+}; 2 mM for Ca^{2+} and Zn^{2+}; 20 μM for Co^{2+}, Cd^{2+}, Mn^{2+}, Ni^{2+}, Pb^{2+}, Cu^{2+}, Fe^{3+}; reaction with Cu^{+} and Fe^{2+} was carried out in an oxygen-free environment to prevent oxidation of metal ions). As shown in Figure 2.8, the sensor maintains excellent selectivity for uranyl over other various biologically relevant metal ions at physiologically relevant concentrations.

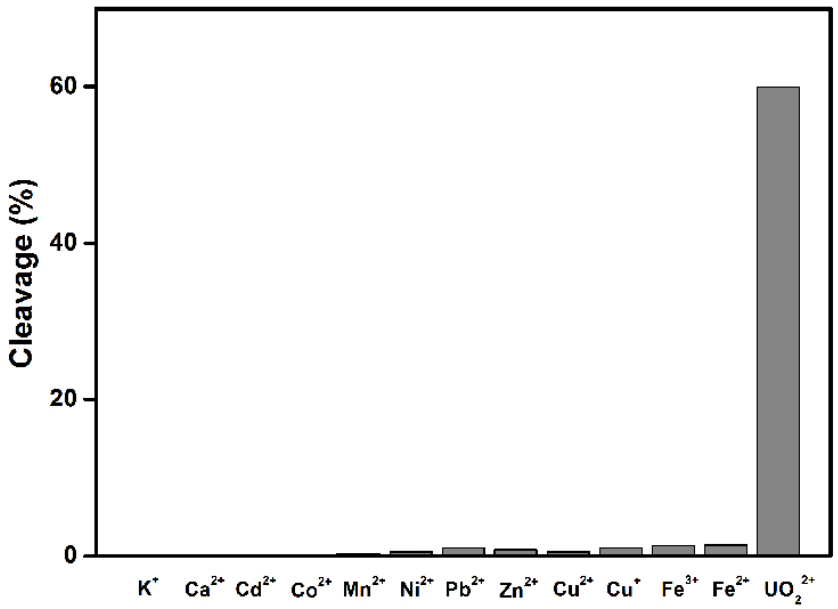

Figure 2.8 Selectivity of the 39ES-AuNP probe.

2.3.3 Stability of 39ES-AuNPs

Stability of 39ES-AuNPs was test in 80% bovine serum, HeLa cell lysate, or buffer B (see 2.2.3) for 3 hours at 37°C. As a positive control, uranyl citrate was added into 39ES-AuNPs at a final concentration of 50 μM. As shown in Figure 2.9, no obvious cleavage of substrate strand was observed, suggesting that the stability of the sensor is sufficient for application in cellular environment.

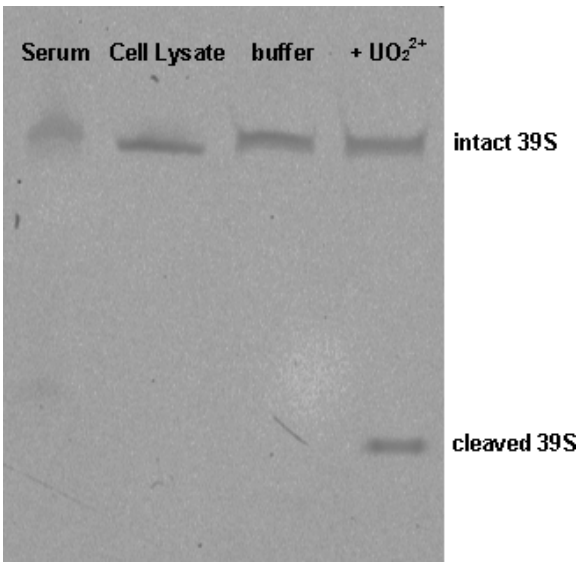

Figure 2.9 Stability of 39ES-AuNPs in the presence of buffer, serum and cell lysate.

2.3.4 39ES-AuNPs uptake and imaging

Having demonstrated the effectiveness of the 39ES-AuNP cellular sensor in buffer, we next tested its cellular uptake and fluorescence changes using HeLa cells (human cervical cancer) as a model. HeLa cells were first treated with 750 μM uranyl citrate for 12 hours to allow sufficient uranyl uptake. The cell viability tested via MTT assay suggests that no obvious toxicity up to 1,000 μM of uranyl citrate or uranyl bicarbonate (Figure 2.10). Based on ICP-MS, the intracellular concentration of uranyl under these conditions is estimated to reach 100 μM.

HeLa cells that were pretreated with uranyl citrate were incubated with the probes for another 2 hours before images were taken using confocal microscopy. The amount of 39ES-AuNP was estimated to be 1×10^6/cell based on ICP-MS measurement (see Section 2.2.9).

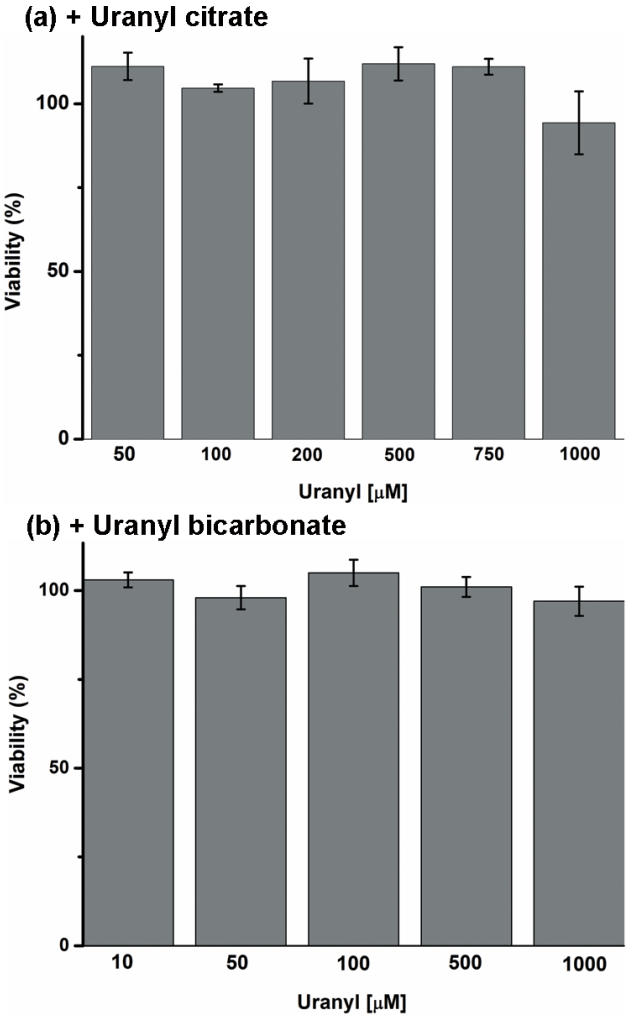

Figure 2.10 Viability of cells incubated with different concentrations of uranyl citrate or uranyl bicarbonate.

We further used live cell imaging to evaluate the performance of 39ES-AuNPs in the cellular environment. Figure 2.11 shows the Z-stack images of cells delivered with 39ES-AuNPs. The red fluorescence from the probe was localized on the same plane as the nucleus, indicating the intracellular localization of the probe.

Figure 2.12 is the typical images from confocal microscopy imaging. The red channel is Cy3 fluorescence from activated 39ES-AuNP and the blue channel is Hoechst 33258 for nucleus

staining. Differential interference contrast microscopy (DIC) images of cells are shown in the third column (Scale bar = 20 μm). As shown in Figure 2.12 (a) and (b), HeLa cells incubated with uranyl citrate showed more fluorescence than those without uranyl citrate. To further demonstrate that the fluorescence observed was due to the activity of the DNAzyme, an inactive DNAzyme substrate strand was prepared in which the adenosine ribonucleotide at the cleavage site was replaced with a deoxyribonucleotide. HeLa cells using such an inactive probe showed less fluorescence than those with the active probe (Figure 2.12 (c) and (d)).

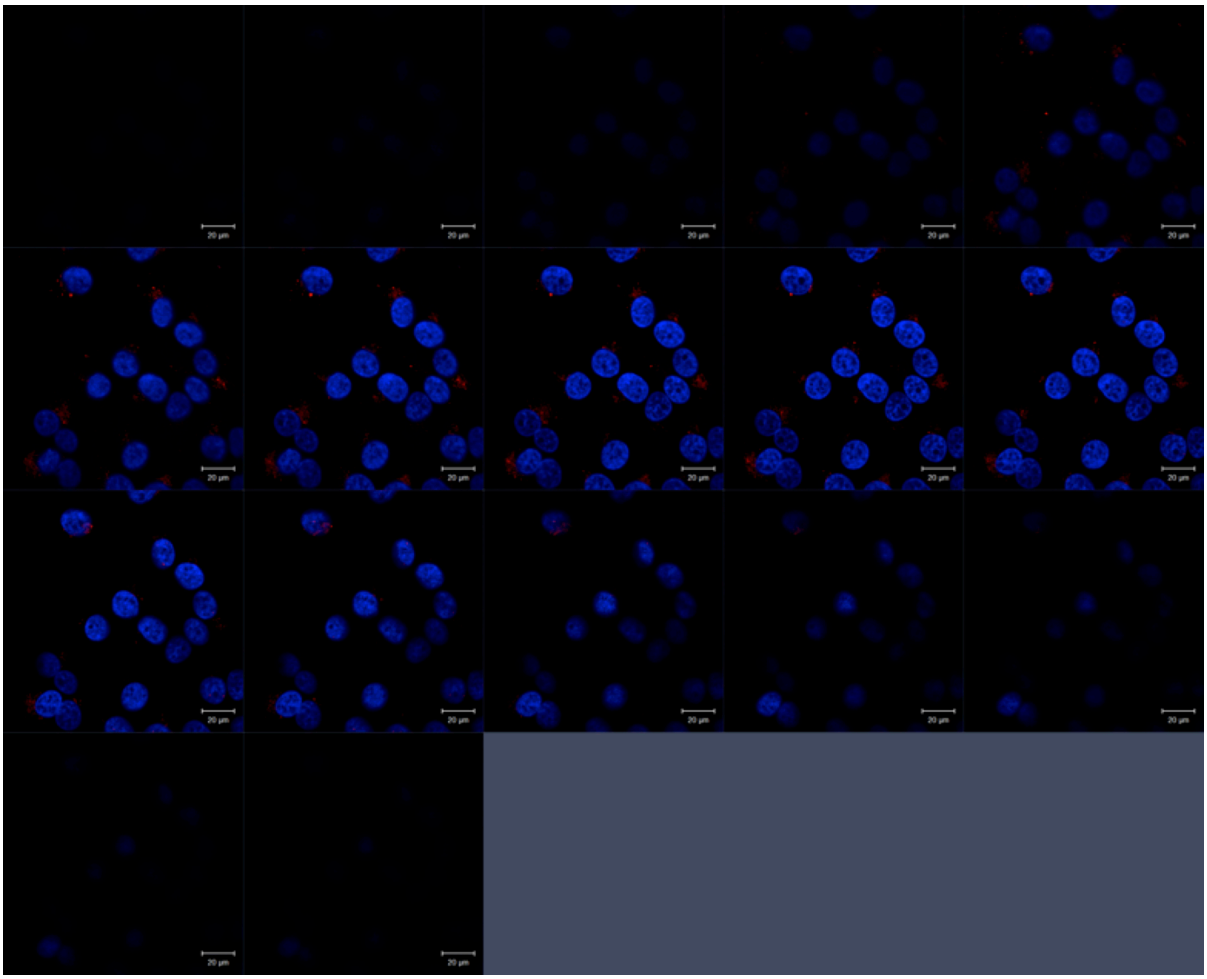

Figure 2.11 Z-stack images of cells with uranyl and 39ES-AuNP probes.

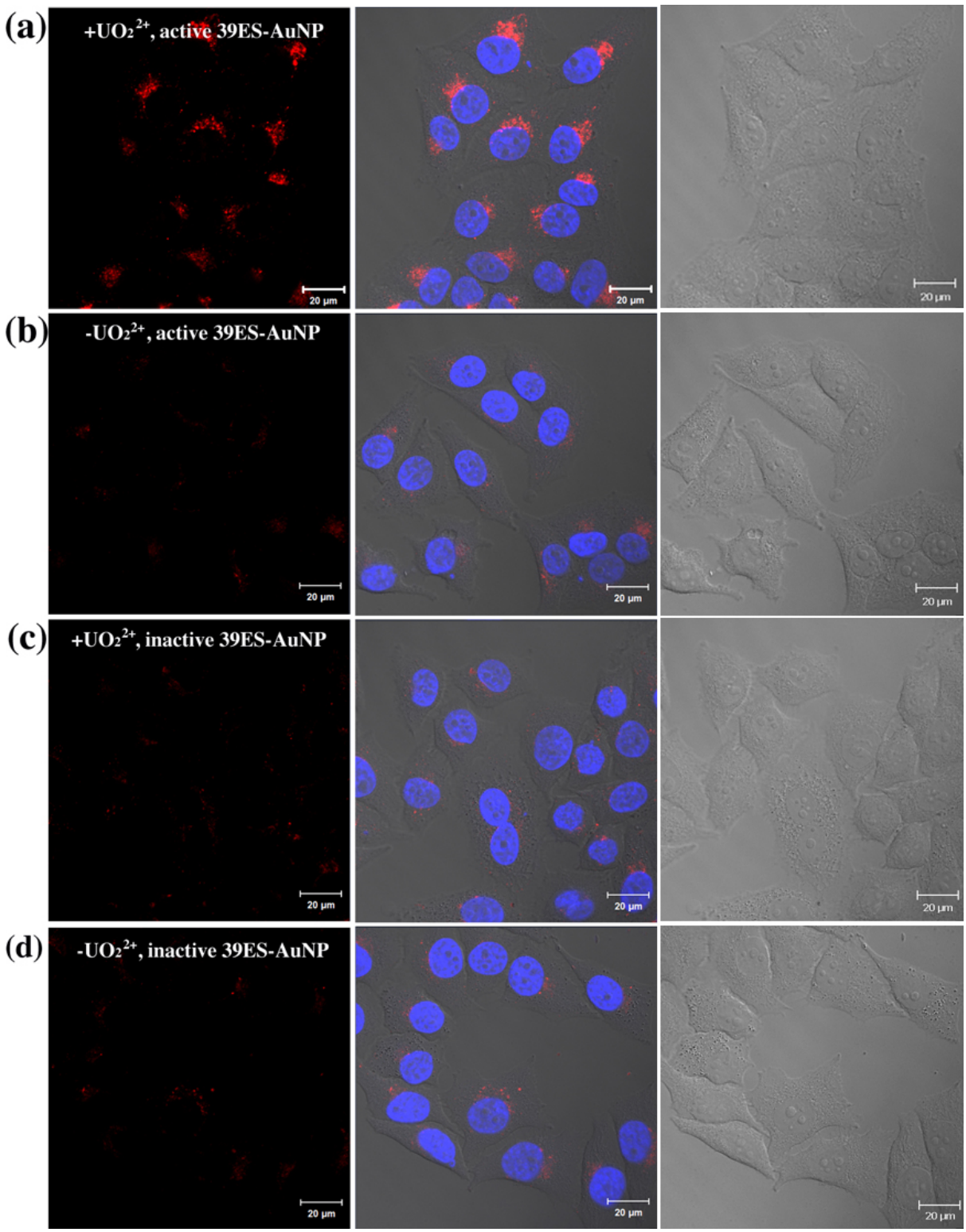

Figure 2.12 Confocal microscopy images of HeLa cells treated with or without uranyl and incubated with active or inactive 39ES-AuNPs.

2.3.5 Intracellular location of 39ES-AuNPs

To study the distribution of 39ES-AuNP inside cells, Lysotracker was used to specifically stain the lysosomes of cells. Fluorescence from 39ES-AuNP and Lysotracker showed good colocalization (Pearson's correlation coefficient=0.61), which indicates that the 39ES-AuNP probe is mainly transported to the lysosomes (Figure 2.13). This result is consistent with DNA-AuNPs being known to enter HeLa cells via receptor-mediated endocytosis. To ensure that the lysosome-specific localization was not due to the DNAzymes we used in this study, we did a control experiment using double-stranded DNA (dsDNA) with a random sequence and functionalized AuNPs with this dsDNA. As shown in Figure 2.14, dsDNA-AuNPs also showed lysosome localization inside cells after two-hour incubation, suggesting that the localization of the DNA-AuNP was determined by the mechanism of its uptake, not by specific DNA sequences. Such co-localization may have implications on the mechanism of uranyl detoxification inside cells. Lysosomes have been known to play ubiquitous sequestration and detoxification roles for heavy metals, such as copper, zinc, cadmium and mercury. Although the mechanism for uranyl detoxification inside mammalian cells is unclear, accumulation of uranyl inside lysosomes as detected by our sensor suggest that the cells may use similar strategies to sequester uranyl inside lysosomes as a way for detoxification.

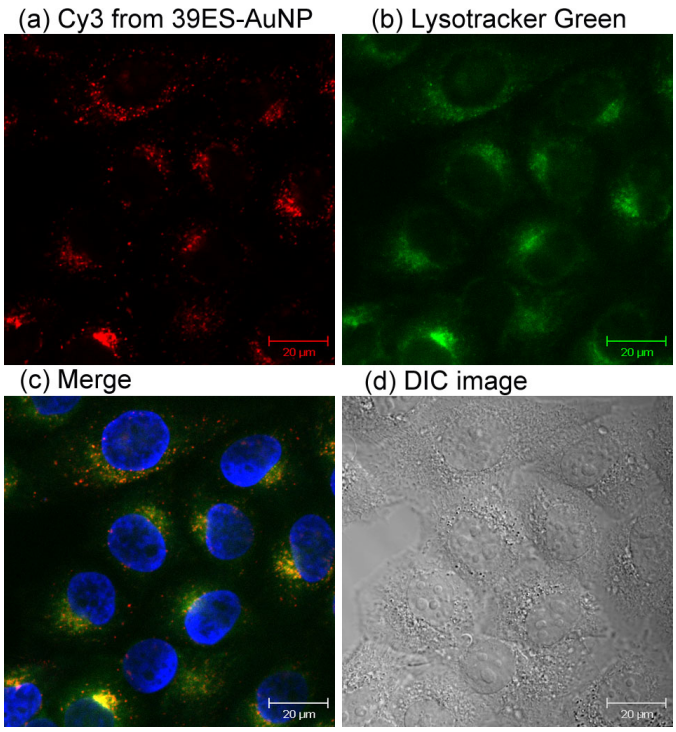

Figure 2.13 Localization of 39ES-AuNPs inside cells.

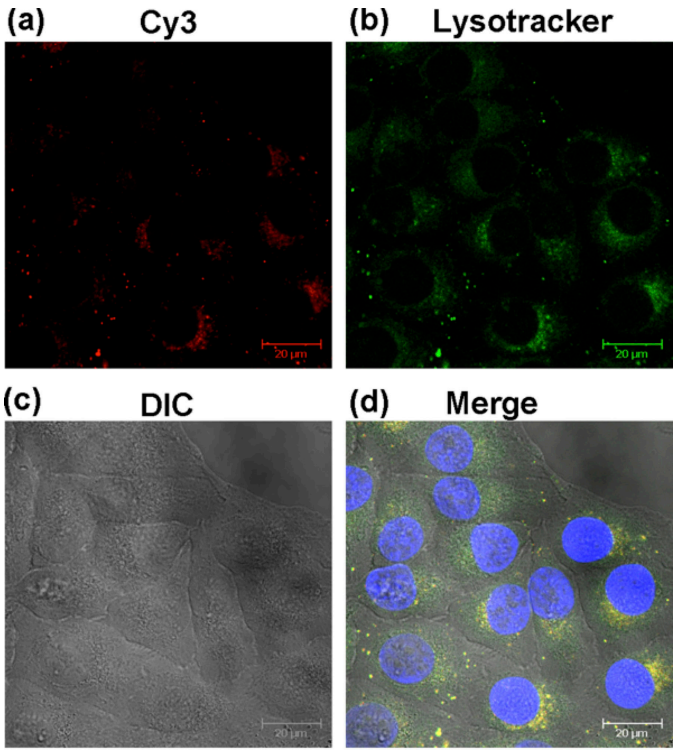

Figure 2.14 Localization of dsDNA-AuNP inside cells.

2.3.6 Flow cytometric quantification

Finally, to ensure that the observations made via confocal microscopy apply to the whole cell population, we examined the fluorescence coming from a population of cells and quantified intracellular fluorescence in cells with or without uranyl using flow cytometry. The results shown in Figure 2.15 suggest that HeLa cells pretreated with uranyl citrate had a higher level of fluorescence than untreated cells. Compared with the active 39ES-AuNP probe, the inactive 39ES-AuNP probe showed less fluorescence in both uranyl-treated and untreated cells. The difference between the positive group and all three control groups is statistically significant ($p<0.001$). These results demonstrate retention of signaling ability of the probes within live cells.

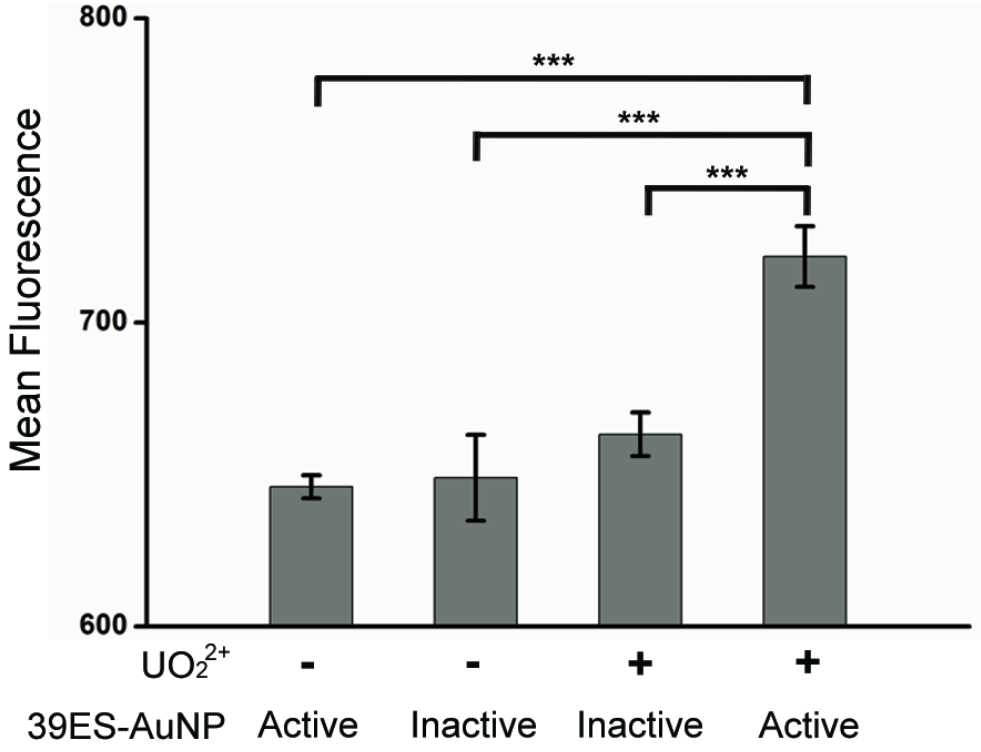

Figure 2.15 Flow cytometric quantification of cell associated fluorescence.

2.4 Conclusions

In conclusion, we have developed the first DNAzyme-based probe of metal ions in living cells by conjugation of a fluorescent DNAzyme onto AuNPs. Since a number of DNAzymes specific for different metal ions have been obtained and additional DNAzymes for other metal ions can be selected using *in vitro* selection, the method demonstrated here provides us with a simple and general platform to convert any of these DNAzymes into intracellular probes for a wide range of metal ions. Continued development of these DNAzyme-AuNP probes will allow for a better understanding of the localization and distribution of metal ions in biological systems.

2.5 References

1. Finney L, Mandava S, Ursos L, Zhang W, Rodi D, Vogt S, Legnini D, Maser J, Ikpatt F, Olopade OI, Glesne D, X-ray fluorescence microscopy reveals large-scale relocalization and extracellular translocation of cellular copper during angiogenesis. *Proc. Natl. Acad. Sci. U. S. A.* **2007** *104*, 2247-2252.

2. Dodani SC, Domaille DW, Nam CI, Miller EW, Finney LA, Vogt S, Chang CJ, Calcium-dependent copper redistributions in neuronal cells revealed by a fluorescent copper sensor and X-ray fluorescence microscopy. *Proc. Natl. Acad. Sci. U. S. A.* **2011** *108*, 5980-5985.

3. Zhang J, Campbell RE, Ting AY, Tsien RY, Creating new fluorescent probes for cell biology. *Nat. Rev. Mol. Cell Biol.* **2002** *3*, 906-918.

4. Kerr R, Lev-Ram V, Baird G, Vincent P, Tsien RY, Schafer WR, Optical imaging of calcium transients in neurons and pharyngeal muscle of C. elegans. *Neuron* **2000** *26*, 583-594.

5. Qian F, Zhang C, Zhang Y, He W, Gao X, Hu P, Guo Z, Visible light excitable Zn2+ fluorescent sensor derived from an intramolecular charge transfer fluorophore and its in vitro and in vivo application. *J. Am. Chem. Soc.* **2009** *131*, 1460-1468.

6. Tomat E, Lippard SJ, Ratiometric and intensity-based zinc sensors built on rhodol and rhodamine platforms. *Inorg. Chem.* **2010** *49*, 9113-9115.

7. Qin Y, Dittmer PJ, Park JG, Jansen KB, Palmer AE, Measuring steady-state and dynamic endoplasmic reticulum and Golgi Zn2+ with genetically encoded sensors. *Proc. Natl. Acad. Sci. U. S. A.* **2011** *108*, 7351-7356.

8. Zeng L, Miller EW, Pralle A, Isacoff EY, Chang CJ, A selective turn-on fluorescent sensor for imaging copper in living cells. *J. Am. Chem. Soc.* **2006** *128*, 10-11.

9. Wegner SV, Arslan H, Sunbul M, Yin J, He C, Dynamic copper(I) imaging in mammalian cells with a genetically encoded fluorescent copper(I) sensor. *J. Am. Chem. Soc.* **2010** *132*, 2567-2569.

10. Hirayama T, Van de Bittner GC, Gray LW, Lutsenko S, Chang CJ, Near-infrared fluorescent sensor for in vivo copper imaging in a murine Wilson disease model. *Proc. Natl. Acad. Sci. U. S. A.* **2012** *109*, 2228-2233.

11. Fakih S, Podinovskaia M, Kong X, Schaible UE, Collins HL, Hider RC, Monitoring intracellular labile iron pools: A novel fluorescent iron(III) sensor as a potential non-invasive diagnosis tool. *J. Pharm. Sci.* **2009** *98*, 2212-2226.

12. Sen S, Sarkar S, Chattopadhyay B, Moirangthem A, Basu A, Dhara K, Chattopadhyay P, A ratiometric fluorescent chemosensor for iron: discrimination of Fe2+ and Fe3+ and living cell application. *Analyst* **2012** *137*, 3335-3342.

13. Hirayama T, Okuda K, Nagasawa H, A highly selective turn-on fluorescent probe for iron(ii) to visualize labile iron in living cells. *Chem. Sci.* **2013** *4*, 1250-1256.

14. Au-Yeung HY, Chan J, Chantarojsiri T, Chang CJ, Molecular imaging of labile iron(II) pools in living cells with a turn-on fluorescent probe. *J. Am. Chem. Soc.* **2013** *135*, 15165-15173.

15. Niwa M, Hirayama T, Okuda K, Nagasawa H, A new class of high-contrast Fe(II) selective fluorescent probes based on spirocyclized scaffolds for visualization of intracellular labile iron delivered by transferrin. *Org. Biomol. Chem.* **2014** *12*, 6590-6597.

16. Sivaraman G, Sathiyaraja V, Chellappa D, Turn-on fluorogenic and chromogenic detection of Fe(III) and its application in living cell imaging. *J. Lumin.* **2014** *145*, 480-485.

17. Nolan EM, Lippard SJ, Tools and tactics for the optical detection of mercuric ion. *Chem. Rev.* **2008** *108*, 3443-3480.

18. Cheng T, Xu Y, Zhang S, Zhu W, Qian X, Duan L, A highly sensitive and selective OFF-ON fluorescent sensor for cadmium in aqueous solution and living cell. *J. Am. Chem. Soc.* **2008** *130*, 16160-16161.

19. Dodani SC, He Q, Chang CJ, A turn-on fluorescent sensor for detecting nickel in living cells. *J. Am. Chem. Soc.* **2009** *131*, 18020-18021.

20. Au-Yeung HY, New EJ, Chang CJ, A selective reaction-based fluorescent probe for detecting cobalt in living cells. *Chem. Commun.* **2012** *48*, 5268-5270.

21. Deo S, Godwin HA, A Selective, Ratiometric Fluorescent Sensor for Pb2+. *J. Am. Chem. Soc.* **2000** *122*, 174-175.

22. He Q, Miller EW, Wong AP, Chang CJ, A selective fluorescent sensor for detecting lead in living cells. *J. Am. Chem. Soc.* **2006** *128*, 9316-9317.

23. Breaker RR, Joyce GF, A DNA enzyme that cleaves RNA. *Chem. Biol.* **1994** *1*, 223-229.

24. Li J, Lu Y, A highly sensitive and selective catalytic DNA biosensor for lead ions. *J. Am. Chem. Soc.* **2000** *122*, 10466-10467.

25. Liu J, Brown AK, Meng X, Cropek DM, Istok JD, Watson DB, Lu Y, A catalytic beacon sensor for uranium with parts-per-trillion sensitivity and millionfold selectivity. *Proc. Natl. Acad. Sci. U. S. A.* **2007** *104*, 2056-2061.

26. Liu J, Lu Y, Rational design of "Turn-On" allosteric DNAzyme catalytic beacons for aqueous mercury ions with ultrahigh sensitivity and selectivity. *Angew. Chem., Int. Ed.* **2007** *46*, 7587-7590.

27. Liu J, Lu Y, A DNAzyme catalytic beacon sensor for paramagnetic Cu2+ ions in aqueous solution with high sensitivity and selectivity. *J. Am. Chem. Soc.* **2007** *129*, 9838-9839.

28. Lin RH, Wu LJ, Lee CH, Lin-Shiau SY, Cytogenetic toxicity of uranyl nitrate in Chinese hamster ovary cells. *Mutat. Res.* **1993** *319*, 197-203.

29. Briner W, The toxicity of depleted uranium. *Int. J. Environ. Res. Public. Health* **2010** *7*, 303-313.

30. Craft E, Abu-Qare A, Flaherty M, Garofolo M, Rincavage H, Abou-Donia M, Depleted and natural uranium: chemistry and toxicological effects. *J Toxicol Environ Health B Crit Rev* **2004** *7*, 297-317.

31. Domingo JL, Reproductive and developmental toxicity of natural and depleted uranium: a review.

Reprod. Toxicol. **2001** *15*, 603-609.

32. Carrière M, Thiebault C, Milgram S, Avoscan L, Proux O, Gouget B, Citrate Does Not Change Uranium Chemical Speciation in Cell Culture Medium but Increases Its Toxicity and Accumulation in NRK-52E Cells. *Chem. Res. Toxicol.* **2006** *19*, 1637-1642.

33. Kathren RL, Burklin RK, Acute chemical toxicity of uranium. *Health Phys.* **2008** *94*, 170-179.

34. Seferos DS, Prigodich AE, Giljohann DA, Patel PC, Mirkin CA, Polyvalent DNA nanoparticle conjugates stabilize nucleic acids. *Nano Lett.* **2009** *9*, 308-311.

35. Liu J, Lu Y, Preparation of aptamer-linked gold nanoparticle purple aggregates for colorimetric sensing of analytes. *Nat. Protoc.* **2006** *1*, 246-252.

36. Mei Q, Wei X, Su F, Liu Y, Youngbull C, Johnson R, Lindsay S, Yan H, Meldrum D, Stability of DNA origami nanoarrays in cell lysate. *Nano Lett.* **2011** *11*, 1477-1482.

37. Giljohann DA, Seferos DS, Patel PC, Millstone JE, Rosi NL, Mirkin CA, Oligonucleotide loading determines cellular uptake of DNA-modified gold nanoparticles. *Nano Lett.* **2007** *7*, 3818-3821.

3 Chapter 3. Intracellular Detection of Sodium Ions Using a DNAzyme-Based Probe[2]

3.1 Introduction

Over the past two decades, enormous progress has been made in designing fluorescent sensors or probes for divalent metal ions. In contrast, designing a fluorescent sensor for monovalent metal ions such as sodium (Na^+) is still underdeveloped, even though Na^+ is the most abundant metal ion in biological systems and plays critical role in diverse biological processes. As one of the most abundant metal ions in extracellular fluid, Na^+ affects cellular processes by triggering the activation of many signal transduction pathways, as well as regulating the functions of hormones.[1-4] Therefore, it is important to carefully monitor the concentrations of the Na^+ in biological systems under various conditions in order to understand its role. Toward this goal, instrumental analyses by atomic absorption spectroscopy (AAS),[5] X-ray fluorescence microscopy (XFM),[6] and ^{23}Na NMR[7] have been used to detect the concentration of intracellular Na^+. However, it is difficult to use these methods to obtain real time dynamics of Na^+ distribution in living cells, since they often require pre-treatment of samples, such as fixation or lysis. To overcome these drawbacks, fluorescent sensors specific for Na^+ have been the focus for sensor development, as they can provide sensitive detection with high spatial and temporal resolution.[8-15] However, despite numerous efforts in developing fluorescent metal ion sensors,[16,17] such as those based on either genetically encoded probes or small molecular sensors, most fluorescent sensors reported so far can detect divalent or trivalent metal ions such as

[2] Reprinted, with permission, from Torabi S-F, Wu P, McGhee CE, Chen L, Hwang K, Zheng N, Cheng J, Lu Y, "*In vitro* selection of a sodium-specific DNAzyme and its application in intracellular sensing," *Proc. Natl. Acad. Sci. U. S. A.* **2015** *112*, 5903-5908.

Ca^{2+},[18-20] Zn^{2+},[21,22] Cu^{2+},[23,24] Fe^{2+},[25-27] and Fe^{3+}.[28] Among the limited number of Na^+ sensors, such as sodium-binding benzofuran isophthalate (SBFI),[29] Sodium Green,[30] CoroNa Green/Red,[31,32] and Asante NaTRIUM Green-1/2 (ANG-1/2),[33-35] most of them are not selective against K^+ [29-32,35] or they have a low binding affinity for Na^+ (with a K_d higher than 100 mM).[32,36,37] Furthermore, the presence of organic solvents is required to achieve desired sensitivity and selectivity for many of the Na^+ probes,[38-40] making it difficult to study Na^+ under physiological conditions. Therefore, it is still a major challenge to design fluorescent sensors with strong affinity for Na^+ and high selectivity over other mono- and multi-valent metal ions that work under physiological conditions.

To meet this challenge, we took advantages of DNAzymes. As demonstrated in Chapter 2, DNAzymes with high sensitivity and specificity for metal ions can be converted into sensors for metal ion detection in live cells. However, most of the previously reported DNAzymes have selectivity for divalent or trivalent metal ions.[41-45] To our knowledge, no DNAzymes have been reported to have high selectivity towards a specific monovalent metal ion. Although DNAzymes that are independent of divalent metal ions have been reported, including those employing modified nucleotides with protein-like functionalities (*i.e.* guanidinium and imidazole),[46-48] no DNAzymes have been found to have selectivity for a certain monovalent metal ion over other monovalent metal ions. Based on a comprehensive search of the literature, the DNAzyme with the highest selectivity for Na^+ has only one-fold selectivity over K^+.[49] Moreover, those DNAzymes require high concentration of monovalent metal ions (molar ranges) in order to function efficiently, and they display very slow catalytic rate (e.g., 10^{-3} min^{-1}).[49-51] Such poor selectivity, high metal ion concentration requirement, and slow catalytic rate render these

DNAzymes unsuitable for cellular detection of Na^+, due to interferences from other monovalent ions such as K^+ (which is present in concentrations about 10-fold higher than Na^+), and the need to image Na^+ rapidly.

This chapter covers the progress toward engineering a Na^+-specific DNAzyme into an intracellular probe for Na^+ detection. A former group member, Dr. Seyed-Fakhreddin Torabi, carried out selection of the Na^+-specific DNAzyme.[52] Therefore, I will mainly focus on the application of this DNAzyme as an intracellular sensor in this chapter.

3.2 Materials and Methods

3.2.1 Sequences

Table 3.1 Sequences of fluorescent sensors for *in vitro* activity test based on the Na^+-specific DNAzyme.

Name	Sequences (5′ to 3′)
NaA43S FAM/IABkFQ	6-FAM/CTCTATCTAT(rA)GGAAGTACCGCCGC/IABkFQ
NaA43E IABkFQ	GCGGCGGTACCAGGTCAAAGGTGGGTGAGGGGACGCCAA GAGTCCCCGCGGTTAGATAGAG/IABkFQ

IABkFQ represents Iowa Black FQ quencher; 6-FAM represents FAM fluorophore.

Table 3.2 Sequences for colocalization study.

Name	Sequences (5′ to 3′)
FAM-dANaS	/6-FAM/ACTCACTATAGGAAGAGATGGACGTG
NaE	ACGTCCATCTCCAGGTCAAAGGTGGGTGAGGGGACGCCAA GAGTCCCCGCGGTTAGTGAG
NaE-Cy3	A*C*GTCCATCTCCAGGTCAAAGGTGGGTGAGGGGACGCC AAGAGTCCCCGCGGTTAGTG*A*G/3Cy3ph/

* represents phosphorothioate modification; 3Cy3ph represents Cy3 modification.

Table 3.3 Sequences for intracellular imaging: positive group

Name	Sequences (5′ to 3′)
Active NaE-IBQ	A*C*GTCCATCTCCAGGTCAAAGGTGGGTGAGGGGACGCCAA GAGTCCCCGCGGTTAGTG*A*G/3IABkFQ/
FAM-caged NaS-BHQ	/6-FAM/ACTCACTAT/iNiBenz rA/GGAAGAGATGG ACGTG/BHQ_1/
FAM-non-cleavable NaS-BHQ	/6-FAM/ACTCACTATAGGAAGAGATGGACGTG/BHQ_1/
TAMRA-caged NaS-BHQ2	/6-TAMN/ACTCACTAT/iNiBenz rA/GGAAGAGATGG ACGTG/BHQ_2/
Inactive NaE-IBRQ	A*C*GTCCATCTCCAGGACAAAGGTGGGTGAGGGGACGCCAA GAGTCCCCGCGGTTAGTG*A*G/IAbRQSp/

iNiBenz represents photocaging group; 6-TAMN represents TAMRA fluorophore; IAbRQSp represents Iowa Black RQ quencher; BHQ_1 and BHQ_2 represent BHQ1 and BHQ2 quencher, respectively.

3.2.2 *In vitro* selection for a Na^+-specific DNAzyme

To select Na^+-specific DNAzyme, two parallel *in vitro* selections were performed with 135 mM (selection A) or 400 mM (selection B) total Na^+, respectively. The starting library was based on a 110-mer oligonucleotide with a random region containing 50 nucleotides (Figure 3.1). Fifteen rounds of selection were conducted for both pools, and the most active pools from selection A (round 13) and selection B (round 15) were chosen for cloning and sequencing. Overall, the selection B pool showed higher signal over background ratio and more cleavage than the selection A pool, while selection A pool showed higher rate of cleavage at lower Na^+ concentrations and better selectivity.[52] In total, there were 48 and 47 clones obtained from selection A and B pool, respectively. These sequences were further categorized into different

classes based on sequence similarities. Sequences from selection A were grouped into two major classes, and selection B resulted in three classes. After testing the activity of individual clones from different classes, one clone, which was from selection A and was the forty-third clone in the sequencing order, displayed the highest k_{obs} (0.11 ± 0.01 min^{-1}) in the presence of 400 mM at room temperature (Figure 3.4A). Therefore, it was named as NaA43 DNAzyme and was chosen for further studies. For more detailed description of the selection progress, please refer to Dr. Seyed-Fakhreddin Torabi's thesis.[52]

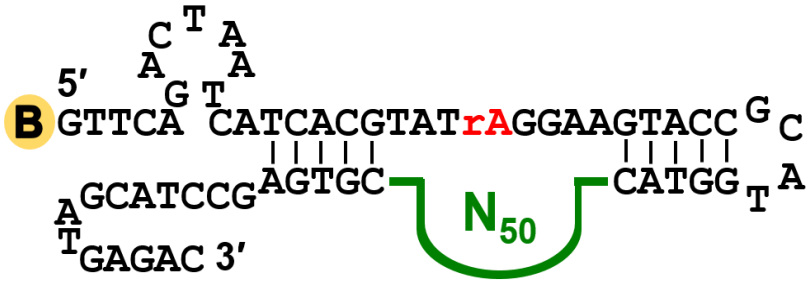

Figure 3.1 Design of randomized oligonucleotide pool for *in vitro* selection for Na^+-specific DNAzymes.

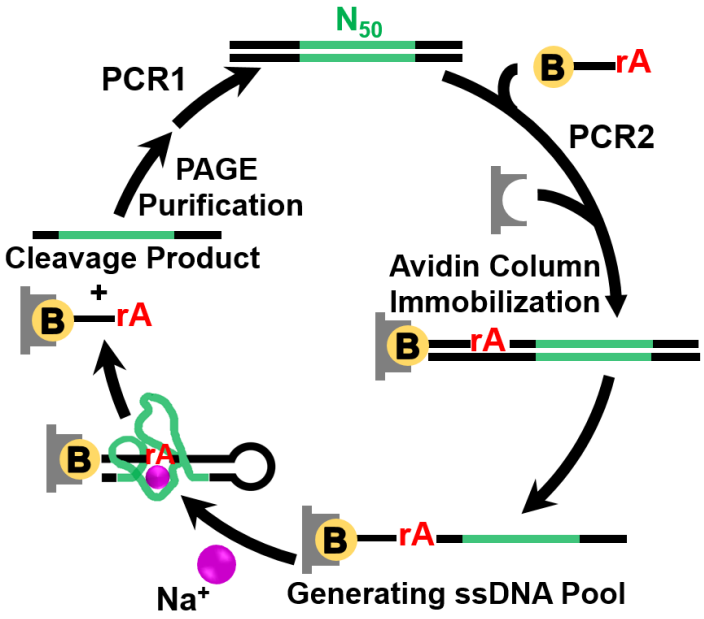

Figure 3.2 Scheme of column-based *in vitro* selection strategy.

3.2.3 Radioisotopic labeling of 5′ end of oligonucleotides

- **REAGENTS**

Oligonucleotides; supplies for PAGE (refer to Section 2.2.4); T4 Polynucleotide kinase (M0201S, New England BioLabs®, available from biology stock room); [ϒ-^{32}P] ATP (PerkinElmer®).

- **EQUIPMENT**

Phosphorimager (STORM 840 optical scanner, Amersham Biosciences); thermocycler (PCR machine, Bio-Rad); Centrifuge.

- **METHODS**

To label 100 pmol of oligonucleotides, mix the following components (Table 3.4) in a PCR tube and put in the thermocycler. Heat the reaction at 37 °C for 1.5 hours.

Table 3.4 ^{32}P-labeling of oligonucleotides.

50 μM oligonucleotide	2 μl
T4 kinase buffer (10 ×)	2.5 μl
[ϒ-^{32}P] ATP*	2 μl
H_2O	17.5 μl
T4 kinase	1 μl
Total	25 μl

* Note that the amount used here is based on the assumption that the [ϒ-^{32}P] ATP is fresh. Use half life of ^{32}P (14.3 days) to calculate the actual amount.

3.2.4 Activity assay

- **REAGENTS**

Buffer A: 50 mM Bis-Tris, 90 mM LiCl, pH 7.0; Stop solution (9 M urea, 1× TBE, 0.05 % bromophenol blue, 0.05 % xylene cyanol).

- **EQUIPMENT**

Phosphorimager (STORM 840 optical scanner, Amersham Biosciences); PAGE equipment.

- **METHODS**

Activity of selected pools and *cis*-cleaving form of the DNAzyme was tested in 50 mM Bis-Tris (pH 7.0) and the reaction was initiated by addition of Na^+ at desired concentration. Activities of trans-cleaving NaA43 DNAzyme was tested by using substrate labeled at 5′-end with [γ-^{32}P]-ATP.

The DNAzyme complex containing the NaA43E and ^{32}P-labeled NaA43S was denatured by heating the mixture at 90°C for 3 min and annealed in buffer A by gradual cooling to room temperature over 30 min. For all activity assay experiments, reaction samples were quenched by addition of 2 µl of reaction mixture to 30 µl of stop solution. We verified that using a large volume (15×) of stop solution with a high urea concentration would denature the DNAzyme and dilute Na^+ concentration significantly, and therefore quench the DNAzyme reaction effectively. The zero time point samples were mixed with the stop solution at the end of the activity assay to test the cleavage in the absence of Na^+. The cleaved and uncleaved DNA were separated by 10%

or 20% denaturing PAGE and gel images were taken by phosphorimager. Kinetic curves were plotted using OriginLab 9.1 and fit to the equation of $\%P_{cleavage.t} = \%P_{max}\ (1-e^{-kt})$, where $\%P_{cleavage.t}$ is the cleavage percentage at time point t, $\%P_{max}$ is the maximum cleavage percentage of substrate at the end of the reaction, and *k* is the rate of cleavage.

3.2.5 Fluorescent activity test of the intracellular sensor in buffer

- **REAGENTS**

Buffer K: 12.5 mM HEPES, 140 mM KCl, 10 mM Glucose, 1.2 mM $MgCl_2$, 1 mM $CaCl_2$, pH 7.4; Buffer Na: 12.5 mM HEPES, 140 mM NaCl, 10 mM Glucose, 1.2 mM $MgCl_2$, 1 mM $CaCl_2$, pH 7.4.

- **EQUIPMENT**

Hand-held UV lamp; Fluorometer (Jobin Yvon FluoroMax-P).

- **METHODS**

Active NaE-IBRQ and TAMRA-caged NaS-BHQ2 were mixed in Buffer K at a final concentration of 10 μM. The two strands were annealed by heating the solution to 75°C for 2 min followed by slowly cooling down to room temperature over 1h. To restore the activity of the caged substrate strand, the solution was added into one of the wells in a 12-well plate, and exposed to UV light at 365 nm for 30 min. Buffer solutions with different concentrations of Na^+ were prepared by mixing Buffer K with Buffer Na at different ratios. Buffer solutions were spiked with the sensor solution after the decaging process, and fluorescence change was monitored using a fluorometer (Jobin Yvon FluoroMax-P) at 541 nm excitation and 568 nm

emission over a time period of 20 min.

3.2.6 Cell culture, sensor delivery and co-localization study

- **REAGENTS**

PBS solution; Dulbecco's modification of Eagle's medium (DMEM); Opti-MEM (gibco®); Fetal Bovine Serum (FBS); penicillin; streptomycin; trypsin-EDTA (0.25%).

- **EQUIPMENT**

Hand-held UV lamp; Cell incubator (cell facility, Room 429 in RAL at UIUC); 24-well plates; glass-bottom dishes (MatTek).

- **METHODS**

HeLa cells were cultured in DMEM supplemented with 10% FBS, 100 U/mL penicillin, and 100 μg/mL streptomycin, on 25 cm^2 culture flasks at 37°C in a humidified 5% CO_2 incubator. Before imaging, cells were plated in 35 mm glass-bottom dishes (MatTek) and grown to 70-90% confluence.

For the delivery of DNAzyme sensors using cationic helical polypeptide G8, the corresponding NaA43E and NaA43S (final concentration of 0.1 mM) were mixed in the buffer containing 20 mM MOPS, 100 mM NaCl with pH at 7.1. To anneal the DNAzyme for better hybridization, the mixture was heated to 75°C for 2 min and slowly cooled down to room temperature for 30 min. G8 polypeptide (degree of polymerization = 50) was dissolved in water at 0.2 mg/ml and the pH of the solution was adjusted to 6 using diluted HCl for better solubility. 45 μl of polypeptide G8 was mixed and incubated with 2 μl of the aforementioned NaA43ES

construct for another 30 min to allow the formation of polymer-DNA complex (G8-NaA43ES). Normal cell culture medium was replaced with Opti-MEM before the G8-NaA43ES complex solution was added to the cells grown in the plates.

After incubating HeLa cells with G8-NaA43ES complex for 4 hours, cells were washed thoroughly with PBS to remove excess amount of G8-NaA43ES complex in the medium. Specific organelles inside cells were stained with commercial dyes, such as Hoechst 33258, CellLight® early endosomes-RFP, LysoTracker Red DND-99, MitoTracker Red CMXRos, and ER tracker Red. Images were obtained using a Zeiss LSM 710 NLO confocal microscope at 63x magnification equipped with a Mai-Tai Ti-Sapphire laser. Fluorescence emission of Hoechst 33258 was measured over 450-520 ranges, with excitation at 401 nm. Fluorescence of LysoTracker, MitoTracker and ER tracker was obtained by exciting at 561 nm and measuring over 575-620 nm, 585-630 nm, and 600-650 nm, respectively. The pinhole and gain settings were kept constant throughout the whole imaging process. Z-stack images were also obtained to confirm that the fluorescent signal was inside cells.

3.2.7 Imaging

HeLa cells were cultured in glass bottom dishes until about 80% confluence. After treatment with corresponding NaA43ES construct for 4 hours, cells were washed thoroughly with DPBS. Then cells were immersed in DPBS and irradiated with UV lamp at 365 nm for 30 minutes. Immediately after UV treatment, stock solutions of gramicidin D, monensin and ouabain were added to the cells at final concentrations of 3 μM, 10 μM and 100 μM, respectively. Fluorescent images were taken every 5 minutes immediately after addition of ionophores.

3.3 Results and discussion

3.3.1 Characterization of NaA43 DNAzyme

After testing the activity of individual clones from *in vitro* selection, one clone, which was from selection A and was the forty-third clone in the sequencing order, displayed the highest k_{obs} (0.11 ± 0.01 min^{-1}) in the presence of 400 mM Na^+ at room temperature (Figure 3.3A). Therefore, it was named as NaA43 DNAzyme and was chosen for further studies.

The obtained NaA43 DNAzyme from *in vitro* selection was 110 nt long and in the *cis*-cleaving form (catalytic core is in the same strand as the rA cleavage site). In order to convert it into an efficient fluorescent sensor, we first truncated out the flanking regions of the catalytic core (blue in Figure 3.3) to convert the DNAzyme from a *cis*-cleaving form into a *trans*-cleaving form. In this way, it is easier to introduce fluorophore and quencher modifications at the ends of both strands with improved synthesis yield, making sensor application more cost-effective.

After *cis* to *trans* transformation, the NaA43 DNAzyme was separated into an enzyme strand (NaA43E) and a substrate strand (NaA43S) (Figure 3.5). They hybridize to each other through the two binding arms flanking the catalytic core in the middle. To confirm that such transformation would not affect the activity of the DNAzyme, we tested the activity of both constructs using gel-based activity assay and compared the performance of the two. As shown in Figure 3.3B, *cis*- and *trans*-cleaving DNAzymes showed very similar reaction kinetics in response to the addition of 400 mM Na^+, suggesting that the transformation was successful and we obtained a *trans*-cleaving construct that was as active as the *cis*-cleaving form.

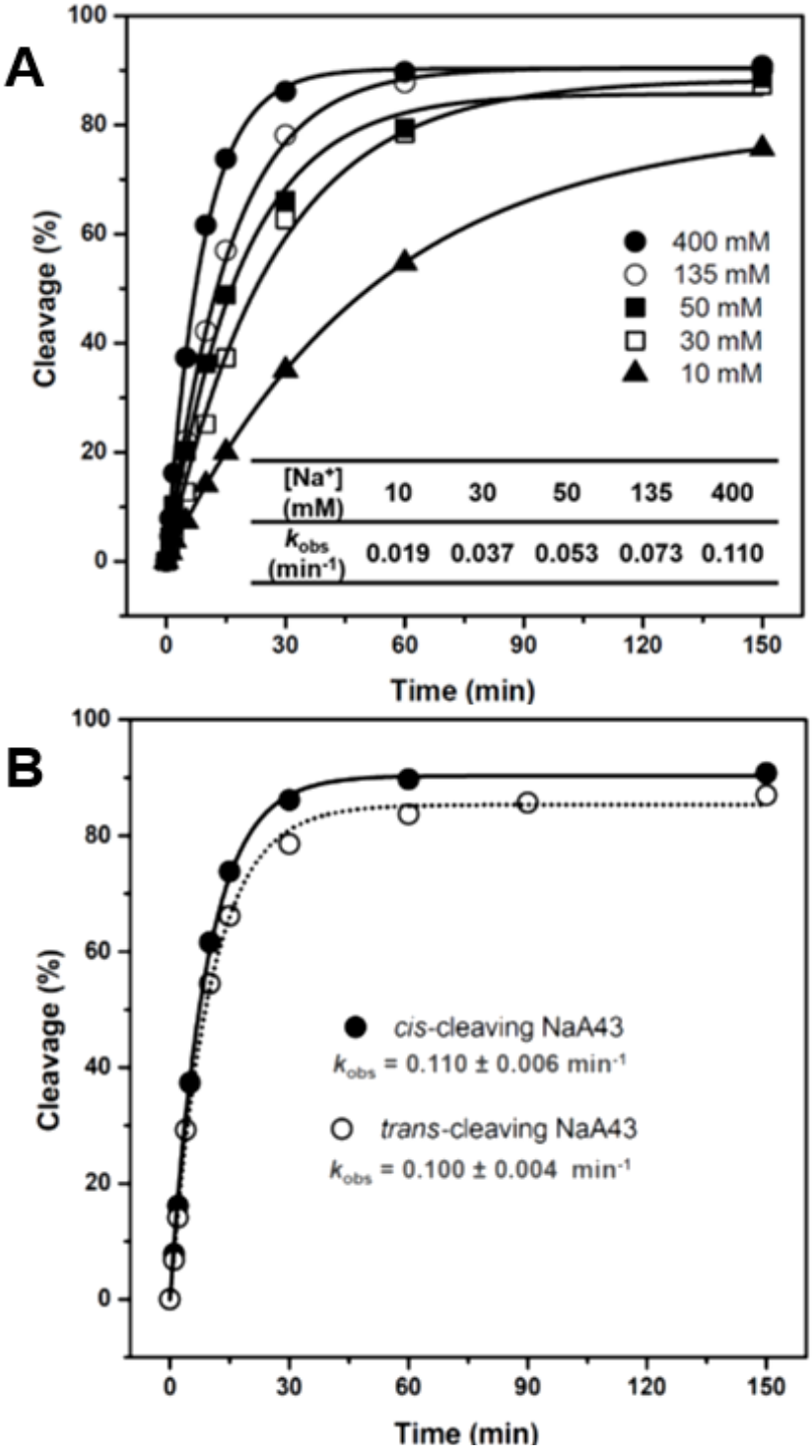

Figure 3.3 Activity of the *cis*-cleaving NaA43 DNAzyme and the comparison between *cis*- and *trans*-cleaving forms.

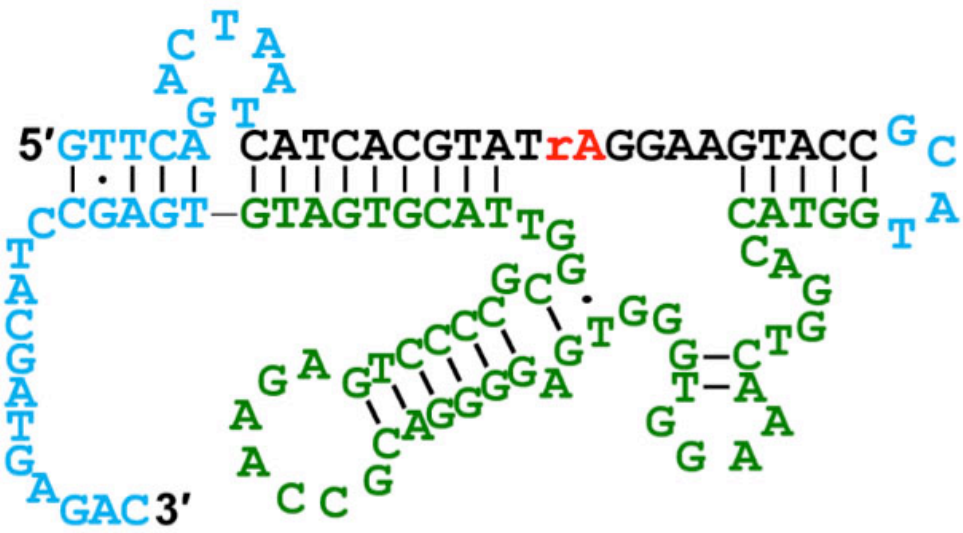

Figure 3.4 Converting NaA43 DNAzyme from a *cis*-cleaving to *trans*-cleaving form.

To see if we could further reduce the size of the DNAzyme by trimming out nucleotides that are not important for the activity, the structural and functional role of each nucleotide in NaA43 was characterized by mutagenesis studies. It was found that six nucleotides (G5, G6, A10, G12, G13, and G17, labeled with red circles in Figure 3.5) were absolutely required for the activity of NaA43. Any single site mutations at these six positions abolished the activity of NaA43 DNAzyme. In addition, another six nucleotides were identified to be critical to the activity, including T7, C8, A11, G16, T18 and G19 (labeled with black circles in Figure 3.5). Single point mutations at these positions resulted in at least 100-fold reduction in activity. The long stem loop in NaA43 (highlighted with blue square in Figure 3.5) was found to play a structural role in the catalytic activity of the DNAzyme, since substitution of the original base pairs with a different type of base pairs in the stem did not affect the activity significantly, as long as the number of base pairs was kept the same.

A more thorough characterization study was carried out by Dr. Seyed-Fakhreddin

Torabi.[52] As shown in Table 3.5, several single point mutations in the catalytic core could lead to complete loss of activity in NaA43 (*e.g.*, T7A). Based on this information, we picked T7A as our inactive construct serving as a negative control in the following studies.

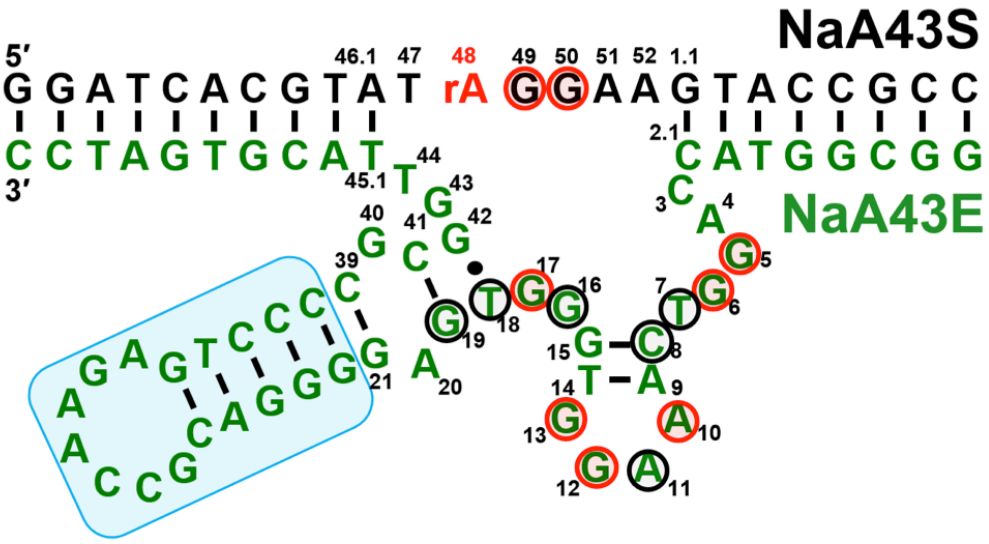

Figure 3.5 Structural and functional significance of specific nucleotides in the NaA43 DNAzyme.

Table 3.5 Mutations introduced into the catalytic core of NaA43 DNAzyme and their corresponding activities (Activity=log ($10^5 \times k_{obs}$).

3										13										23										33										43			Activity
A43E	C	A	G	G	T	C	A	A	A	G	G	T	G	G	G	T	G	A	G	G	G	G	A	C	G	C	C	A	A	G	A	G	T	C	C	C	C	G	C	G	G	T	**4.00**
C3A	A	-	-	-	-	-	-	-	-	-	-	-	-	-	-	-	-	-	-	-	-	-	-	-	-	-	-	-	-	-	-	-	-	-	-	-	-	-	-	-	-	**3.68**
A4G	-	G	-	-	-	-	-	-	-	-	-	-	-	-	-	-	-	-	-	-	-	-	-	-	-	-	-	-	-	-	-	-	-	-	-	-	-	-	-	-	-	**3.29**
A4T	-	T	-	-	-	-	-	-	-	-	-	-	-	-	-	-	-	-	-	-	-	-	-	-	-	-	-	-	-	-	-	-	-	-	-	-	-	-	-	-	-	**3.09**
G5A	-	-	A	-	-	-	-	-	-	-	-	-	-	-	-	-	-	-	-	-	-	-	-	-	-	-	-	-	-	-	-	-	-	-	-	-	-	-	-	-	-	**None**
G5C	-	-	C	-	-	-	-	-	-	-	-	-	-	-	-	-	-	-	-	-	-	-	-	-	-	-	-	-	-	-	-	-	-	-	-	-	-	-	-	-	-	**None**
G5T	-	-	T	-	-	-	-	-	-	-	-	-	-	-	-	-	-	-	-	-	-	-	-	-	-	-	-	-	-	-	-	-	-	-	-	-	-	-	-	-	-	**None**
G6A	-	-	-	A	-	-	-	-	-	-	-	-	-	-	-	-	-	-	-	-	-	-	-	-	-	-	-	-	-	-	-	-	-	-	-	-	-	-	-	-	-	**None**
G6C	-	-	-	C	-	-	-	-	-	-	-	-	-	-	-	-	-	-	-	-	-	-	-	-	-	-	-	-	-	-	-	-	-	-	-	-	-	-	-	-	-	**None**
G6T	-	-	-	T	-	-	-	-	-	-	-	-	-	-	-	-	-	-	-	-	-	-	-	-	-	-	-	-	-	-	-	-	-	-	-	-	-	-	-	-	-	**None**
T7A	-	-	-	-	A	-	-	-	-	-	-	-	-	-	-	-	-	-	-	-	-	-	-	-	-	-	-	-	-	-	-	-	-	-	-	-	-	-	-	-	-	**None**
T7C	-	-	-	-	C	-	-	-	-	-	-	-	-	-	-	-	-	-	-	-	-	-	-	-	-	-	-	-	-	-	-	-	-	-	-	-	-	-	-	-	-	**0.63**
T7G	-	-	-	-	G	-	-	-	-	-	-	-	-	-	-	-	-	-	-	-	-	-	-	-	-	-	-	-	-	-	-	-	-	-	-	-	-	-	-	-	-	**None**
C8A	-	-	-	-	-	A	-	-	-	-	-	-	-	-	-	-	-	-	-	-	-	-	-	-	-	-	-	-	-	-	-	-	-	-	-	-	-	-	-	-	-	**1.88**
C8G	-	-	-	-	-	G	-	-	-	-	-	-	-	-	-	-	-	-	-	-	-	-	-	-	-	-	-	-	-	-	-	-	-	-	-	-	-	-	-	-	-	**1.57**
C8T	-	-	-	-	-	T	-	-	-	-	-	-	-	-	-	-	-	-	-	-	-	-	-	-	-	-	-	-	-	-	-	-	-	-	-	-	-	-	-	-	-	**1.52**
A9C	-	-	-	-	-	-	C	-	-	-	-	-	-	-	-	-	-	-	-	-	-	-	-	-	-	-	-	-	-	-	-	-	-	-	-	-	-	-	-	-	-	**1.44**
A9G	-	-	-	-	-	-	G	-	-	-	-	-	-	-	-	-	-	-	-	-	-	-	-	-	-	-	-	-	-	-	-	-	-	-	-	-	-	-	-	-	-	**3.74**
A9T	-	-	-	-	-	-	T	-	-	-	-	-	-	-	-	-	-	-	-	-	-	-	-	-	-	-	-	-	-	-	-	-	-	-	-	-	-	-	-	-	-	**1.13**
A10C	-	-	-	-	-	-	-	C	-	-	-	-	-	-	-	-	-	-	-	-	-	-	-	-	-	-	-	-	-	-	-	-	-	-	-	-	-	-	-	-	-	**None**
A10G	-	-	-	-	-	-	-	G	-	-	-	-	-	-	-	-	-	-	-	-	-	-	-	-	-	-	-	-	-	-	-	-	-	-	-	-	-	-	-	-	-	**None**
A10T	-	-	-	-	-	-	-	T	-	-	-	-	-	-	-	-	-	-	-	-	-	-	-	-	-	-	-	-	-	-	-	-	-	-	-	-	-	-	-	-	-	**None**
A11C	-	-	-	-	-	-	-	-	C	-	-	-	-	-	-	-	-	-	-	-	-	-	-	-	-	-	-	-	-	-	-	-	-	-	-	-	-	-	-	-	-	**1.33**
A11G	-	-	-	-	-	-	-	-	G	-	-	-	-	-	-	-	-	-	-	-	-	-	-	-	-	-	-	-	-	-	-	-	-	-	-	-	-	-	-	-	-	**None**
A11T	-	-	-	-	-	-	-	-	T	-	-	-	-	-	-	-	-	-	-	-	-	-	-	-	-	-	-	-	-	-	-	-	-	-	-	-	-	-	-	-	-	**None**
G12A	-	-	-	-	-	-	-	-	-	A	-	-	-	-	-	-	-	-	-	-	-	-	-	-	-	-	-	-	-	-	-	-	-	-	-	-	-	-	-	-	-	**None**
G12C	-	-	-	-	-	-	-	-	-	C	-	-	-	-	-	-	-	-	-	-	-	-	-	-	-	-	-	-	-	-	-	-	-	-	-	-	-	-	-	-	-	**None**
G12T	-	-	-	-	-	-	-	-	-	T	-	-	-	-	-	-	-	-	-	-	-	-	-	-	-	-	-	-	-	-	-	-	-	-	-	-	-	-	-	-	-	**None**
G13A	-	-	-	-	-	-	-	-	-	-	A	-	-	-	-	-	-	-	-	-	-	-	-	-	-	-	-	-	-	-	-	-	-	-	-	-	-	-	-	-	-	**None**
G13C	-	-	-	-	-	-	-	-	-	-	C	-	-	-	-	-	-	-	-	-	-	-	-	-	-	-	-	-	-	-	-	-	-	-	-	-	-	-	-	-	-	**None**
G13T	-	-	-	-	-	-	-	-	-	-	T	-	-	-	-	-	-	-	-	-	-	-	-	-	-	-	-	-	-	-	-	-	-	-	-	-	-	-	-	-	-	**None**
T14G	-	-	-	-	-	-	-	-	-	-	-	G	-	-	-	-	-	-	-	-	-	-	-	-	-	-	-	-	-	-	-	-	-	-	-	-	-	-	-	-	-	**3.27**
G15T	-	-	-	-	-	-	-	-	-	-	-	-	T	-	-	-	-	-	-	-	-	-	-	-	-	-	-	-	-	-	-	-	-	-	-	-	-	-	-	-	-	**3.56**
G16A	-	-	-	-	-	-	-	-	-	-	-	-	-	A	-	-	-	-	-	-	-	-	-	-	-	-	-	-	-	-	-	-	-	-	-	-	-	-	-	-	-	**None**
G16C	-	-	-	-	-	-	-	-	-	-	-	-	-	C	-	-	-	-	-	-	-	-	-	-	-	-	-	-	-	-	-	-	-	-	-	-	-	-	-	-	-	**0.79**
G16T	-	-	-	-	-	-	-	-	-	-	-	-	-	T	-	-	-	-	-	-	-	-	-	-	-	-	-	-	-	-	-	-	-	-	-	-	-	-	-	-	-	**1.55**
G17A	-	-	-	-	-	-	-	-	-	-	-	-	-	-	A	-	-	-	-	-	-	-	-	-	-	-	-	-	-	-	-	-	-	-	-	-	-	-	-	-	-	**None**
G17C	-	-	-	-	-	-	-	-	-	-	-	-	-	-	C	-	-	-	-	-	-	-	-	-	-	-	-	-	-	-	-	-	-	-	-	-	-	-	-	-	-	**None**
G17T	-	-	-	-	-	-	-	-	-	-	-	-	-	-	T	-	-	-	-	-	-	-	-	-	-	-	-	-	-	-	-	-	-	-	-	-	-	-	-	-	-	**None**
T18A	-	-	-	-	-	-	-	-	-	-	-	-	-	-	-	A	-	-	-	-	-	-	-	-	-	-	-	-	-	-	-	-	-	-	-	-	-	-	-	-	-	**1.06**
T18C	-	-	-	-	-	-	-	-	-	-	-	-	-	-	-	C	-	-	-	-	-	-	-	-	-	-	-	-	-	-	-	-	-	-	-	-	-	-	-	-	-	**1.00**
T18G	-	-	-	-	-	-	-	-	-	-	-	-	-	-	-	G	-	-	-	-	-	-	-	-	-	-	-	-	-	-	-	-	-	-	-	-	-	-	-	-	-	**1.06**
G19A	-	-	-	-	-	-	-	-	-	-	-	-	-	-	-	-	A	-	-	-	-	-	-	-	-	-	-	-	-	-	-	-	-	-	-	-	-	-	-	-	-	**1.34**
G19C	-	-	-	-	-	-	-	-	-	-	-	-	-	-	-	-	C	-	-	-	-	-	-	-	-	-	-	-	-	-	-	-	-	-	-	-	-	-	-	-	-	**2.10**
G19T	-	-	-	-	-	-	-	-	-	-	-	-	-	-	-	-	T	-	-	-	-	-	-	-	-	-	-	-	-	-	-	-	-	-	-	-	-	-	-	-	-	**2.17**
A20T	-	-	-	-	-	-	-	-	-	-	-	-	-	-	-	-	-	T	-	-	-	-	-	-	-	-	-	-	-	-	-	-	-	-	-	-	-	-	-	-	-	**3.06**
G40C	-	-	-	-	-	-	-	-	-	-	-	-	-	-	-	-	-	-	-	-	-	-	-	-	-	-	-	-	-	-	-	-	-	-	-	-	-	-	-	-	-	**2.61**
C41T	-	-	-	-	-	-	-	-	-	-	-	-	-	-	-	-	-	-	-	-	-	-	-	-	-	-	-	-	-	-	-	-	-	-	-	-	-	-	-	-	-	**3.31**
G42A	-	-	-	-	-	-	-	-	-	-	-	-	-	-	-	-	-	-	-	-	-	-	-	-	-	-	-	-	-	-	-	-	-	-	-	-	-	-	-	-	-	**2.99**
G42T	-	-	-	-	-	-	-	-	-	-	-	-	-	-	-	-	-	-	-	-	-	-	-	-	-	-	-	-	-	-	-	-	-	-	-	-	-	-	-	-	-	**3.05**
G43A	-	-	-	-	-	-	-	-	-	-	-	-	-	-	-	-	-	-	-	-	-	-	-	-	-	-	-	-	-	-	-	-	-	-	-	-	-	-	-	-	-	**2.55**
G43T	-	-	-	-	-	-	-	-	-	-	-	-	-	-	-	-	-	-	-	-	-	-	-	-	-	-	-	-	-	-	-	-	-	-	-	-	-	-	-	-	-	**2.28**
T44A	-	-	-	-	-	-	-	-	-	-	-	-	-	-	-	-	-	-	-	-	-	-	-	-	-	-	-	-	-	-	-	-	-	-	-	-	-	-	-	-	-	**3.33**
T44C	-	-	-	-	-	-	-	-	-	-	-	-	-	-	-	-	-	-	-	-	-	-	-	-	-	-	-	-	-	-	-	-	-	-	-	-	-	-	-	-	-	**2.51**

3.3.2 Activity check under strict RNase-free conditions

Since it was rare to see that DNA could evolve to adopt monovalent metal ion specificity, one concern was that the observed activity was due to RNase contamination in the Na salt, although several results from selection experiment suggested that this was very unlikely, such as no cleavage was observed for several variants of NaA43 even in the presence of Na^+. To completely eliminate the concern about RNase contamination, I tested the NaA43 DNAzyme under strict RNase-free conditions.

I first baked NaCl salt (purchased from Alfa Asar, 99.999% purity) at 260 °C for 36 hours, and used ultrapure DEPC-treated water to make a fresh NaCl stock solution with a final concentration of 3 M. All the bench surface and pipettes were wiped with RNase AWAY® decontamination reagent. All the buffers used in the activity assays were freshly prepared with DEPC-treated water. NaA43 DNAzyme was annealed following the protocol in Section 3.2.4, and the solution was spiked with final concentration of 400 mM NaCl to start the reaction. Both baked and unbaked NaCl were tested, and I observed very similar activities under these two conditions, indicating that RNase is not the cause of cleavage (Figure 3.6).

In addition to using baked NaCl, I also tried to destroy any potential RNases in salt solutions using protease. To accomplish this goal, I treated the stock solution of NaCl with Protease K at 37 °C for 24 hours before use. Proteinase K is known to inactivate most DNases and RNases rapidly. As shown in Figure 3.6, the cleavage activity of the NaA43 DNAzyme remained the same as that in the presence of untreated NaCl. This result further confirms that nucleases did not contribute to the cleavage activity.

At the same time, I did two negative controls. One is the substrate (NaA43S) dissolved in DEPC-treated water and left on bench for 2 hours (Figure 3.7, lane 6 and Figure 3.9, bar 1), and the other is NaA43ES left in annealing buffer containing 50 mM Bis-Tris, 112 mM LiCl, pH 7.0 in DEPC-treated water for 2 hours (Figure 3.7, lane 5 and Figure 3.9, bar 5). No obvious degradation was observed for both negative controls (less than 1%), indicating that the substrate is quite stable during the time period of activity assays. In addition, I spiked NaA43S solution with unbaked NaCl at a final concentration of 400 mM, and only 0.8% cleavage was observed after 2 hours (Figure 3.7, lane 4 and Figure 3.9, bar 2), suggesting the fast cleavage we observed in activity assays was resulted from the activity of Na^+-specific DNAzyme, not from RNase contamination in NaCl.

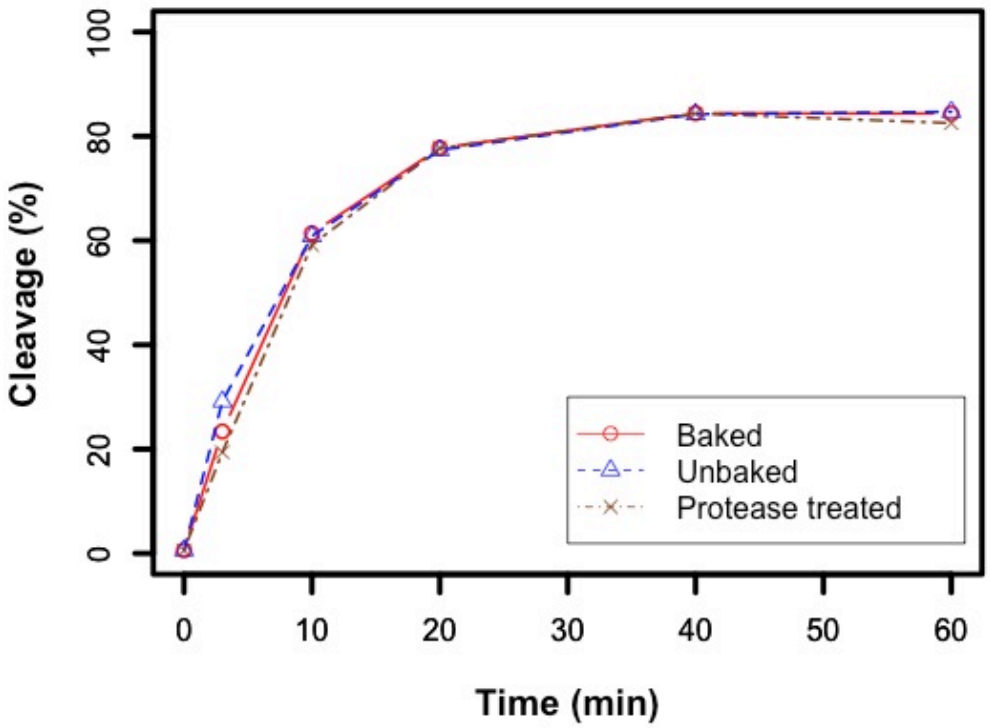

Figure 3.6 Activity of NaA43 DNAzyme in the presence of 400 mM of NaCl from different Na salt sources.

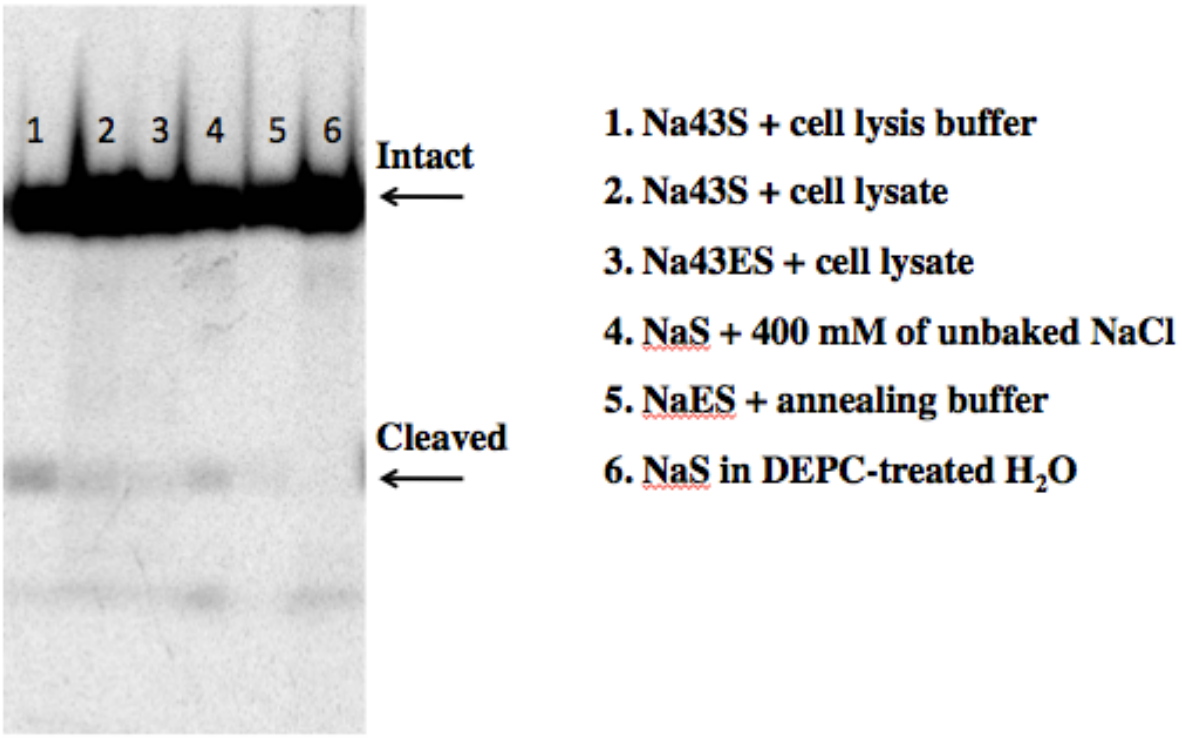

Figure 3.7 Gel image of activity and stability test of NaA43 DNAzyme (with ^{32}P-labeled substrate strand) under different conditions for 2 hours.

3.3.3 Stability of NaA43 DNAzyme in the presence of RNases and cell lysate

Since the ultimate goal of this project was to use NaA43 DNAzyme as an intracellular sensor for Na+, I evaluated the stability of the DNAzyme in the presence of different types of RNases as well as in Na^+-free cell lysate, over the period of 1 hour. RNase A and RNase H, which are two of the most common RNases found in organisms and environment, were used for the initial tests.

Specifically, five units of RNase A or one unit of RNase H were incubated with 100 fmol of NaA43 DNAzyme, which was in the complex form with ^{32}P-labeled substrate strand, at 37 °C

for 1 hour (1 unit of RNase A is defined as the amount of enzyme that causes an increase in absorbance at 260 nm of 1.0 when yeast RNA is hydrolyzed at 37 °C and pH 5.0; 1 unit of RNase H is defined as the concentration at which 1 nmol of RNA in the form of poly(rA)• poly(dT) could be digested into acid-soluble ribonucleotides in 20 minutes at 37 °C). As shown in Figure 3.8, our DNAzyme showed minimal degradation in the presence of these RNases (Figure 3.8 and Figure 3.9, bar 7 and 8). Furthermore, I prepared Na^+-free cell lysate from HeLa cells and tested the stability of the NaA43 DNAzyme in the presence of cell lysate. As shown in Figure 3.7 (lane 2 and 3), the substrate strand was very stable over the course of 2 hours in cell lysate. In contrast, when we spiked the above lysate with 400 mM NaCl, the substrate was cleaved rapidly within 40 min (bar 9 in Figure 3.9).

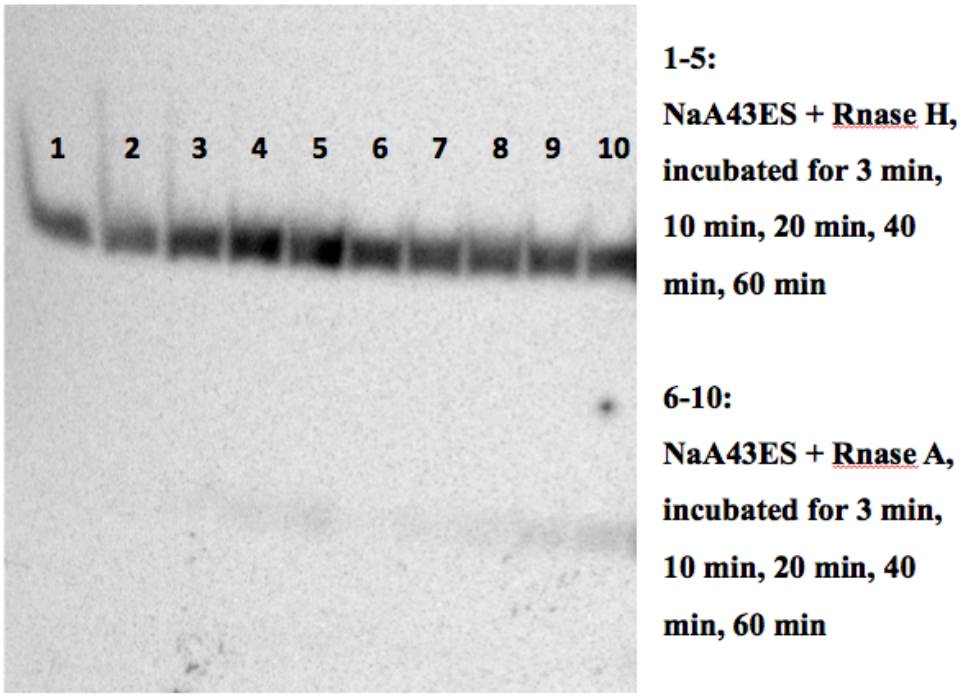

Figure 3.8 Stability of NaA43 DNAzyme in the presence of RNase H and RNase A.

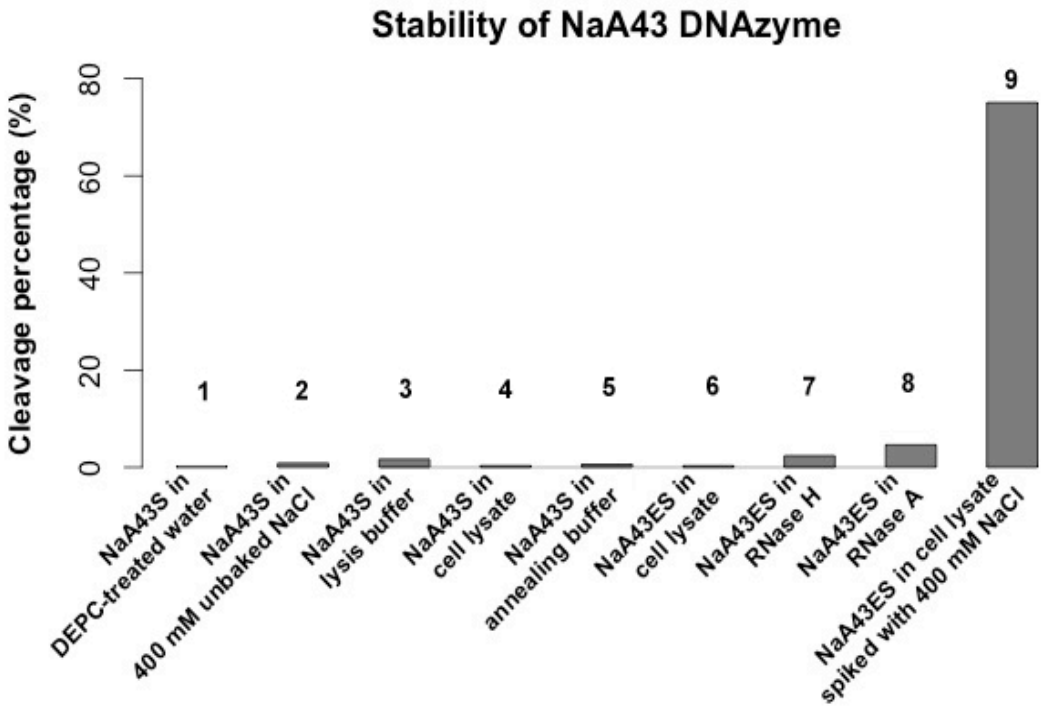

Figure 3.9 Bar graph of stability of NaA43 DNAzyme under different conditions.

3.3.4 Converting the DNAzyme into a Fluorescent Sensor for Na^+

Having confirmed that the NaA43 DNAzyme is resistant to RNase degradation and has good sensitivity for Na^+, we converted the *trans*-cleaving construct into a fluorescent sensor by incorporating a fluorophore and two quenchers at the ends of the two strands (Figure 3.10). More specifically, we designed a catalytic beacon by labeling the NaA43S with a TAMRA fluorophore at its 5′ end and the NaA43E with BHQ-2 quencher at its 3′ end (Figure 3.10).[43,53] In addition, a second quencher was added at the 3′ end of the NaA43S to minimize background fluorescence (Figure 3.10). To ensure stable duplex formation at room temperature, the 3′ arm of NaA43S was designed to have a high (~ 80%) GC-content. To ensure the release of the product fragment

containing the fluorophore after cleavage, the 5′ end of NaA43S was designed with a much lower (33%) GC-content (Figure 3.10). In the presence of sufficient Li^+, the NaA43S-NaA43E complex was formed because it has a melting temperature higher than room temperature (>44 °C). As a result, the fluorescence signal was quenched due to the close proximity of the fluorophore and quencher. Upon addition of Na^+, NaA43S was cleaved at the rA in the middle. Since the melting temperature of the fluorophore-containing arm after cleavage is below room temperature (~10 °C), dehybridization causes the fluorophore to release from its quenchers, resulting in fluorescence increase (Figure 3.11). Due to the technical difficulty in synthesizing BHQ-2 modified oligonucleotides with length more than 60 nt, we cut one deoxynucleotide at the 3′ end of the enzyme strand. The cleavage site is labeled with red circle in Figure 3.10, and "PG" stands for "photocaging group" (see Section 3.3.6). The sensor showed fast response to Na^+ and strong turn-on fluorescence at physiological concentrations of Na^+ (Figure 3.12).

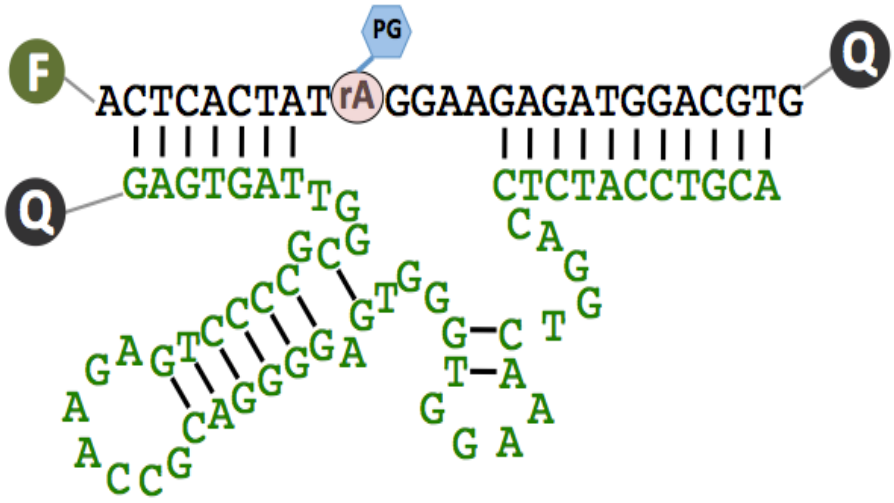

Figure 3.10 Scheme of a fluorescent sensor for Na^+ based on the NaA43 DNAzyme.

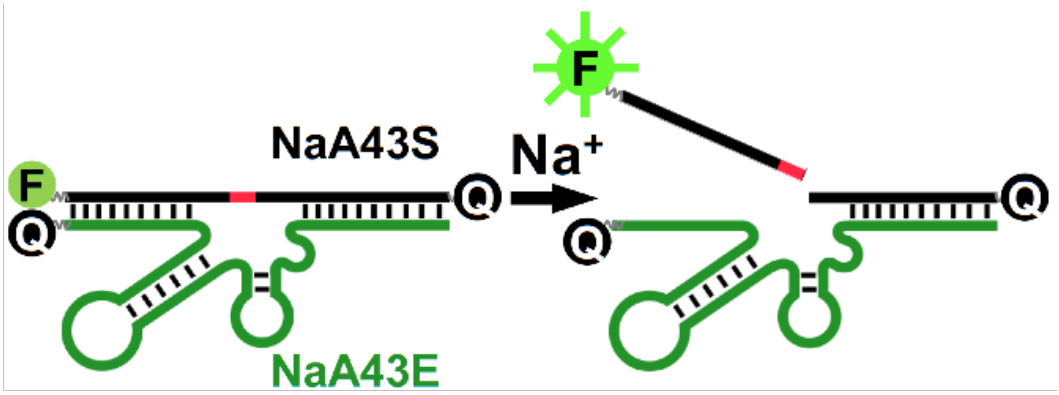

Figure 3.11 Scheme of the turn-on response of the NaA43 fluorescent sensor in the presence of Na^+.

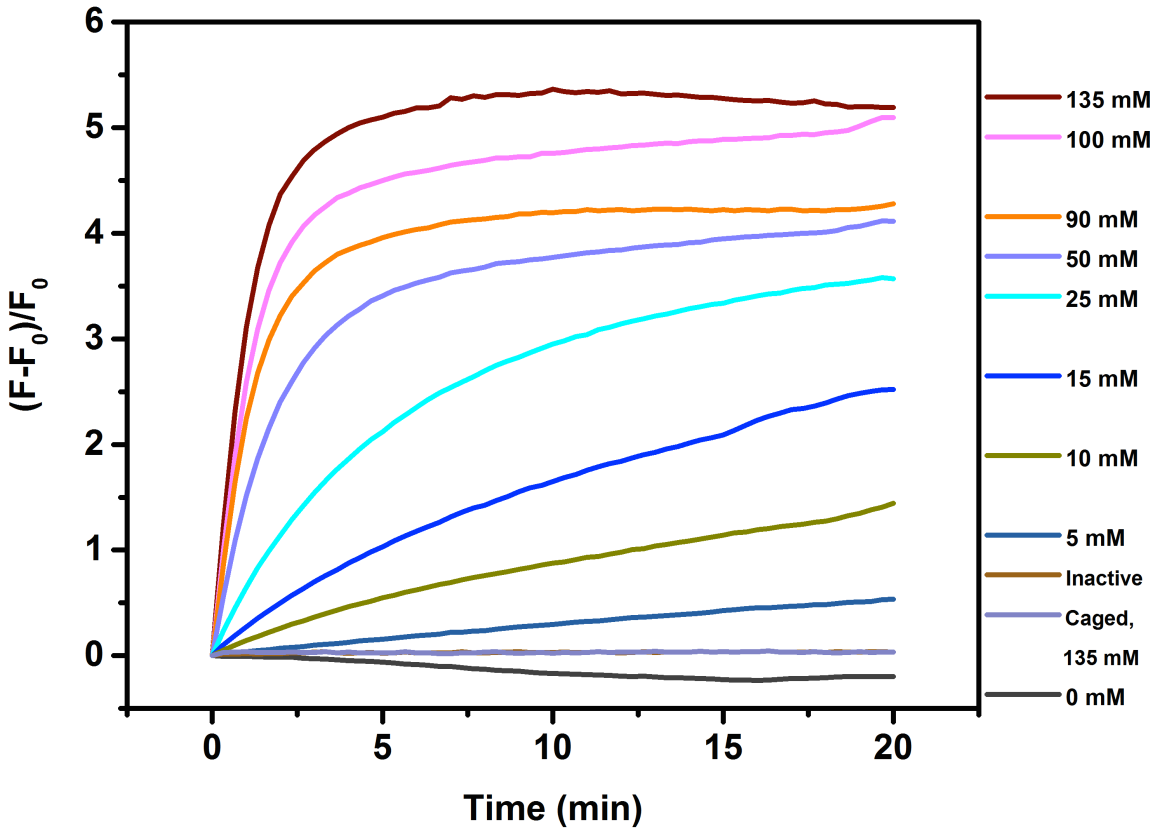

Figure 3.12 Turn-on fluorescence of NaA43 sensor in buffer solution with different concentrations of Na^+.

Another set of fluorescent activity test was performed by Dr. Seyed-Fakhreddin Torabi, using a slightly different construct (different sequences in the binding arms). As shown in Figure 3.13, the observed rate of fluorescence increase was accelerated with additional Na^+, until saturation at ~135 mM of Na^+, with an apparent dissociation constant (K_d) of 39.1±2.3 mM (Figure 3.15).[52,54] The limit of detection was determined to be 135 μM or 3.1 parts per million (3σ/slope), with dynamic range up to 50 mM (Figure 3.14 inset). This range covers the likely cellular concentrations of Na^+ very well.

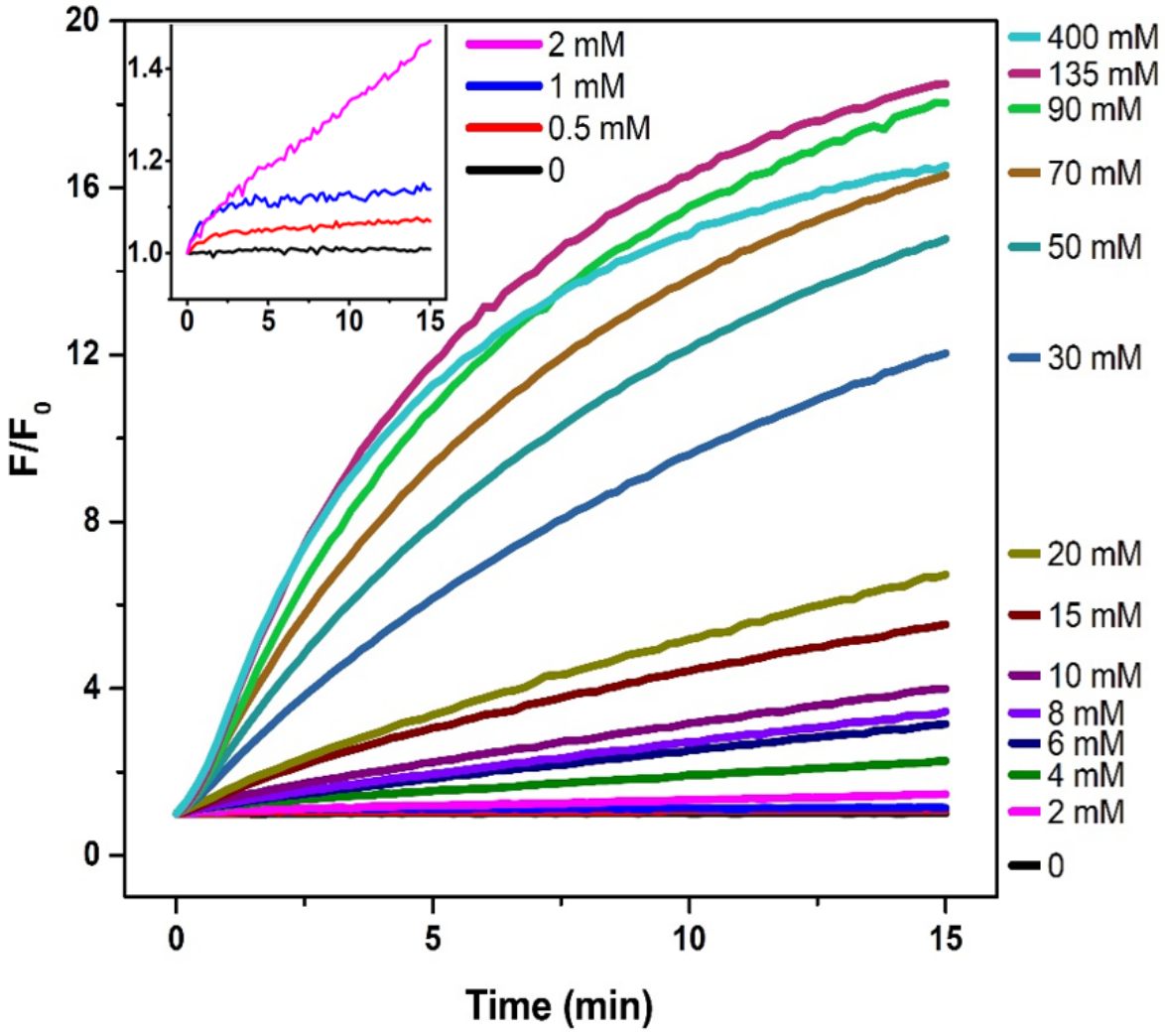

Figure 3.13 Time-dependent fluorescence increase of NaA43 sensor at various concentrations of Na^+ (mM).

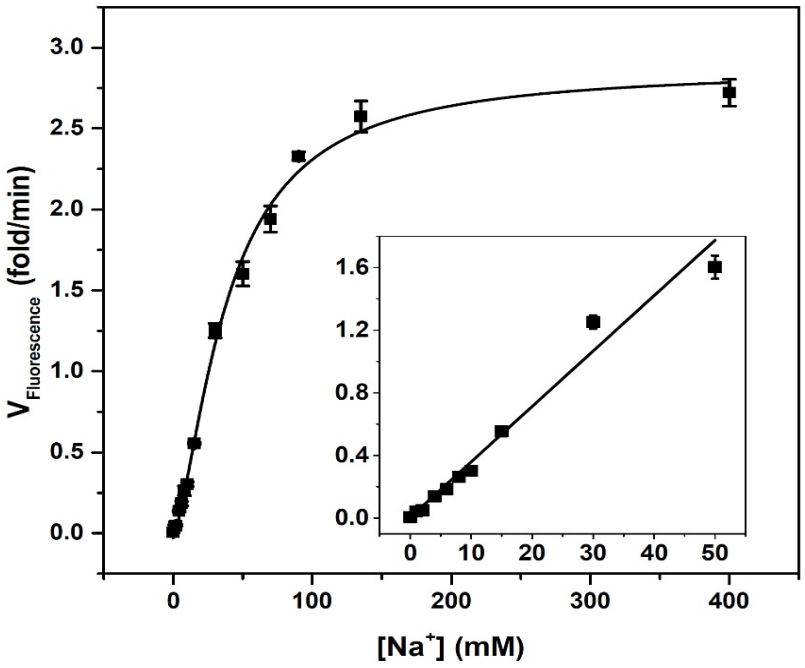

Figure 3.14 Rate of fluorescence increase under different concentrations of Na^+ (mM), and the dynamic range of the sensor.

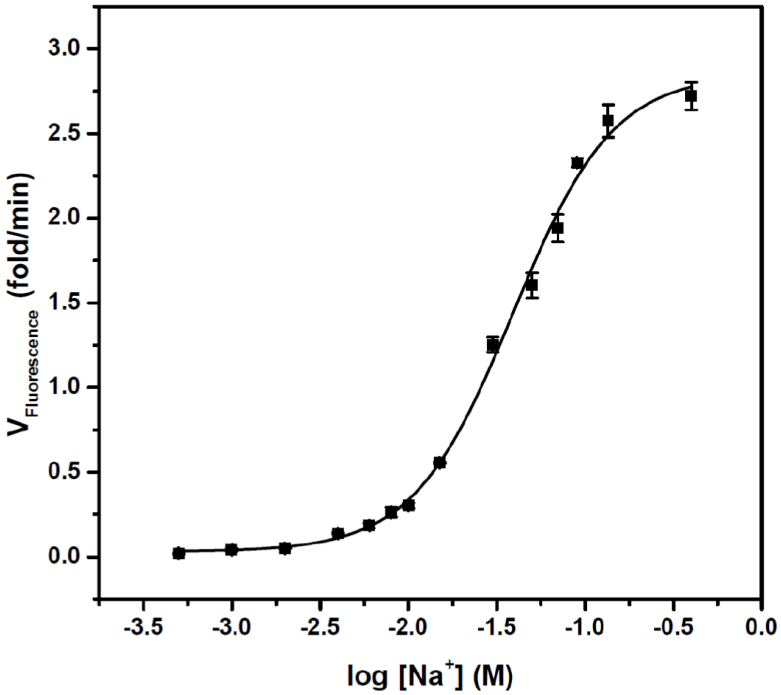

Figure 3.15 Rate of initial fluorescence increase vs. log([Na^+]) (M), for determining the apparent K_d (39.1 ± 2.3 mM).

3.3.5 Selectivity of NaA43 fluorescent sensor

To determine the selectivity of the sensor for Na^+ over other metal ions, we monitored sensor response to 22 different metal ions (Figure 3.16). Sensor complex was formed in 90 mM LiCl and the rate of fluorescence enhancement was measured in presence of 100 mM, 2 mM and 0.2 mM of mono-, di- and trivalent metal ions, respectively. For Cu^{2+} and Hg^{2+}, since they are known to quench fluorophores, activity of the fluorescent sensor was tested using gel-based assay with ^{32}P-radiolabeled substrate in the presence of Na^+. None of the tested metal ions showed a significant change in fluorescence signal, suggesting that the NaA43 DNAzyme based sensor has excellent selectivity for Na^+, with at least 10,000-fold better activity versus the next best competing metal ion (Li^+). The sensor remained selective in the presence of a mixture of 100 mM Na^+ and other mono- or divalent metal ions in their physiologically relevant concentrations.

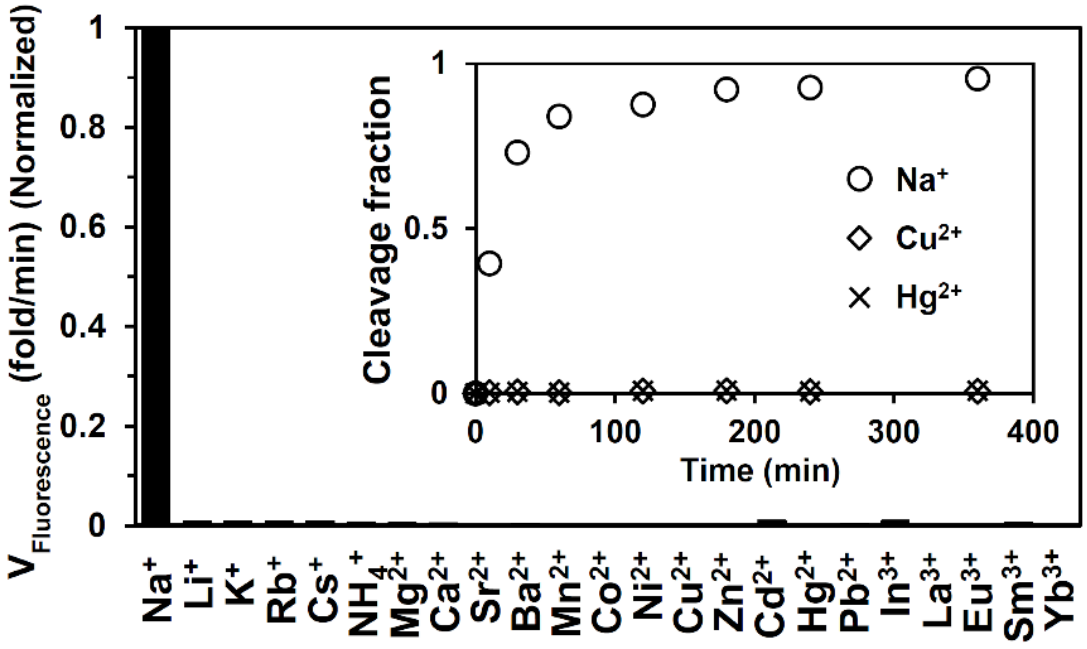

Figure 3.16 Selectivity of the NaA43 fluorescent sensor.

3.3.6 Photocaging strategy

Having demonstrated detection of Na^+ in buffer, we then explored application of the Na^+-specific DNAzyme for imaging Na^+ in living cells. To prevent cleavage of NaA43S during the delivery of the DNAzyme into cells so that the activation of the sensor for Na^+ detection can be controlled with temporal resolution, we employed a photocaging strategy, in which the 2′-hydroxyl (2′-OH) group at the rA cleavage site in the substrate strand (NaA43S) was modified with a photolabile *o*-nitrobenzyl group (Figure 3.17).[55] The caging of the 2′-OH group prevents the cleavage of NaA43S by blocking the activity of 2′-OH as a nucleophile in a transesterification reaction.[56] The caging group can be readily removed upon brief irradiation at 365 nm, which switches the substrate from being non-cleavable to cleavable.

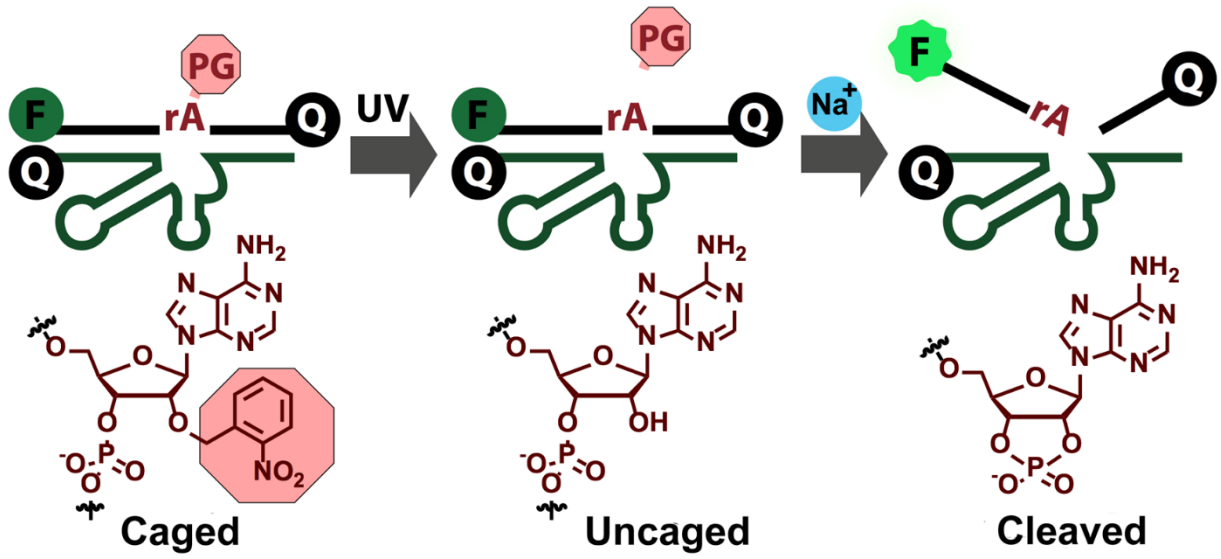

Figure 3.17 Scheme of the decaging process for the photolabile Na^+-specific DNAzyme.

To convert the caged DNAzyme into a fluorescent sensor, fluorophore and quenchers were attached to the DNAzyme in the way as shown in Figure 3.17. The caged DNAzyme showed no activity even in the presence of a high concentration of Na^+ (300 mM) (Figure 3.12). After 365 nm irradiation for 30 minutes, ~ 80% of the DNAzymes were decaged, estimated based on HPLC carried out in previous studies.[57] Two saline solutions, commonly used for *in vivo* calibration of Na^+ probes were made for testing the performance of the decaged DNAzyme.[58] One solution contains 12.5 mM HEPES (pH 7.4), 140 mM NaCl, 10 mM glucose, 1.2 mM $MgCl_2$, and 1 mM $CaCl_2$. The other buffer has the same components except that 140 mM NaCl was replaced by 140 mM KCl. A mixture of these two solutions was used to generate buffers with a range of different concentrations of Na^+. Increased fluorescent signal with increasing concentrations of Na^+ was observed, indicating that the activity of the DNAzyme can be restored after reactivation by 365 nm irradiation (Figure 3.12).

3.3.7 Delivery of the NaA43 sensor into cells

To use the photocaged Na^+-specific DNAzyme to image Na^+ in cells, a delivery method that can transport DNA into the cytoplasm of cells without accumulation in specific sub-cellular organelles is required. I tried different delivery vehicles, including a cell-penetrating peptide (CPP) (EB1) and two types of α-helical cationic polypeptides (PVBLG-8 and G8). The initial tests were conducted using 8-17 DNAzyme, in which the substrate strand was labeled with a FAM fluorophore. Further optimization was performed using the NaA43 DNAzyme with a fluorophore labeled all-DNA substrate.

3.3.7.1 Cell-penetrating peptide EB1

The history of cell-penetrating peptides dates back to 1988, when the HIV TAT transactivating factor was discovered.[59,60] A few years later, it was found that the *Drosophila* Antennapedia transcription factor proteins were able to translocate cell membrane and enter cells.[61] These discoveries lead to the further discoveries that short sequences of these proteins have cell-penetrating properties. A 16-mer peptide derived from Antennapedia was named penetratin and an 11-mer peptide derived from TAT protein was referred as TAT since then (Table 3.6). These two CPPs have been widely used in the delivery of various cargos, including nucleic acids, liposomes, nanoparticles, and polymers.[62] CPPs can be attached to their cargos through covalent bonds, which is usually used for neutral cargo, such as peptide nucleic acids (PNAs) and small drug molecules. CPPs can also form complexes with their cargos by noncovalent bond formed via electrostatic or hydrophobic interactions between negatively charged cargo and positively charged CPPs. CPPs are known to be able to escape endocytosis once they enter the cells. Different theories have been developed to explain such phenomenon, such as proton sponge theory, as well as hydrophobic and electrostatic interactions between the endosomal membrane and the CPP complexes.

EB1, an analogue of penetratin, has been found to have better delivery efficiency in transporting siRNA and promote endosomelysis than penetratin (Table 3.6).[63] It was hypothesized that EB1 was able to be protonated in the early-to-late endosomes and form an amphipathic alpha helix, resulting in disruption of the endosomal membrane.[63]

Table 3.6 Sequences of cell-penetrating peptides.

Name	Sequence	Refs
TAT	GRKKRRQRRRPPQ	[59]
penetratin	RQIKIWFQNRRMKWKK	[60]
EB1	LIRLWSHLIHIWFQNRRLKWKKK-amide	[63]

EB1 peptide was kindly provided by Kevin Hwang, who did the synthesis using the peptide synthesizer in the lab. I first dissolved EB1 in Millipore water at a final concentration of 1 mM. FAM fluorophore labeled substrate strand of 8-17 DNAzyme (FAM-17S-iT) was annealed with its enzyme strand (17E-iT) at final concentration of 0.4 mM. Both of the two sequences had an inverted T modification introduced at the end in order to increase the half-life time of the construct inside cells (Table 3.7). 8-17ES DNAzyme complex was formed by denaturing the DNA at 70 °C for 2 minutes followed by cooling down to room temperature over half an hour. EB1 peptide and 8-17ES were mixed at molar ratio of 10:1, 25:1, 50:1 or 100:1. The mixture was incubated at room temperature for half an hour to form CPP-DNA complexes. The resulting complexes were incubated with HeLa cells in Opti-MEM for 2 hours. The total amount of 8-17ES per imaging plate was kept 0.2 nmol.

Table 3.7 Sequences of 8-17 DNAzyme used in delivery studies.

Name	Sequence	MW
FAM-17S-iT	5’-FAM- ACT CAC TAT rAGG AAG AGA TGG ACG TG -3’InvdT	~8,200
17E-3-iT	5’-CAC GTC CAT CTC TTC TCC GAG CCG GTC GAA ATA GTG AG-3’InvdT	11,918

However, aggregations were observed immediately after mixing EB1 with the DNAzyme, especially at the ratio of 50:1 and 100:1. As shown in Figure 3.18 and Figure 3.19, most of the FAM fluorescence was observed from aggregated complexes absorbed on the surface of the imaging plate, and no obvious uptake inside cells was observed. The observation of aggregation was very consistent for several different trials, even at low molar ratios. Due to this issue, I did not continue pursuing this approach.

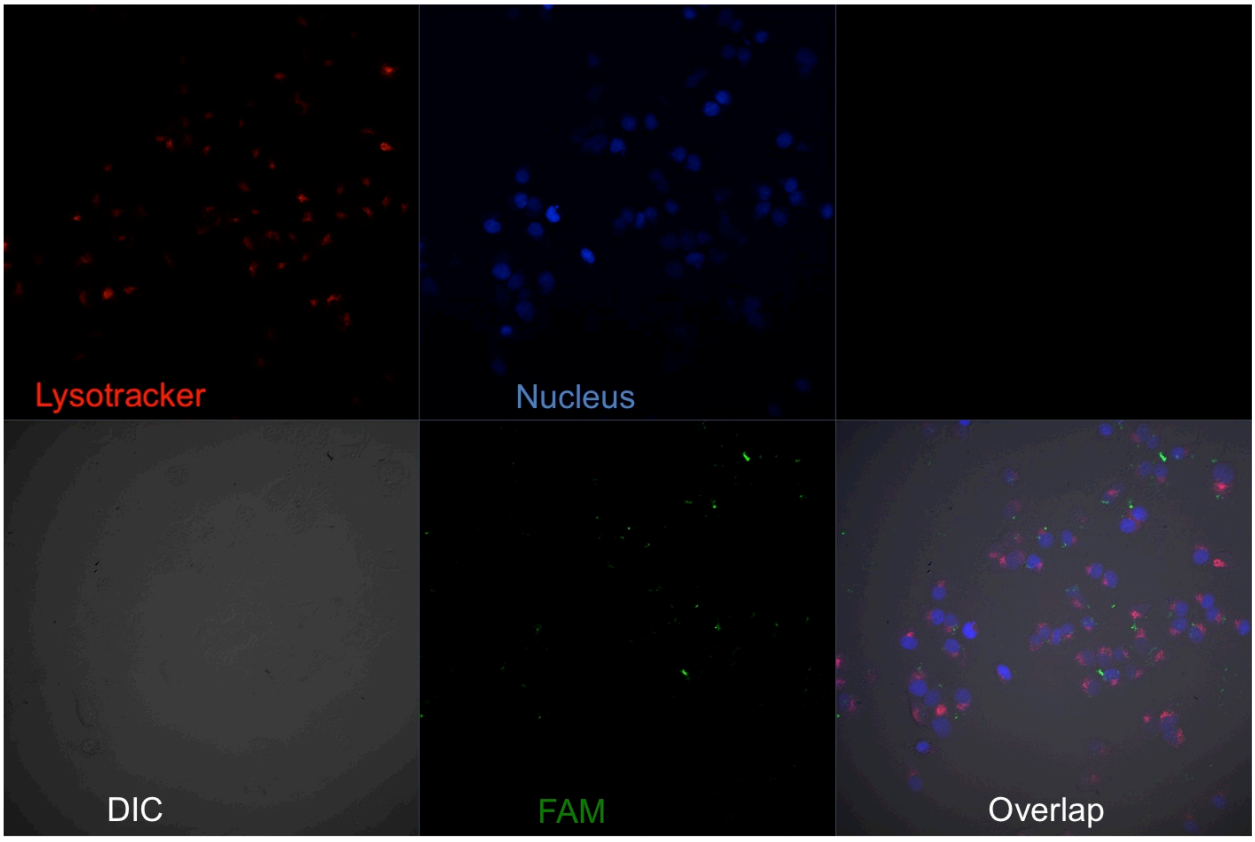

Figure 3.18 Confocal images of 8-17 DNAzyme delivered by cell-penetrating peptide EB1 (Molar ratio of EB1: DNAzyme = 10:1).

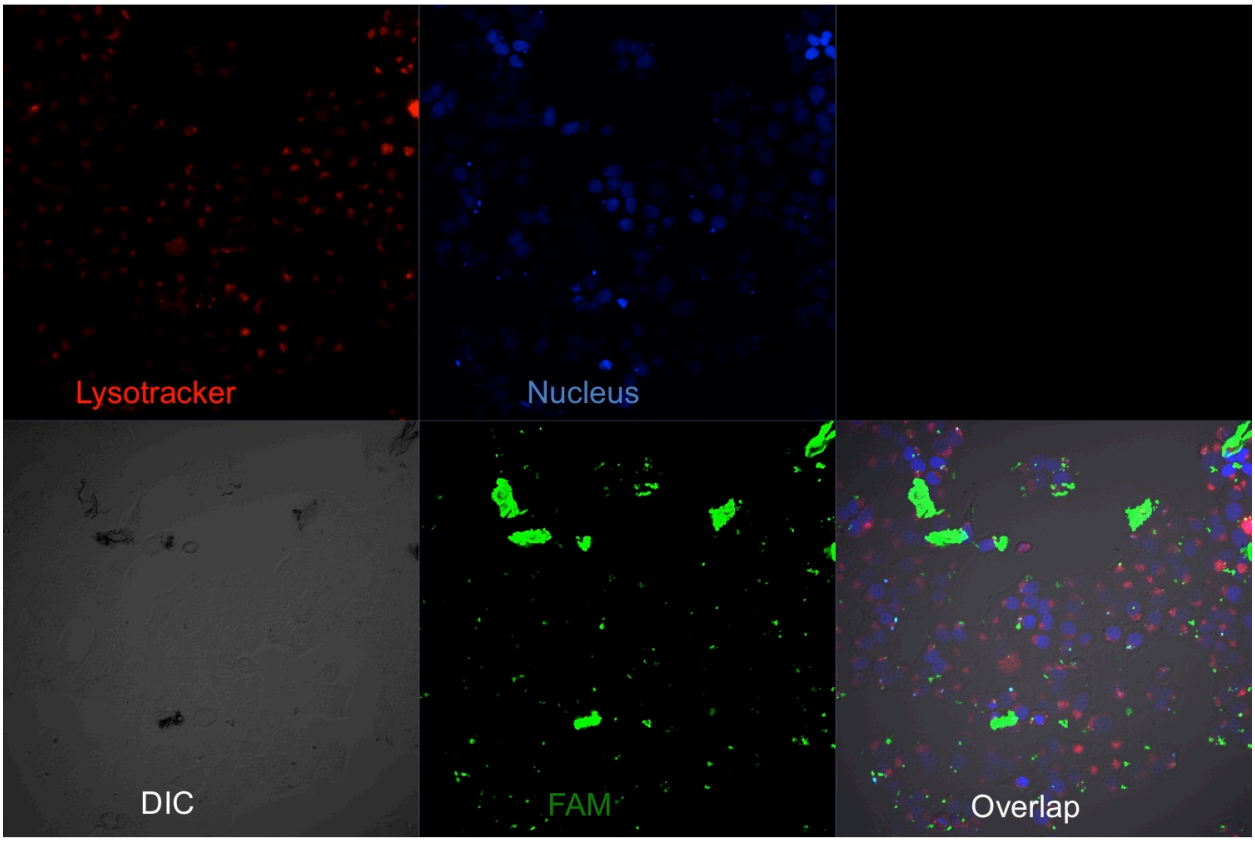

Figure 3.19 Confocal images of 8-17 DNAzyme delivered by cell-penetrating peptide EB1 (molar ratio of EB1: DNAzyme = 25:1).

Table 3.8 Parameters of the confocal microscope used for imaging.

Channel	Excitation (nm)	Emission (nm)
H33258	405	453 - 520
Lysotracker Red	561	586 - 624
FAM	488	504 - 560
Bright field	633	NA

* pinhole size was set at 1 AU for 20 × lens, 96.7 for 63 × oil lens; Gain was kept below 800; Digital gain was kept at 1; Zoom was set at 0.8 for oil lens, 1 for 20 × lens

3.3.7.2 α-helical cationic polypeptide

It has been shown previously that a class of α-helical cationic polypeptide was able to deliver siRNA and DNA plasmid into various types of mammalian cells with high efficacy and capability of escaping the endocytic pathway.[64-66] As an alternative approach to CPPs, I chose two α-helical cationic polypeptides, PVBLG-8 (Figure 3.20) and G8 (Figure 3.27). Both of them were kindly provided by our collaborator, Dr. Nan Zheng from Dr. Jianjun Cheng's lab at UIUC.

PVBLG-8 polymer has an α-helical core structure with positively charged aminoethyl piperidine side chains. It has been shown that PVBLG-8 could be used to deliver siRNA into cells and provide better protection for siRNA during the delivery process.[67-69] PVBLG-8 outperformed 25-kDa polyethylenimine (PEI) in cells generally amenable to transfection, such as COS-7 and HEK293. Moreover, it also showed better transfection performance in traditionally hard-to-transfect cells, such as H9 human embryonic stem cells.

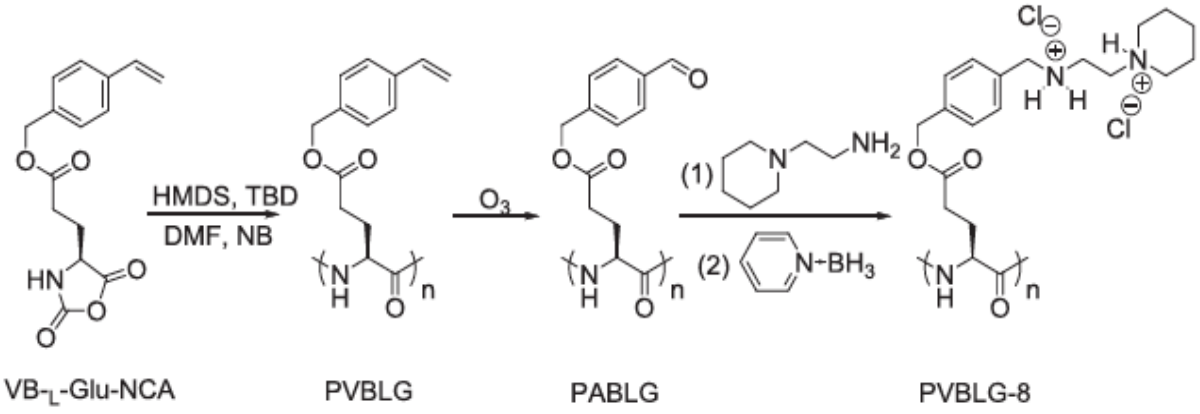

Figure 3.20 Scheme of synthesis of PVBLG-8 helical cationic peptide. (Adapted from Ref[65])

I first tested the delivery efficiency of PVBLG-8 using 8-17 DNAzyme as the cargo (Table 3.7). The PVBLG-8 polymer I obtained from Cheng lab had a degree of polymerization of about 200 (200 units per polymer chain). The molecular weight of one unit in the polymer was calculated to be about 458. PVBLG-8 was first dissolved in Millipore water at a final concentration of 1 mg/ml (~2.2 mM for polymer unit). FAM-17S-iT and 17E-iT were mixed at a final concentration of 0.22 mM for each strand in 1.5 M NaCl (Table 3.9). Different molar ratios of PVBLG-8 to DNAzyme were tested, such as 50:1, 25:1, 10:1 and 5:1. The amount of DNAzyme was kept at ~1 nmol per imaging plate for all the conditions (Table 3.10). The mixture of PVBLG-8 and DNAzyme was kept at room temperature for half an hour to allow the formation of complexes. Then, each of the 30 μl mixture was diluted into 1 ml of Opti-MEM and added into a glass-bottom imaging plate with HeLa cells grown to ~80% confluence. After three-hour incubation, cells were checked using confocal microscope. As shown in Figure 3.21 and Figure 3.22, 5:1 ratio gave reasonable good delivery efficiency, as indicated by the bright FAM signal from cells. The poor co-localization of FAM and lysotracker suggested that the DNAzyme was not trapped inside endosomes or lysosomes. If 10:1 ratio was used, more DNAzyme uptake was observed compared to the ratio of 5:1 (Figure 3.23 and Figure 3.24). If the ratio was increased further to 25:1, cells started to detach from the plate, indicating toxicity from the overload of the complex (data not shown).

Table 3.9 Preparation of 17ES DNAzyme for forming complex with PVBLG-8.

Name	Sequence	MW
FAM-17S-iT	0.88 mM	5 μl
17E-3-iT	0.88 mM	5 μl
Buffer	1.5 M NaCl	10 μl

Table 3.10 Different molar ratios of PVBLG-8 to DNAzyme.

Molar ratio	PVBLG-8 (2.2 mM)	DNAzyme (0.22 mM)	H_2O
50:1	25 µl	5 µl	0 µl
25:1	12.5 µl	5 µl	12.5 µl
10:1	5 µl	5 µl	20 µl
5:1	2.5 µl	5 µl	22.5 µl

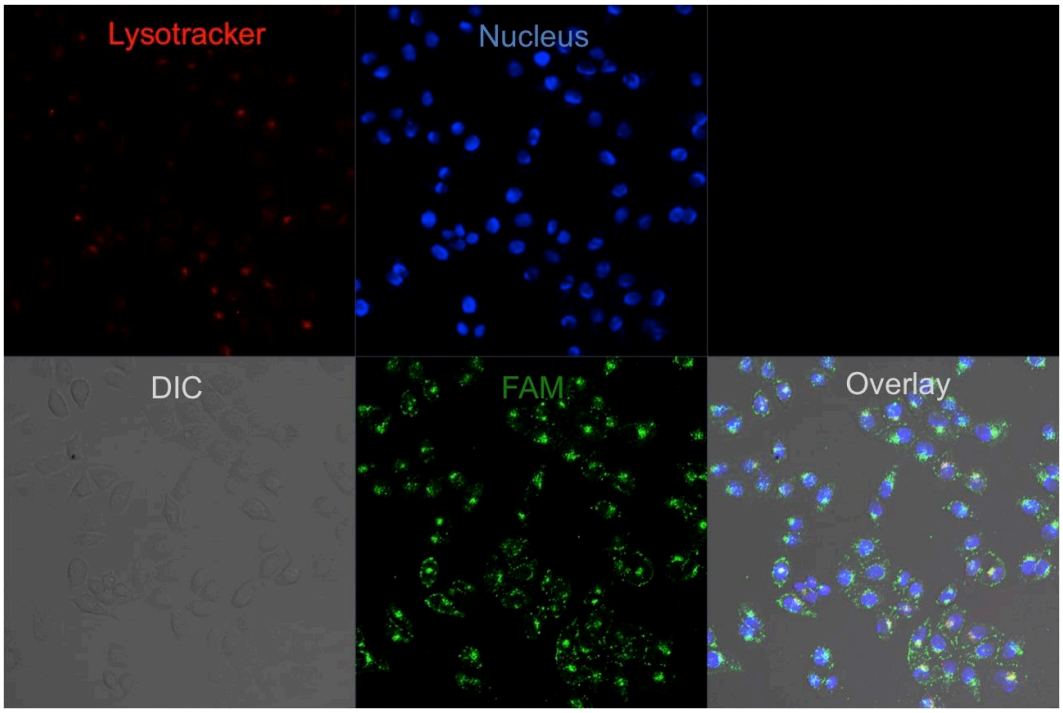

Figure 3.21 Fluorescent images of HeLa cells delivered with PVBLG-8 and 8-17 DNAzyme complex (PVBLG-8:DNAzyme = 5:1 (molar ratio), 20 × lens).

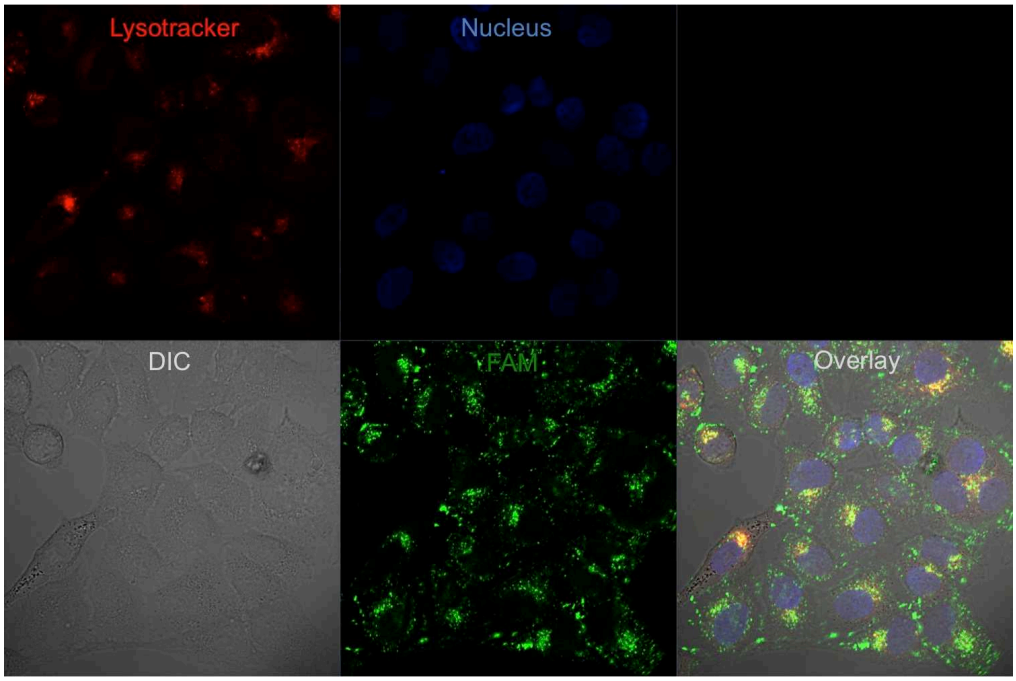

Figure 3.22 Fluorescent images of HeLa cells delivered with PVBLG-8 and 8-17 DNAzyme complex (PVBLG-8:DNAzyme = 5:1(molar ratio), 63 × oil lens).

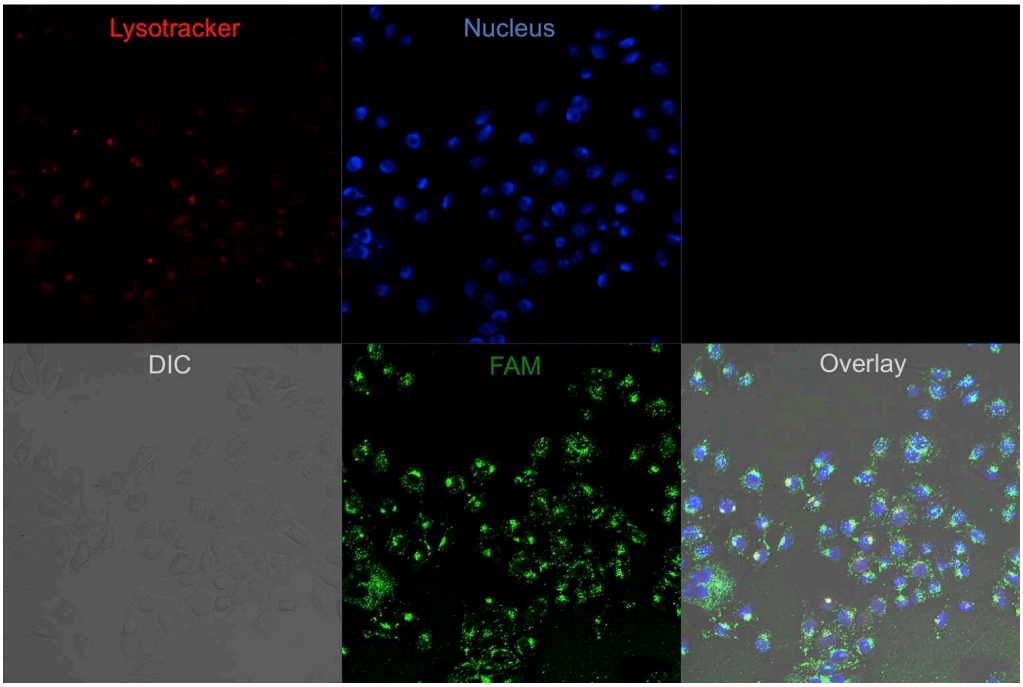

Figure 3.23 Fluorescent images of HeLa cells delivered with PVBLG-8 and 8-17 DNAzyme complex (PVBLG-8:DNAzyme = 10:1 (molar ratio), 20 × lens).

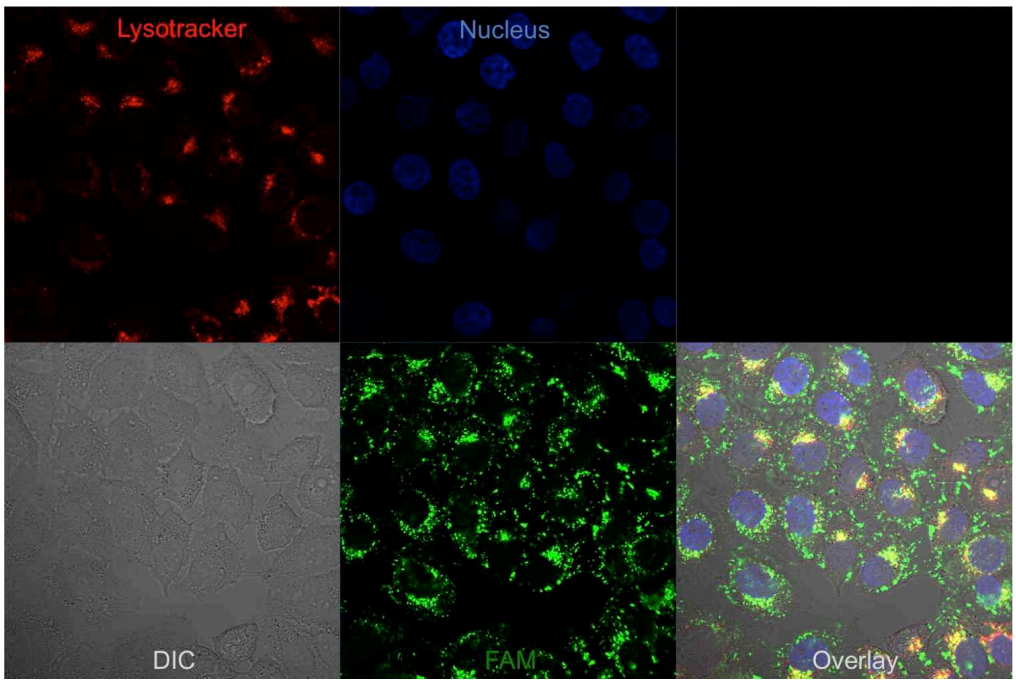

Figure 3.24 Fluorescent images of HeLa cells delivered with PVBLG-8 and 8-17 DNAzyme complex (PVBLG-8 to DNAzyme = 10:1 (molar ratio), 63 × oil lens).

Having demonstrated that PVBLG-8 served as a good delivery vehicle for 8-17 DNAzyme, I switched to NaA43 DNAzyme to see if PVBLG-8 would work as well. NaA43 DNAzyme containing a FAM labeled all-DNA substrate strand was used for the following tests (Table 3.2). However, to my surprise, PVBLG-8 showed a dramatically reduced delivery capability when NaA43 DNAzyme was used. As shown in Figure 3.25, when the ratio of PVBLG-8 to NaA43 DNAzyme was 10 to 1, under the same imaging parameters, only very weak FAM signal was observed. Similar result was observed for 20:1 ratio. When the ratio increased to 60:1, large aggregates of polymer in complex with DNAzyme started to show up as background and appeared to be outside cells (Figure 3.26). If the ratio increased to 100:1, more aggregates were observed, and the cells did not seem to be healthy.

In summary, although PVBLG-8 polypeptide showed excellent delivery capability for 8-

17 DNAzyme, it appeared to be much less effective for NaA43 DNAzyme. It might be due to the size difference between the two DNAzymes. 8-17 DNAzyme is much smaller in size compared to NaA43 DNAzyme, and PVBLG-8 seemed to be less effective in delivering larger DNAzymes.

In order to find a proper delivery vehicle for NaA43 DNAzyme, I chose to use another α-helical cationic polypeptides, G8, as an alternative to PVBLG-8. The intuitive of using G8 was that it has a longer side chain compared to PVBLG-8 (Figure 3.27A), which might be helpful for translocating bigger DNAzymes across cell membrane. Its guanidine side chains are also known to play a crucial role in cell penetration efficiency.[70] It has been demonstrated that G8 forms an ultrastable helical structure within a pH range of 1-9, and has sufficient water solubility.[70] By maintaining its helical structure at both neutral and acidic pH, G8 was able to penetrate cell membranes as well as escape from endosomes and lysosomes, resulting in highly efficient gene delivery (Figure 3.27B).[70]

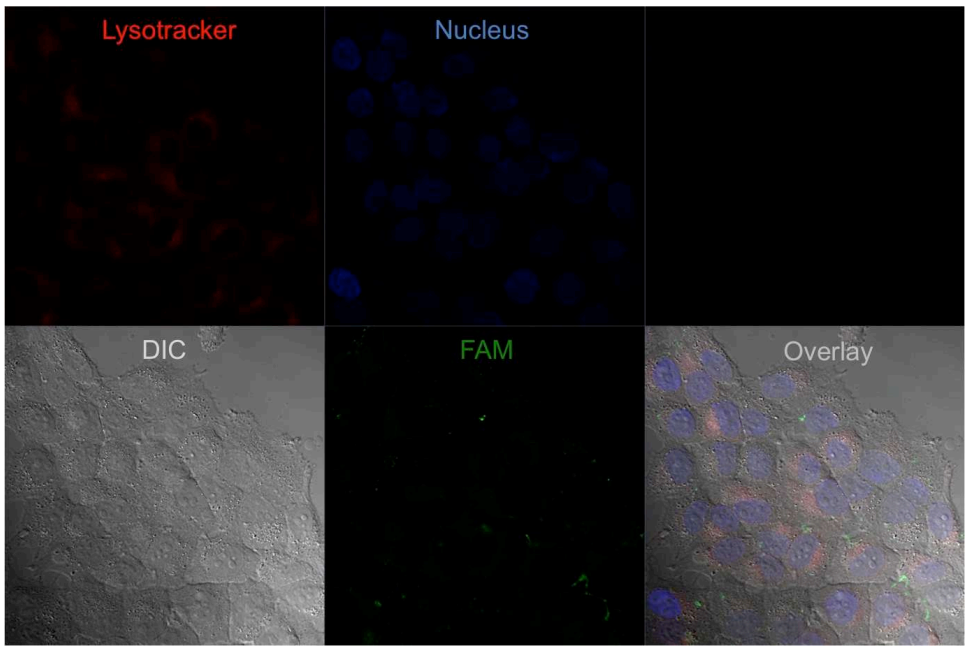

Figure 3.25 Fluorescent images of HeLa cells delivered with PVBLG-8 and NaA43 DNAzyme complex (PVBLG-8 to DNAzyme = 10:1 (molar ratio), 63 × oil lens).

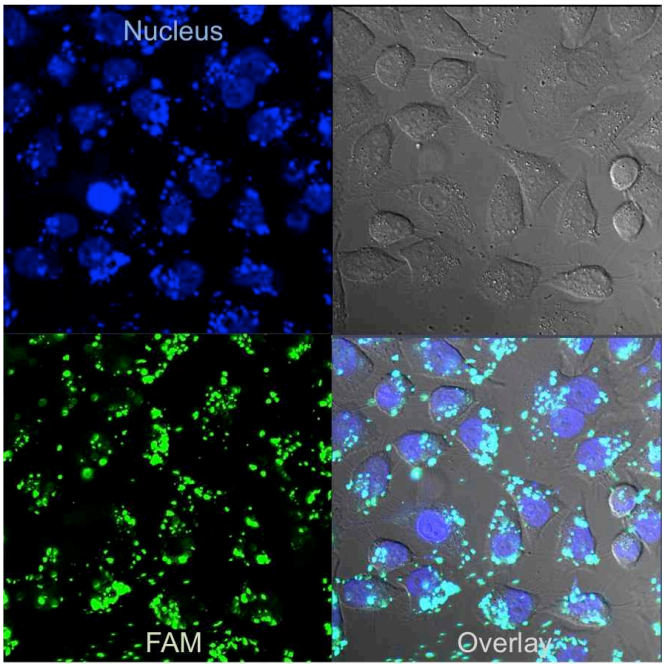

Figure 3.26 Fluorescent images of HeLa cells delivered with PVBLG-8 and NaA43 DNAzyme complex (PVBLG-8 to DNAzyme = 60:1 (molar ratio), 63 × oil lens).

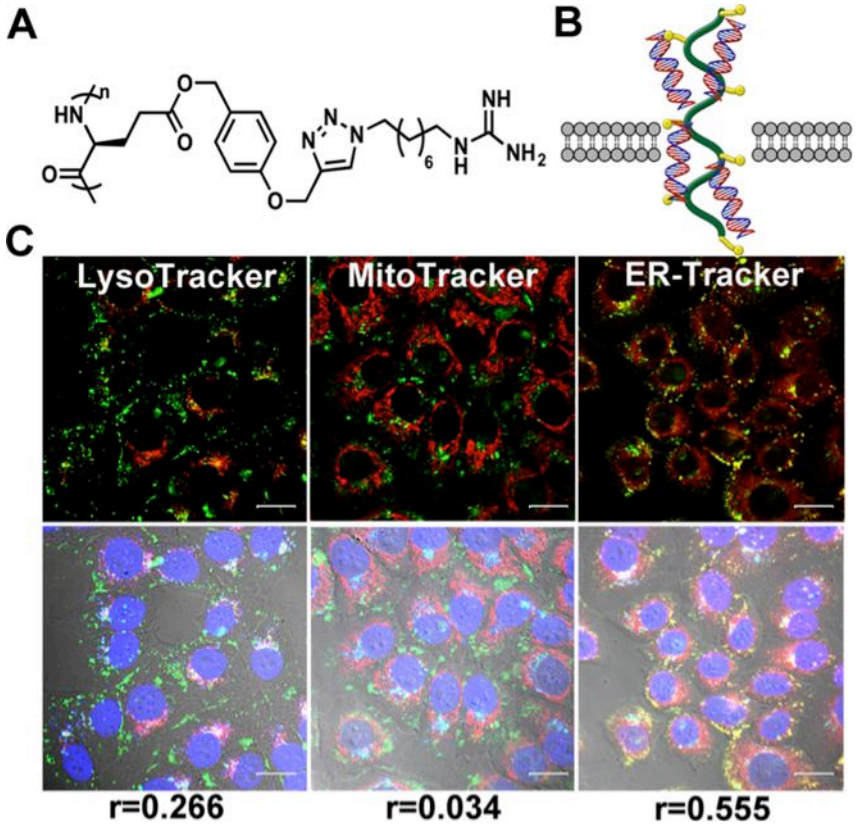

Figure 3.27 Intracellular localization of NaA43ES DNAzymes delivered by G8 polypeptide.

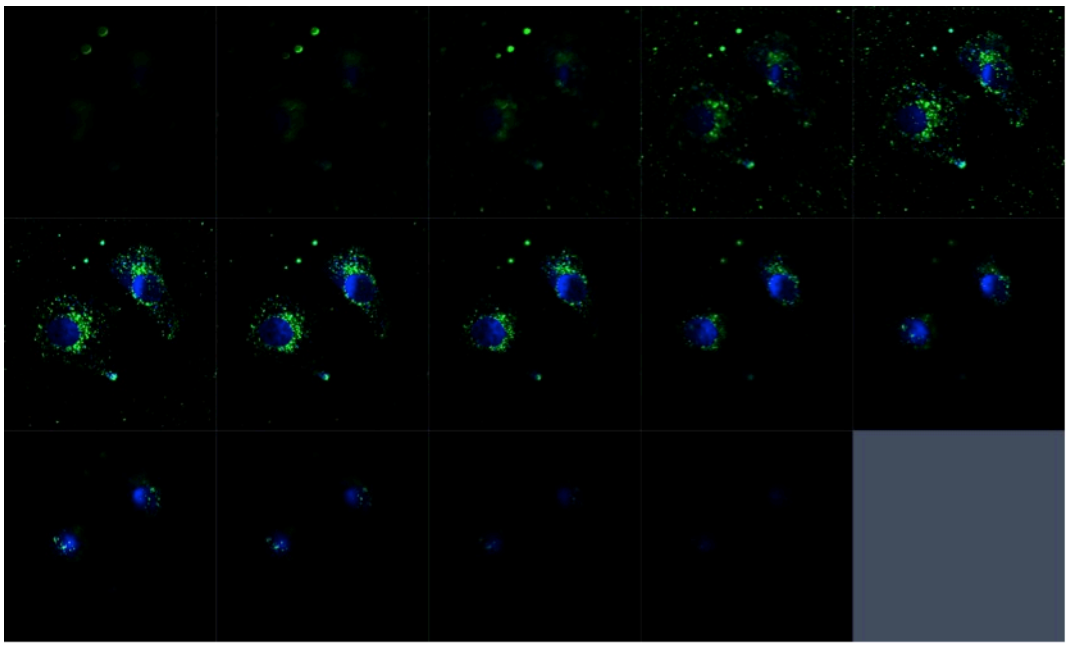

Figure 3.28 Z-stack images of HeLa cells with G8-NaA43ES complex.

Using G8 polypeptide, I achieved high delivery efficiency of the NaA43ES DNAzymes into the cytoplasm of living HeLa cells after a 4 h incubation (Figure 3.27C, Figure 3.28). To further investigate localization of the DNAzymes inside cells, staining using organelle-specific dyes was carried out subsequently. The degree of co-localization of two fluorophores was quantified by Pearson correlation coefficient as a standard technique.[71] As suggested by both this calculation and microscopic images (Figure 3.27C), NaA43ES was mainly located inside the cytoplasm of the cell, without showing organelle localization in lysosomes, mitochondria, or the endoplasmic reticulum.

Since Lysotracker tracks lysosomes by lighting up at low pH, it does not track early endosomes or late endosomes, where pH has not yet dropped much. Therefore, to further rule out this major vesicular sink, I used CellLight® early endosomes-RFP protein as a different tracker.

I transfected HeLa with the CellLight® early endosomes-RFP protein overnight before adding G8 polypeptide-DNAzyme complexes. Early endosomes-RFP is a construct where RFP is fused to Rab5a, providing specific targeting to cellular early endosomes without being affected by organelle pH. As shown in Figure 3.29, the red fluorescence from early endosomes-RFP co-localized poorly with the green fluorescence from polypeptide-DNAzyme complex, with Pearson's coefficient as 0.168±0.098, suggesting that the majority of polypeptide-DNAzyme complex was not trapped in the early endosomes. Therefore, we can rule out the possibility of early endosomes being the major vesicular sink for the NaA43 DNAzyme. Furthermore, other experiments carried out on the G8 peptide (also explained below) indicate that endocytosis may not be the major mechanism of delivery, and so endosomal or lysosomal encapsulation and sequestration might not be expected.

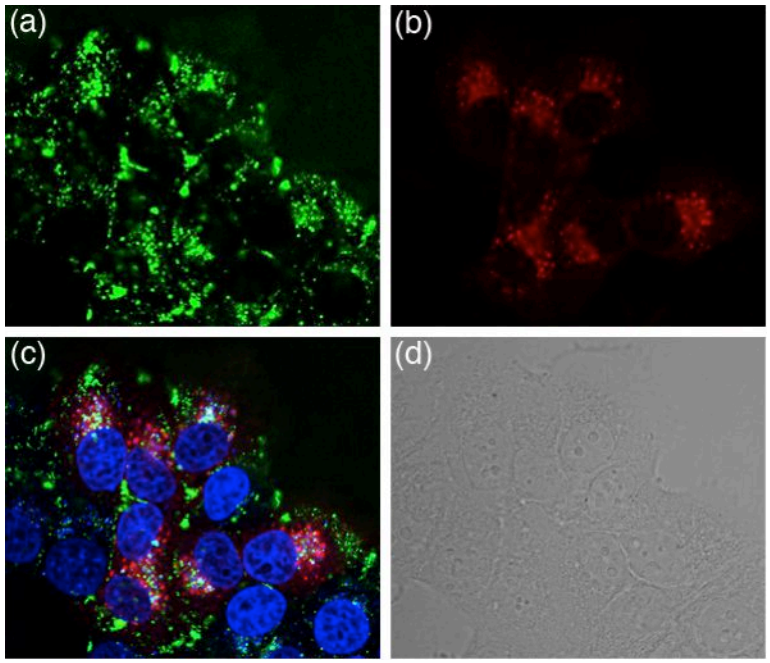

Figure 3.29 Co-localization of G8-NaA43 DNAzyme complex with early endosomes-RFP tracker.

3.3.8 Intracellular Na^+ imaging using the caged NaA43 DNAzyme

Given the fact that G8 polypeptide is a very efficient carrier for NaA43ES, we used it to deliver the caged NaA43ES complex into living HeLa cells (Figure 3.30) for the detection of Na^+. The sensor showed minimal background fluorescence after its delivery, indicating that most of the caged NaA43S remained intact during the delivery process. After washing the cells to remove excess probes and G8 in the culture medium, the cells were incubated in Dulbecco's Phosphate-Buffered Saline (DPBS) solution and irradiated with light at 365 nm for 30 minutes in order to uncage the DNAzyme complex. Immediately after uncaging, the intracellular Na^+ level was elevated by adding gramicidin, monensin and ouabain. The combination of these three ionophores is known to equilibrate the intracellular Na^+ concentration with extracellular concentration within several minutes.[58,72] The influx of Na^+ from extracellular medium caused the fluorescence inside cells to gradually increase over a time course of 30 minutes (Figure 3.30). In comparison, with the same treatment, but using a non-cleavable NaA43S, the turn-on fluorescence was not observed inside cells (Figure 3.30).

To further confirm that the turn-on fluorescence was a result from the cleavage of uncaged NaA43S by active NaA43E, we also used the combination of caged NaA43S with an inactive variant of NaA43E as a negative control (forming catalytically inactive NaA43ES complex). The inactive NaA43E contains a single point mutation, which completely abolishes the DNAzyme activity. In this case, fluorescence from the probes was maintained at a constant background level over 30 minutes (Figure 3.31), which strongly suggests that the turn-on fluorescence we observed from the active NaA43ES resulted from successful decaging and subsequent Na^+-specific DNAzyme cleavage activity.

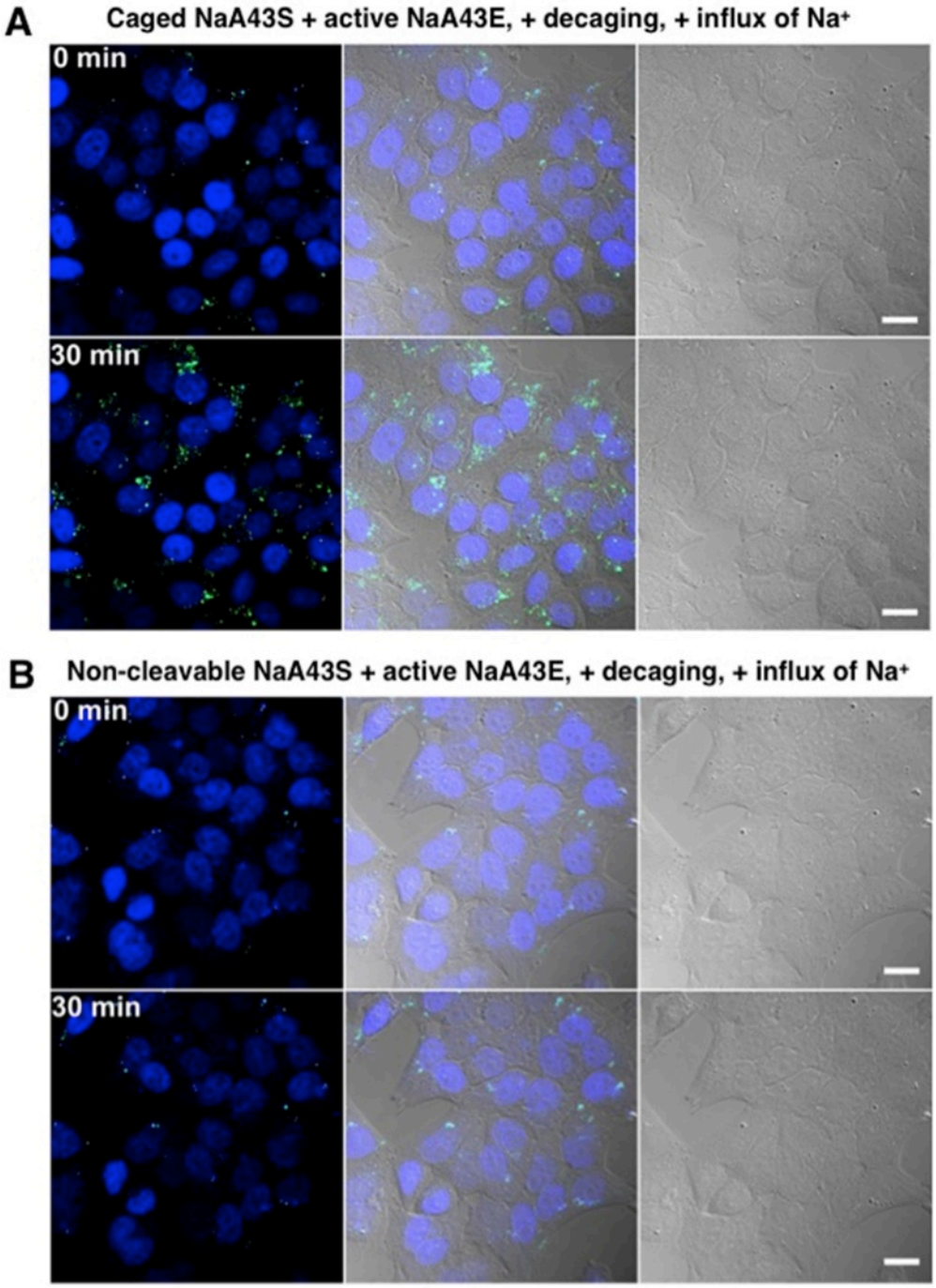

Figure 3.30 Confocal microscopy images of HeLa cells transfected with (A) caged NaA43ES complex and (B) Non-cleavable NaA43S in complex with NaA43E.

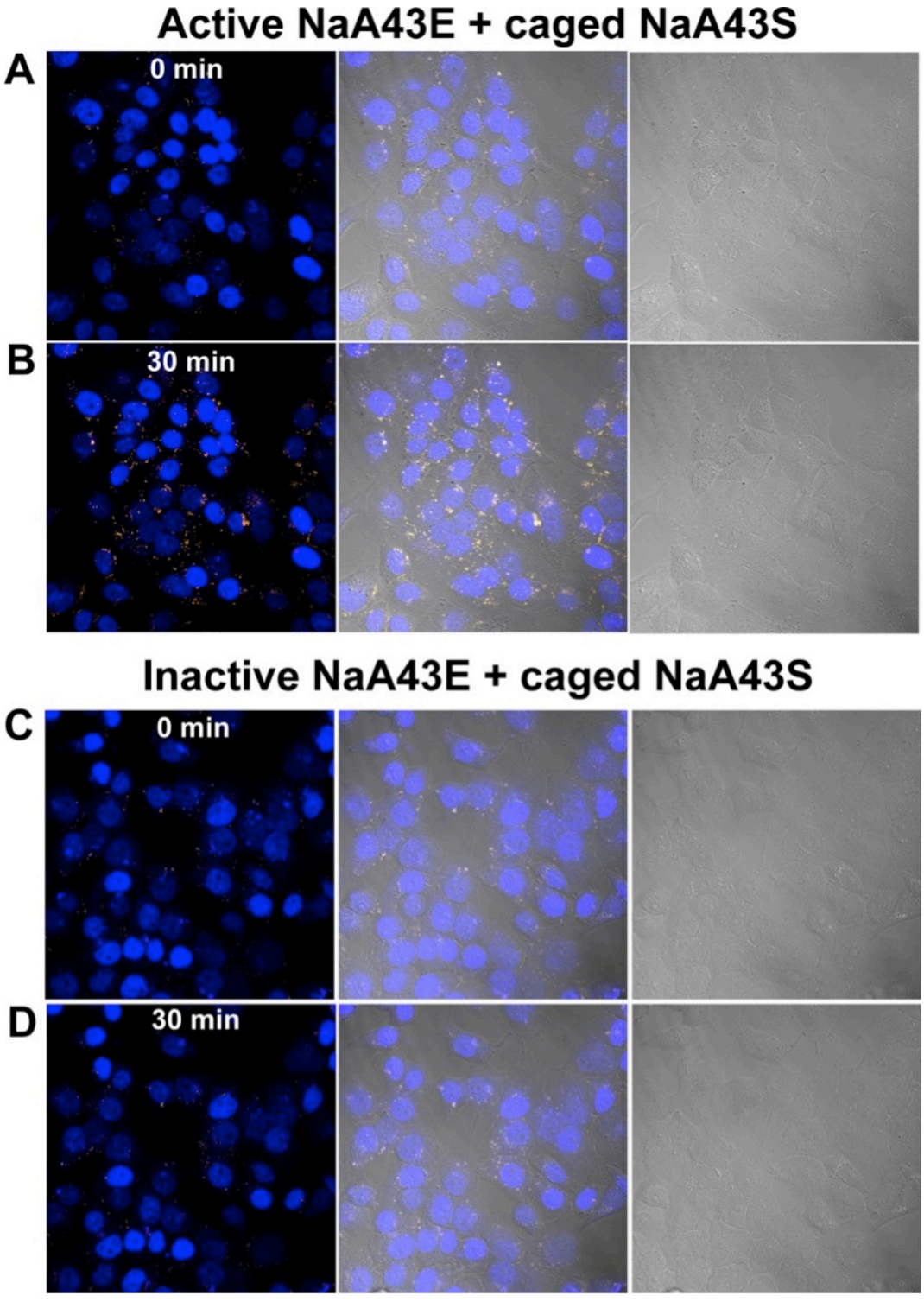

Figure 3.31 Confocal images of Na^+ sensing using TAMRA-caged NaA43S-BHQ2 as the substrate, and an inactive NaA43E in the control group.

3.3.9 Flow cytometry results

To support that the increased fluorescence intensity with Na^+ uptake noted in confocal imaging applies to the whole cell population, I employed flow cytometry. As shown in Figure 3.32, cells incubated with caged NaA43ES and an influx of 143 mM Na^+ were the only group that showed a significant increase in fluorescence, after photo-decaging. In contrast, cells incubated with non-cleavable NaA43ES complex delivered to them showed a shift in fluorescence intensity from that of blank cells after decaging, which can be attributed to background fluorescence. Additionally, without an influx of Na^+, cells delivered with caged active NaA43ES did not show increased fluorescence, suggesting that the fluorescent signal came from the Na^+-dependent activity of the probe rather than from any degradation of the DNAzyme probe by endogenous nucleases. Moreover, no turn-on fluorescence was observed in the populations of cells delivered with non-cleavable NaA43ES, regardless of whether the Na^+ level inside cells was elevated or not, which is a strong indication that the fluorescent signal resulted from the activity of DNAzymes inside cells.

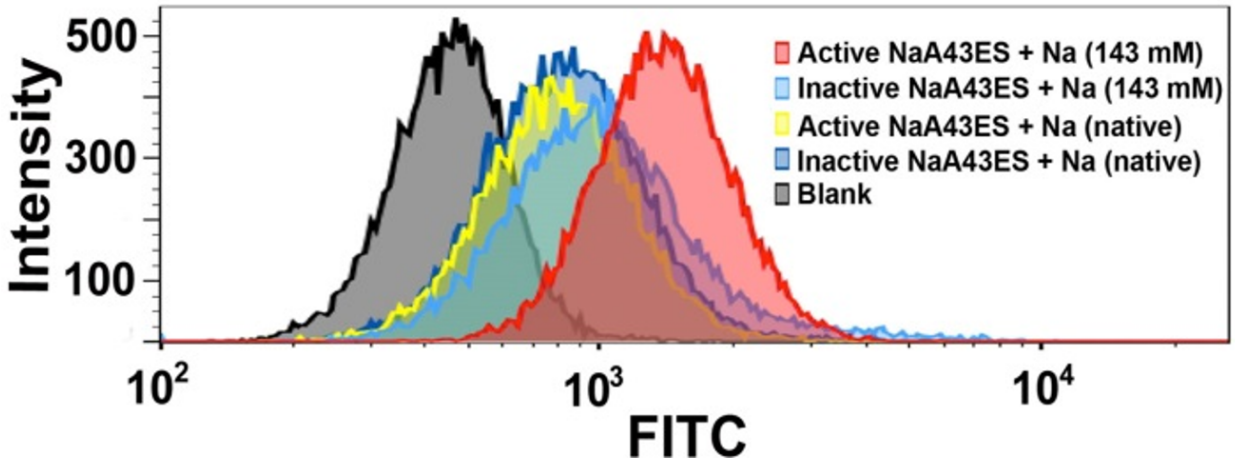

Figure 3.32 Flow cytometric quantification of cell associated fluorescence.

3.4 Conclusions

In conclusion, we have obtained the first Na^+-specific RNA-cleaving DNAzyme (NaA43ES) with fast catalytic rate and exceptionally high selectivity over other metal ions, and demonstrated the use of this DNAzyme for sensing and imaging intracellular Na^+ in living cells, by adopting an efficient DNAzyme delivery method using a cationic polypeptide, together with a photo-caging strategy to allow controllable activation of the probe inside cells. In the field of sensing monovalent metal ions, in particular Na^+, obtaining highly selective sensors with proper sensitivity and selectivity has been a major challenge. Most previously developed Na^+ fluorescent sensors suffer from poor sensitivity or are also responsive to other metal ions such as K^+. The *in vitro* selection of DNAzymes selective for Na^+ has allowed for the identification of a fluorescent sensor with exceptional selectivity and sensitivity, further validating this method for the simple identification of sensors for many other metal ions, even where existing design strategies may be lacking. Finally, cellular sensing of sodium using DNAzyme sensors will allow for greater insight into the mechanisms and importance of sodium homeostasis in biology.

It is also remarkable that the NaA43 DNAzyme has such a high selectivity for Na^+ against Li^+, K^+, and other monovalent, divalent, and trivalent metal ions. To our knowledge, no Na^+-specific nucleic acid, whether naturally occurring or in vitro selected has been previously reported. In the protein world, although K^+ channels are quite selective for K^+ over other metal ions, the Na^+ channels are much less selective.[73,74] Being able to obtain the NaA43 DNAzyme with such a high selectivity for Na^+ will not only provide a highly selective sensor for Na^+, as demonstrated here, it will also give us an opportunity to elucidate the origin of such a high selectivity. Previous studies of a Pb^{2+}-DNAzyme have shown the high selectivity is mainly due

to the DNAzyme forming a specific binding pocket for the metal ion.[75] It would be interesting to find out if the NaA43 DNAzyme uses the same mechanism for selectivity.

3.5 References

1. Jaitovich A, Bertorello AM, Intracellular sodium sensing: SIK1 network, hormone action and high blood pressure. *BBA-Mol. Basis Dis.* **2010** *1802*, 1140-1149.

2. Ingelfinger JR, Pratt RE, Ellison K, Dzau VJ, Sodium regulation of angiotensinogen mRNA expression in rat kidney cortex and medulla. *J. Clin. Invest.* **1986** *78*, 1311-1315.

3. Kalra PR, Anker SD, Coats AJ, Water and sodium regulation in chronic heart failure: the role of natriuretic peptides and vasopressin. *Cardiovasc. Res.* **2001** *51*, 495-509.

4. Catterall WA, Hulme JT, Jiang X, Few WP, Regulation of sodium and calcium channels by signaling complexes. *J. Recept. Sig. Transd.* **2006** *26*, 577-598.

5. Malloy CR, Buster DC, Castro MMCA, Geraldes CFGC, Jeffrey FMH, Sherry AD, Influence of Global-Ischemia on Intracellular Sodium in the Perfused Rat-Heart. *Magn. Reson. Med.* **1990** *15*, 33-44.

6. Grubman A, James SA, James J, Duncan C, Volitakis I, Hickey JL, Crouch PJ, Donnelly PS, Kanninen KM, Liddell JR, Cotman SL, de Jonge MD, White AR, X-ray fluorescence imaging reveals subcellular biometal disturbances in a childhood neurodegenerative disorder. *Chem. Sci.* **2014** *5*, 2503-2516.

7. Ivanics T, Blum H, Wroblewski K, Wang DJ, Osbakken M, Intracellular Sodium in Cardiomyocytes Using Na-23 Nuclear-Magnetic-Resonance. *BBA-Mol. Cell Res.* **1994** *1221*, 133-144.

8. de Silva AP, Gunaratne HQ, Gunnlaugsson T, Huxley AJ, McCoy CP, Rademacher JT, Rice TE, Signaling Recognition Events with Fluorescent Sensors and Switches. *Chem. Rev.* **1997** *97*, 1515-1566.

9. Johnson I, Review: Fluorescent probes for living cells. *The Histochemical Journal* **1998** *30*, 123-140.

10. Valeur B, Leray I, Design principles of fluorescent molecular sensors for cation recognition. *Coord. Chem. Rev.* **2000** *205*, 3-40.

11. Burdette SC, Walkup GK, Spingler B, Tsien RY, Lippard SJ, Fluorescent sensors for Zn2+ based on a fluorescein platform: Synthesis, properties and intracellular distribution. *J. Am. Chem. Soc.* **2001** *123*, 7831-7841.

12. Domaille DW, Que EL, Chang CJ, Synthetic fluorescent sensors for studying the cell biology of metals. *Nat. Chem. Biol.* **2008** *4*, 168-175.

13. Nolan EM, Lippard SJ, Small-molecule fluorescent sensors for investigating zinc metalloneurochemistry. *Acc. Chem. Res.* **2009** *42*, 193-203.

14. Schaferling M, The art of fluorescence imaging with chemical sensors. *Angew Chem Int Ed Engl* **2012** *51*, 3532-3554.

15. Carter KP, Young AM, Palmer AE, Fluorescent sensors for measuring metal ions in living systems. *Chem. Rev.* **2014** *114*, 4564-4601.

16. McRae R, Bagchi P, Sumalekshmy S, Fahrni CJ, In Situ Imaging of Metals in Cells and Tissues.

Chem. Rev. **2009** *109*, 4780-4827.

17. Kikuchi K, Design, synthesis and biological application of chemical probes for bio-imaging. *Chem. Soc. Rev.* **2010** *39*, 2048-2053.

18. Grynkiewicz G, Poenie M, Tsien RY, A new generation of Ca2+ indicators with greatly improved fluorescence properties. *J. Biol. Chem.* **1985** *260*, 3440-3450.

19. Minta A, Kao JP, Tsien RY, Fluorescent indicators for cytosolic calcium based on rhodamine and fluorescein chromophores. *J. Biol. Chem.* **1989** *264*, 8171-8178.

20. Stosiek C, Garaschuk O, Holthoff K, Konnerth A, In vivo two-photon calcium imaging of neuronal networks. *Proc. Natl. Acad. Sci. U. S. A.* **2003** *100*, 7319-7324.

21. Fahrni CJ, O'Halloran TV, Aqueous coordination chemistry of quinoline-based fluorescence probes for the biological chemistry of zinc. *J. Am. Chem. Soc.* **1999** *121*, 11448-11458.

22. Chang CJ, Jaworski J, Nolan EM, Sheng M, Lippard SJ, A tautomeric zinc sensor for ratiometric fluorescence imaging: Application to nitric oxide-induced release of intracellular zinc. *Proc. Natl. Acad. Sci. U. S. A.* **2004** *101*, 1129-1134.

23. You Y, Han Y, Lee YM, Park SY, Nam W, Lippard SJ, Phosphorescent sensor for robust quantification of copper(II) ion. *J. Am. Chem. Soc.* **2011** *133*, 11488-11491.

24. Price KA, Hickey JL, Xiao ZG, Wedd AG, James SA, Liddell JR, Crouch PJ, White AR, Donnelly PS, The challenges of using a copper fluorescent sensor (CS1) to track intracellular distributions of copper in neuronal and glial cells. *Chem. Sci.* **2012** *3*, 2748-2759.

25. Au-Yeung HY, Chan J, Chantarojsiri T, Chang CJ, Molecular Imaging of Labile Iron(II) Pools in Living Cells with a Turn-On Fluorescent Probe. *J. Am. Chem. Soc.* **2013** *135*, 15165-15173.

26. Hirayama T, Okuda K, Nagasawa H, A highly selective turn-on fluorescent probe for iron(II) to visualize labile iron in living cells. *Chem. Sci.* **2013** *4*, 1250-1256.

27. Niwa M, Hirayama T, Okuda K, Nagasawa H, A new class of high-contrast Fe(II) selective fluorescent probes based on spirocyclized scaffolds for visualization of intracellular labile iron delivered by transferrin. *Org. Biomol. Chem.* **2014** *12*, 6590-6597.

28. Fakih S, Podinovskaia M, Kong XL, Schaible UE, Collins HL, Hider RC, Monitoring Intracellular Labile Iron Pools: A Novel Fluorescent Iron(III) Sensor as a Potential Non-Invasive Diagnosis Tool. *J. Pharm. Sci.* **2009** *98*, 2212-2226.

29. Donoso P, Mill JG, Oneill SC, Eisner DA, Fluorescence Measurements of Cytoplasmic and Mitochondrial Sodium Concentration in Rat Ventricular Myocytes. *J. Physiol.-London* **1992** *448*, 493-509.

30. Amorino GP, Fox MH, Intracellular Na+ Measurements Using Sodium Green Tetraacetate with Flow-Cytometry. *Cytometry* **1995** *21*, 248-256.

31. Meier SD, Kovalchuk Y, Rose CR, Properties of the new fluorescent Na+ indicator CoroNa

Green: Comparison with SBFI and confocal Na+ imaging. *J. Neurosci. Meth.* **2006** *155*, 251-259.

32. Jayaraman S, Song YL, Vetrivel L, Shankar L, Verkman AS, Noninvasive in vivo fluorescence measurement of airway-surface liquid depth, salt concentration, and pH. *J. Clin. Invest.* **2001** *107*, 317-324.

33. Lamy CM, Chatton JY, Optical probing of sodium dynamics in neurons and astrocytes. *Neuroimage* **2011** *58*, 572-578.

34. Kim MK, Lim CS, Hong JT, Han JH, Jang HY, Kim HM, Cho BR, Sodium-Ion-Selective Two-Photon Fluorescent Probe for In Vivo Imaging. *Angew. Chem., Int. Ed.* **2010** *49*, 364-367.

35. Sarkar AR, Heo CH, Park MY, Lee HW, Kim HM, A small molecule two-photon fluorescent probe for intracellular sodium ions. *Chem. Commun.* **2014** *50*, 1309-1312.

36. Dubach JM, Lim E, Zhang N, Francis KP, Clark H, In vivo sodium concentration continuously monitored with fluorescent sensors. *Integr. Biol.* **2011** *3*, 142-148.

37. Bernardinelli Y, Azarias G, Chatton JY, In situ fluorescence imaging of glutamate-evoked mitochondrial Na+ responses in astrocytes. *Glia* **2006** *54*, 460-470.

38. Gunnlaugsson T, Nieuwenhuyzen M, Richard L, Thoss V, Novel sodium-selective fluorescent PET and optically based chemosensors: towards Na+ determination in serum. *J. Chem. Soc. Perk. T. 2* **2002**, 141-150.

39. Leray I, O'Reilly F, Jiwan JLH, Soumillion JP, Valeur B, A new calix[4]arene-based fluorescent sensor for sodium ion. *Chem. Commun.* **1999**, 795-796.

40. Leray I, Lefevre JP, Delouis JF, Delaire J, Valeur B, Synthesis and photophysical and cation-binding properties of mono- and tetranaphthylcalix[4]arenes as highly sensitive and selective fluorescent sensors for sodium. *Chem. Eur. J.* **2001** *7*, 4590-4598.

41. Li J, Lu Y, A highly sensitive and selective catalytic DNA biosensor for lead ions. *J. Am. Chem. Soc.* **2000** *122*, 10466-10467.

42. Li J, Zheng W, Kwon AH, Lu Y, In vitro selection and characterization of a highly efficient Zn(II)-dependent RNA-cleaving deoxyribozyme. *Nucleic Acids Res.* **2000** *28*, 481-488.

43. Liu J, Brown AK, Meng X, Cropek DM, Istok JD, Watson DB, Lu Y, A catalytic beacon sensor for uranium with parts-per-trillion sensitivity and millionfold selectivity. *Proc. Natl. Acad. Sci. U. S. A.* **2007** *104*, 2056-2061.

44. Liu J, Lu Y, A DNAzyme catalytic beacon sensor for paramagnetic Cu2+ ions in aqueous solution with high sensitivity and selectivity. *J. Am. Chem. Soc.* **2007** *129*, 9838-9839.

45. Liu J, Lu Y, Rational design of "Turn-On" allosteric DNAzyme catalytic beacons for aqueous mercury ions with ultrahigh sensitivity and selectivity. *Angew. Chem., Int. Ed.* **2007** *46*, 7587-7590.

46. Hollenstein M, Hipolito CJ, Lam CH, Perrin DM, A self-cleaving DNA enzyme modified with amines, guanidines and imidazoles operates independently of divalent metal cations (M2+). *Nucleic Acids*

Res. **2009** *37*, 1638-1649.

47. Smuga D, Majchrzak K, Sochacka E, Nawrot B, RNA-cleaving 10-23 deoxyribozyme with a single amino acid-like functionality operates without metal ion cofactors. *New J. Chem.* **2010** *34*, 934-948.

48. Hollenstein M, Hipolito CJ, Lam CH, Perrin DM, Toward the Combinatorial Selection of Chemically Modified DNAzyme RNase A Mimics Active Against all-RNA Substrates. *Acs Combinatorial Science* **2013** *15*, 174-182.

49. Geyer CR, Sen D, Evidence for the metal-cofactor independence of an RNA phosphodiester-cleaving DNA enzyme. *Chem. Biol.* **1997** *4*, 579-593.

50. Faulhammer D, Famulok M, Characterization and divalent metal-ion dependence of in vitro selected deoxyribozymes which cleave DNA/RNA chimeric oligonucleotides. *J. Mol. Biol.* **1997** *269*, 188-202.

51. Carrigan MA, Ricardo A, Ang DN, Benner SA, Quantitative analysis of a RNA-cleaving DNA catalyst obtained via in vitro selection. *Biochemistry* **2004** *43*, 11446-11459.

52. Torabi S-F. In vitro selection and characterization of mono-, di-, and trivalent metal-dependent DNAzymes and their sensing applications: University of Illinois at Urbana-Champaign; 2014.

53. Liu J, Lu Y, Improving fluorescent DNAzyme biosensors by combining inter- and intramolecular quenchers. *Anal. Chem.* **2003** *75*, 6666-6672.

54. Torabi S-F, Wu P, McGhee CE, Chen L, Hwang K, Zheng N, Cheng J, Lu Y, In vitro selection of a sodium-specific DNAzyme and its application in intracellular sensing. *Proc. Natl. Acad. Sci. U. S. A.* **2015** *112*, 5903-5908.

55. Chaulk SG, MacMillan AM, Synthesis of oligo-RNAs with photocaged adenosine 2'-hydroxyls. *Nat. Protoc.* **2007** *2*, 1052-1058.

56. Brown AK, Li J, Pavot CM, Lu Y, A lead-dependent DNAzyme with a two-step mechanism. *Biochemistry* **2003** *42*, 7152-7161.

57. Hwang K, Wu P, Kim T, Lei L, Tian S, Wang Y, Lu Y, Photocaged DNAzymes as a General Method for Sensing Metal Ions in Living Cells. *Angew. Chem., Int. Ed.* **2014** *53*, 13798-13802.

58. Donoso P, Mill JG, O'Neill SC, Eisner DA, Fluorescence measurements of cytoplasmic and mitochondrial sodium concentration in rat ventricular myocytes. *J Physiol* **1992** *448*, 493-509.

59. Frankel AD, Pabo CO, Cellular uptake of the tat protein from human immunodeficiency virus. *Cell* **1988** *55*, 1189-1193.

60. Green M, Loewenstein PM, Autonomous functional domains of chemically synthesized human immunodeficiency virus tat trans-activator protein. *Cell* **1988** *55*, 1179-1188.

61. Derossi D, Joliot AH, Chassaing G, Prochiantz A, The 3rd Helix of the Antennapedia Homeodomain Translocates through Biological-Membranes. *J. Biol. Chem.* **1994** *269*, 10444-10450.

62. Heitz F, Morris MC, Divita G, Twenty years of cell-penetrating peptides: from molecular

mechanisms to therapeutics. *Br. J. Pharmacol.* **2009** *157*, 195-206.

63. Lundberg P, El-Andaloussi S, Sutlu T, Johansson H, Langel U, Delivery of short interfering RNA using endosomolytic cell-penetrating peptides. *FASEB J.* **2007** *21*, 2664-2671.

64. Lu H, Wang J, Bai Y, Lang JW, Liu S, Lin Y, Cheng J, Ionic polypeptides with unusual helical stability. *Nat. Commun.* **2011** *2*, 206.

65. Gabrielson NP, Lu H, Yin L, Kim KH, Cheng J, A Cell-penetrating Helical Polymer For siRNA Delivery to Mammalian Cells. *Mol. Ther.* **2012** *20*, 1599-1609.

66. Gabrielson NP, Lu H, Yin L, Li D, Wang F, Cheng J, Reactive and bioactive cationic alpha-helical polypeptide template for nonviral gene delivery. *Angew Chem Int Ed Engl* **2012** *51*, 1143-1147.

67. Gabrielson NP, Lu H, Yin L, Kim KH, Cheng J, A cell-penetrating helical polymer for siRNA delivery to mammalian cells. *Mol. Ther.* **2012** *20*, 1599-1609.

68. Yen J, Zhang Y, Gabrielson NP, Yin L, Guan L, Chaudhury I, Lu H, Wang F, Cheng J, Cationic, helical polypeptide-based gene delivery for IMR-90 fibroblasts and human embryonic stem cells. *Biomater Sci* **2013** *1*, 719-727.

69. Zhang R, Song Z, Yin L, Zheng N, Tang H, Lu H, Gabrielson NP, Lin Y, Kim K, Cheng J, Ionic alpha-helical polypeptides toward nonviral gene delivery. *Wiley Interdiscip. Rev. Nanomed. Nanobiotechnol.* **2015** *7*, 98-110.

70. Zhang R, Zheng N, Song Z, Yin L, Cheng J, The effect of side-chain functionality and hydrophobicity on the gene delivery capabilities of cationic helical polypeptides. *Biomaterials* **2014** *35*, 3443-3454.

71. French AP, Mills S, Swarup R, Bennett MJ, Pridmore TP, Colocalization of fluorescent markers in confocal microscope images of plant cells. *Nat. Protoc.* **2008** *3*, 619-628.

72. Bernardinelli Y, Azarias G, Chatton JY, In situ fluorescence imaging of glutamate-evoked mitochondrial Na+ responses in astrocytes. *Glia* **2006** *54*, 460-470.

73. Sheng S, McNulty KA, Harvey JM, Kleyman TR, Second transmembrane domains of ENaC subunits contribute to ion permeation and selectivity. *J. Biol. Chem.* **2001** *276*, 44091-44098.

74. Doyle DA, Morais Cabral J, Pfuetzner RA, Kuo A, Gulbis JM, Cohen SL, Chait BT, MacKinnon R, The structure of the potassium channel: molecular basis of K+ conduction and selectivity. *Science* **1998** *280*, 69-77.

75. Kim HK, Rasnik I, Liu J, Ha T, Lu Y, Dissecting metal ion-dependent folding and catalysis of a single DNAzyme. *Nat. Chem. Biol.* **2007** *3*, 763-768.

4 Chapter 4 Attempts to detect labile iron in mammalian and bacterial cells using Fe(II) and Fe(III) DNAzymes

4.1 Introduction

4.1.1 Iron homeostasis in biological system

Iron, the most abundant transitional metal ion in biological systems, plays an important role as a metal cofactor for various enzymes, as well as a signaling molecule involved in different pathways.[1-4] Because of its ability to exist in one of two oxidation states (Fe(II) and Fe(III)), iron is an ideal redox catalyst for diverse biological processes, such as respiratory chain reaction[5-7] and DNA replication[8-11]. However, the redox potential of iron also contributes to its toxicity.[12,13] Homeostasis of iron is exquisitely controlled to ensure that there is adequate iron for basal functions but no excess iron. It is known that free iron can promote formation of reactive oxygen species (ROS), leading to damage of cellular components.[14-16]

Intracellular iron balance is achieved through at least two mechanisms. First, all mammalian cells produce ferritin, which is a polymer composed of two similar polypeptide chains, L-ferritin and H-ferritin.[17-24] Each ferritin polymer has a central cavity to store hydrated iron oxides, and can accommodate up to 4500 iron atoms.[25] Ferritin serves as an iron tank, which stores excess iron and allows the use of iron when there is a need. Another mechanism is based on iron regulatory proteins (IRPs).[26-29] When iron is limiting, these proteins bind to iron regulatory elements (IREs) in the untranslated regions of mRNAs involved in iron transport and storage.[30-33] These mRNAs usually encode ferritin, ferroportin, and heme biosynthetic

enzymes.[34-37] The binding of IRPs to these IREs sterically blocks the initiation of translation by interfering with ribosome assembly at the start codon, and thus interrupts the production of these proteins, leading to less storage of iron and more mobile iron for the cells to use. In the whole body, the plasma iron concentrations remain stable at 10-30 μM.[38] Hepcidin, a circulating peptide hormone, was identified as the systemic iron-regulatory hormone. [39-45] It regulates intestinal iron absorption, plasma iron concentrations, and tissue iron distribution by inducing degradation of its receptor, the cellular iron exporter ferroportin.[46]

4.1.2 Cellular iron uptake

4.1.2.1 Transferrin-mediated mechanisms

In erythroid progenitor cells and other actively dividing cells, iron can be acquired from plasma transferrin (Tf) by receptor-mediated endocytosis.[47-54] Iron-loaded transferrin binds to the cell surface transferrin receptor 1 (TfR1), and the complex undergoes endocytosis via clathrin-coated pits.[55-57] Acidification of the endosome to pH 5.5 triggers a conformational change in Tf, resulting in less binding affinity for iron.[56] Subsequently, literated Fe^{3+} ions get reduced to Fe^{2+} and transported across the endosomal membrane to the cytosol.[50] In the meanwhile, the apo-Tf/TfR1 complex returns to the cell membrane, and the apo-Tf is recycled back to the bloodstream to recapture iron.[58]

Iron chelation by Tf serves as an important mechanism for maintaining Fe^{3+} in a soluble and redox-inert form under physiologic conditions, and preventing the generation of ROS. Tf also plays a defensive role against pathogen infection by depriving the potential pathogens of extracellular iron (*vida infra*). Under normal conditions, approximately 30% of the Tf iron-

binding sites are saturated, which allows Tf to efficiently buffer alterations of plasma iron levels and capture free iron to minimize the risk of toxicity. Under iron overload conditions, the level of redox-active non-transferrin bound iron (NTBI) can increase to 10-15 μM or higher.[59,60] Although the exact chemical nature of NTBI remains unknown, it is hypothesized that it circulates in a form that is loosely coordinated to albumin or small organic acids, such as citrate.[12,61]

4.1.2.2 Transferrin-independent mechanisms

Tf is known to be the main source of iron for tissues. Besides Tf-dependent pathways, specific cell types may use alternative Tf-independent routes to acquire iron. For example, macrophages can also acquire high amounts of iron through phagocytosis of senescent erythrocytes.[62,63] Tissue parenchymal cells can take up NTBI under iron overload states. Cardiomyocytes may take up NTBI through L-type voltage-depended calcium channels too. Moreover, in pathological states, tissue damage results in release of iron-rich intracellular ferritin into plasma, which can be taken up by cells through transferrin-independent endocytosis pathways.

4.1.3 Bacterial iron uptake

Given the fact that iron is essential for all organisms, including all human pathogens, human innate immune system has evolved to limit iron availability to invading microbes in a process called nutritional immunity.[64-70] Therefore, successful human pathogens must possess special mechanisms to circumvent nutritional immunity in order to survive and cause disease. Gram-positive bacteria can obtain iron through the use of heme[71,72] and hemoprotein cell surface

receptors, or through secretion of hemophores.[73-76] Gram-negative pathogens utilize siderophores and heme/hemoprotein receptors to obtain host iron.[77-81]

4.1.4 Current methods of iron sensing

Despite the importance of iron homeostasis in biology, current methods for detecting iron still mainly rely on instrumental analysis, such as atomic absorption spectroscopy, EPR, or ICP-MS, which require tedious sample preparation process and large amount of samples. Moreover, these methods can only provide very rough estimations of intracellular metal concentrations as it was normally calculated by total amount of metals in the sample divided by estimated cell volume. In addition, these methods cannot differentiate between different metal species, such as metals associated with inorganic or organic ligands, or metals incorporated inside proteins.

Of the available methods for real-time sensing/imaging of iron in cells, fluorescent sensors have been the predominant choice, because of advantages of high signal intensity and fast response time.[82] However, the design and synthesis of fluorescent sensors for iron remains a significant challenge, in large part due to the intrinsic non-specific quenching property of iron. Among the published sensors for Fe(II)/Fe(III), most are turn-off sensors, which are generally undesirable due to reduced dynamic range and added potential for false positive signals within a complex cellular environment.[83-87] Therefore, a new type of sensors for iron is needed to better elucidate the roles of iron in biology.

In order to develop an approach to address this challenge, we decide to take advantages of DNAzymes. Previously, we have demonstrated that DNAzyme could be converted into metal ion sensors for UO_2^{2+} and Na^+ detection inside cells. More recently, our lab has selected Fe(II)

and Fe(III) specific DNAzymes. This chapter will cover my initial attempts and preliminary results of applying these two DNAzymes for detecting iron inside mammalian and bacterial cells.

4.2 Materials and Methods

4.2.1 Sequences

Table 4.1 Sequences of Fe(II) and Fe(III) DNAzymes with different linker lengths for gold nanoparticle functionalization.

Name	Sequences (5′ to 3′)
5SH9A Fe2E	/5ThioMC6-D/ AAA AAA AAA TGG ATA TCT CCT AGC CAG ACT GTT ATG TGT GAT ACG GCA AAC TTC GTG ATG CCT CTA CGG GTC CG
5SH12A Fe2E	/5ThioMC6-D/ AAA AAA AAA AAA TGG ATA TCT CCT AGC CAG ACT GTT ATG TGT GAT ACG GCA AAC TTC GTG ATG CCT CTA CGG GTC CG
5SH15A Fe2E	/5ThioMC6-D/ AAA AAA AAA AAA AAA TGG ATA TCT CCT AGC CAG ACT GTT ATG TGT GAT ACG GCA AAC TTC GTG ATG CCT CTA CGG GTC CG
Alx-Q rFe2S	/5IABkFQ/CGG ACC CGT ATC AAT CTC ACG TAT (rA)GG ATA TCC A /3AlexF488N/
3SH9A Fe3E	GCG GCA TGC GCG TTT GCG GCA CCT AAA CGC TCC TAA TAG AGA AAA AAA AA /3ThioMC3-D/
3SH9A Fe3E	GCG GCA TGC GCG TTT GCG GCA CCT AAA CGC TCC TAA TAG AGA AAA AAA AAA AA /3ThioMC3-D/
3SH9A Fe3E	GCG GCA TGC GCG TTT GCG GCA CCT AAA CGC TCC TAA TAG AGA AAA AAA AAA AAA AA /3ThioMC3-D/
Alx-Q rFe3S	/5Alex647N/ CTC TAT TArG GGA GAC TCG CAT GCC GC /3IAbRQSp/

/5ThioMC6-D/ represents 5′ thiol modification; /3ThioMC3-D/ stands for 3′ thiol modification; /3AlexF488N/ represents 3′ Alexa488 fluorophore; /5Alex647N/ represents 5′ Alexa647 fluorophore; /5IABkFQ/ stands for 5′ Iowa Black FQ quencher; /3IAbRQSp/ stands for 3′ Iowa Black RQ quencher.

Table 4.2 FAM-labeled all-DNA substrate strands of Fe(II) and Fe(III) DNAzymes for cellular delivery tests, and quencher-labeled enzyme strands for activity tests.

Name	Sequences (5′ to 3′)
dFe2S 3FAM	C GGA CCC GTA TCA ATC TCA CGT ATA GGA TAT CCA /36-FAM/
NM Fe2E	TGG ATA TCT CCT AGC CAG ACT GTT ATG TGT GAT ACG GCA AAC TTC GTG ATG CCT CTA CGG GTC CG
5Q Fe2E	/5IABkFQ/ TGG ATA TCT CCT AGC CAG ACT GTT ATG TGT GAT ACG GCA AAC TTC GTG ATG CCT CTA CGG GTC CG
dFe3S 5FAM	/56-FAM/ ACC TAT TAG GGA GAC TCG CAT GCC GC
NM Fe3E	GCG GCA TGC GCG TTT GCG GCA CCT AAA CGC TCC TAA TAG AG
3Q Fe3E	GCG GCA TGC GCG TTT GCG GCA CCT AAA CGC TCC TAA TAG AG /3IAbRQSp/

/36-FAM/ represents 3′ FAM fluorophore; /56-FAM/ represents 5′ FAM fluorophore; /5IABkFQ/ stands for 5′ Iowa Black FQ quencher; /3IAbRQSp/ stands for 3′ Iowa Black RQ quencher.

Table 4.3 Fluorophore and quencher labeled all-DNA substrate strands of Fe(II) and Fe(III) DNAzymes as control groups.

Name	Sequences (5′ to 3′)
Alx-Q dFe2S	/5IABkFQ/ C GGA CCC GTA TCA ATC TCA CGT ATA GGA TAT CCA /3AlexF488N/
Alx-Q dFe3S	/5Alex647N/ CTC TAT TAG GGA GAC TCG CAT GCC GC /3IAbRQSp/

4.2.2 Functionalization of gold nanoparticles (AuNPs) with Fe(II) or Fe(III) DNAzyme

In the following protocols, Fe DNAzyme refers to either Fe(II) or Fe(III) DNAzymes. FeES-AuNP refers to AuNPs conjugated with either Fe(II) or Fe(III) DNAzymes. Fe2E refers to the enzyme strand of Fe(II) DNAzyme, and Fe3E refers to the enzyme strand of Fe(III) DNAzyme. Similarly, Fe2S refers to the substrate strand of Fe(II) DNAzyme, and Fe3S refers to the substrate strand of Fe(III) DNAzyme.

- **REAGENTS**

Freshly prepared Tris-(2-carboxymethyl)phosphine hydrochloride (TCEP) (10 mM) (Sigma); Ultrapure Tris-(hydroxymethyl) aminomethane (Tris) (Aldrich); Glacier acetic acid (Fisher); Tris acetate buffer (500 mM, pH 8.2); Acetate buffer (500 mM sodium acetate, pH adjusted to 5.2 by acetic acid); NaOH (12 M); NaCl (1M); KCN (2 mM); Buffer A (25 mM Tris acetate, 100 mM NaCl, pH 8.2); Buffer Fe2 (20 mM Bis-Tris, 200 mM NaCl, pH 7.0); Buffer Fe3 (40 mM NaOAc, 5 mM Bis-Tris, 200 mM NaCl, pH 5.5).

- **EQUIPMENT**

Two disposable scintillation vials (20 ml); 1.7 ml MaxyClear Snaplock Microcentrifuge tube (Axygen®, Product # MCT-175-C); benchtop centrifuge (Eppendorf); Fluorometer (Jobin Yvon FluoroMax-P); pH meter (Fisher Scientific Accumet AB15).

- **METHODS**

AuNPs were synthesized following the protocol in Section 2.2.1. The obtained 13 nm

AuNPs were stored in a clean glass container for later use.

To reduce the disulfide linkage of the thiol-modified Fe DNAzyme strand (Table 4.1), 9 μl of 1 mM thiol-DNAzyme was mixed with 1.5 μl of 10 mM TCEP in 500 mM acetate buffer (pH 5.2). After one hour, the reduced thiol-DNAzyme was added to 3 ml of AuNP solution in a clean glass vial while gently shaking by hand to form FeE-AuNP conjugates through gold-thiol bonds. The vial was stored in the dark for a day. On the second day, 30 μl of 500 mM Tris acetate (pH 8.2) buffer and 300 μl of 1 M NaCl were added dropwise while gently shaking. The vial was stored in the dark for at least another day before use.

To transfer FeE-AuNPs from functionalization buffer to reaction buffer, 500 μl of FeE-AuNP was transferred to a 1.7 ml microcentrifuge tube and centrifuged at 16,100*g* for 18 min. The supernatant containing free DNAzyme was removed. Particles were washed two more times with 200 μl of buffer A, then dispersed in 200 μL of buffer Fe2 or buffer Fe3 (see REAGENTS). It is important to use the specific brand of microcentrifuge tubes (mentioned in the equipment section) to prevent adhesion of AuNP to the wall of tubes. The supernatants obtained from all washes were combined and the absorbance at 260 nm measured. The number of DNAzyme strands per AuNP was estimated by subtracting the amount of DNAzyme in the supernatant mixture from the total amount of DNAzyme added into AuNP solution. The extinction coefficient of AuNP is 1.85×10^{8} $M^{-1}cm^{-1}$ at 520 nm.

To anneal the substrate strands (Table 4.1) with the enzyme strands on gold nanoparticles to form FeES-AuNPs, substrate was added to a FeE-AuNP solution to a final ratio of 1.5:1 substrate to enzyme. The solution was heated at 65°C for 5 min, and cooled down at room

temperature for 1 h. The solution was stored at 4°C overnight to allow full hybridization. After overnight incubation, excess substrate was removed by centrifugation and washing with 3 × 200 µl buffer Fe2 or Fe3. Finally, FeES-AuNP was dispersed in 200 µl buffer Fe2 or buffer Fe3 for further use.

4.2.3 Activity tests

- **REAGENTS**

Buffer Fe2 (20 mM Bis-Tris, 200 mM NaCl, pH 7.0); Freshly prepared Fe^{2+} stock solution (100 mM Fe^{2+} in 1.2 mM HCl); Buffer Fe3 (40 mM NaOAc, 5 mM Bis-Tris, 200 mM NaCl, pH 5.5); Freshly prepared Fe^{3+} stock solution (40 mM Fe^{3+} in 100 mM HNO_3).

- **EQUIPMENT**

Fluorometer (Jobin Yvon FluoroMax-P)

- **METHODS**

To test the activity of Fe DNAzymes conjugated to AuNPs, FeES-AuNP was diluted to a concentration of 1 nM in buffer Fe2 or buffer Fe3, accordingly. Fluorescence intensity of Fe2ES-AuNP samples (with Alexa488 fluorophore) was measured using a fluorometer at 495 nm excitation and 520 nm emission over 30 min. Fluorescence intensity of Fe3ES-AuNP samples (with Alexa647 fluorophore) was measured using a fluorometer at 650 nm excitation and 670 nm emission over 30 min. To start the reaction, a 100× stock solution of Fe^{2+} or Fe^{3+} was added into FeES-AuNP solution while stirring.

4.2.4 Stability tests of Fe(II) DNAzyme in the presence of Fenton reactions

- **REAGENTS**

Buffer Fe2 (20 mM Bis-Tris, 200 mM NaCl, pH 7.0); freshly prepared Fe^{2+} stock solution (100 mM $FeCl_2$ in 1.2 mM HCl); Buffer Fe3 (40 mM NaOAc, 5 mM Bis-Tris, 200 mM NaCl, pH 5.5); freshly prepared Fe^{3+} stock solution (40 mM ammonium ferric sulfate in 100 mM HNO_3); 200 μM Fe(II)-EDTA stock solution (400 μM ammonium ferrous sulfate mixed with 800 μM EDTA with equal volume); 20 × H_2O_2 stock solution (1 mM); 20 × ascorbate stock solution (2 mM); 10 × TBE buffer; 10% and 20% Polyacrylamide gel stock; 25% w/w Ammonium persulfate (APS); TEMED (Bio-Rad®); Stop solution with dyes (8 M urea, 50 mM EDTA in 1× TBE buffer, 0.05 % xylene cyanol and 0.05 % bromophenol blue); Stop solution without dyes (8 M urea, 50 mM EDTA in 1× TBE buffer).

- **EQUIPMENT**

Phosphorimager (STORM 840 optical scanner); Electrophoresis power supply.

- **METHODS**

To test the stability of Fe(II) DNAzyme in the presence of Fenton reactions, a couple of Fenton reaction conditions were chosen. First, to evaluate the activity of the DNAzyme as well as the stability of substrate strand, Fe(II) DNAzyme with ^{32}P-labeled substrate strand was subjected to 100 μM $FeCl_2$ or $MnCl_2$ in buffer Fe2 and kept in air. In comparison, the same construct was also subjected to 100 μM Fe(II)-EDTA or Mn(II)-EDTA in the presence of 50 μM H_2O_2 and 100 μM ascorbate in buffer Fe2 to mimic Fenton reaction conditions. The reactions

were sampled at 2-hour, 6-hour, and 12-hour time points. To test the stability of all-DNA enzyme strand, Fe(II) DNAzyme with ^{32}P-labeled enzyme strand was subjected to the same conditions as above and the reactions were sampled at the same time points.

Due to the fact that Tris and Bis-Tris are known to be hydroxyl radical scavengers, buffer Fe2 was replaced with 20 mM MOPS, 100 mM NaCl, pH7.0 for further stability tests. Fe(II) DNAzyme with ^{32}P-labeled substrate or enzyme strand was incubated with 500 μM $FeCl_2$ or 250 μM $MnCl_2$ in MOPS buffer in air. In addition, the Fe(II) DNAzyme was also subjected to 500 μM $FeCl_2$ or 250 μM $MnCl_2$ in the presence of 50 μM H_2O_2 and 100 μM ascorbate. The reactions were sampled at 2-hour, 6-hour, and 12-hour time point to evaluate the stability of Fe(II) DNAzyme over time. The samples were separated by 15% denaturing PAGE and gel images were taken by phosphorimager.

4.2.5 Delivery of Fe(II) and Fe(III) DNAzymes into mammalian cells using G8 polypeptide

- **REAGENTS**

2 × Buffer Fe2 (40 mM Bis-Tris, 400 mM NaCl, pH 7.0); 2 × Buffer Fe3 (80 mM NaOAc, 10 mM Bis-Tris, 400 mM NaCl, pH 5.5); G8 polypeptide stock solution (0.2 mg/ml, pH 6.0); PVBLG-8 stock solution (1 mg/ml).

- **EQUIPMENT**

Zeiss LSM 710 NLO confocal microscope (IGB imaging center at UIUC)

- **METHODS**

Besides of using AuNP based delivery, I also tried using G8 polypeptide to deliver Fe(II) or Fe(III) DNAzyme into the cytosol of HepG8 or HeLa cells. The enzyme and FAM-labeled all-DNA substrate strands of DNAzyme (Table 4.2) were first annealed in buffer Fe2 or buffer Fe3 accordingly by heating up to 75 °C and then cooling down to room temperature over half an hour (Table 4.4). Final concentration of Fe(II) or Fe(III) DNAzyme after annealing was 0.1 mM. DNAzymes were mixed with either PVBLG-8 or G8 polypeptide with volume ratio of 30:1 or 20:1 (*i.e.* 30 μl of G8 was mixed with 1 μl of annealing product), and the mixture was kept at room temperature to allow the formation of complex for at least half an hour. The total amount of DNAzyme for each imaging plate was kept constant at 0.1 nmol.

Table 4.4 Components of annealing reaction.

Components	Volume
Fe2E/Fe3E	1 μl of 1 mM
Fe2S/Fe3S	1 μl of 1 mM
2 × Buffer Fe2/Fe3	5 μl
H_2O	3 μl

The polypeptide-DNAzyme complex was added to HepG2 or HeLa cells grown on imaging plates in Opti-MEM for 4 hours. After four-hour incubation, cells were thoroughly washed with PBS to remove excess complex. Fresh Opti-MEM was added to the cells, followed by Hoechst stain. The delivery efficiency was checked using confocal microscope at 63× magnification.

4.2.6 Delivery of Fe(II) DNAzyme into bacterial cells

4.2.6.1 Preparation of calcium competent cells for heat shock

- **REAGENTS**

100 ml of autoclaved LB medium; 1 L of 100 mM $CaCl_2$ (cold); 1L of 100 mM $MgCl_2$ (cold); 100 ml of 85 mM $CaCl_2$, 15% glycerol (v/v) (cold); LB plate.

- **EQUIPMENT**

Centrifuge; Shaker at 37 °C.

- **METHODS**

On day 1, streak out frozen glycerol stock of bacterial cells onto an LB plate. Grow plate overnight at 37 °C. On day 2, select a single colony of *E. coli* from the LB plate and inoculate a 5 ml starter culture of LB. Grow culture at 37 °C in shaker overnight. On day 3, inoculate 100 ml of LB media with 1 ml overnight culture. Grow culture at 37 °C in shaker and measure the OD_{600} every hour until OD_{600} reaches 0.2~0.3 (normally it takes about 2 hours). Inoculate another 100 ml of LB medium with 5 ml of the above culture, and grow at 37 °C in shaker until OD_{600} reaches 0.2~0.3 again. It is important not to let the OD get any higher than 0.4.

When the OD_{600} reaches 0.2~0.3, immediately put the cells on ice. Chill the culture for 20-30 minutes, swirling occasionally to ensure even cooling. Place centrifuge tubes on ice at this time. Split the 100 ml culture into 2 parts by pouring 50 ml into ice cold centrifuge tubes. Harvest cells by centrifugation at 4000 rpm for 15 minutes at 4 °C. Decant the supernatant gently and resuspend each pellet in about 20 ml of ice cold $MgCl_2$. Harvest cells by centrifugation at

3000 rpm for 15 minutes at 4 °C. Decant the supernatant gently and resuspend each pellet in about 20 ml of ice cold $CaCl_2$. Harvest cells by centrifugation at 3000 rpm for 15 minutes at 4 °C. Decant the supernatant gently and resuspend each pellet in about 10 ml of ice cold 85 mM $CaCl_2$, 15% glycerol. Harvest cells by centrifugation at 2100 rpm for 15 minutes. Decant the supernatant and resuspend the pellet in 2 ml of ice cold 85 mM $CaCl_2$, 15% glycerol. Aliquot 100 µl into sterile 1.5 ml microfuge tubes and snap freeze with liquid nitrogen. Store frozen cells in -80 °C freezer.

4.2.6.2 Heat shock

Take out competent cells from the freezer and put them on ice until they thaw. 1 nmol of Fe(II) DNAzyme was annealed in Buffer Fe2 (20 mM Bis-Tris, 200 mM NaCl, pH 7.0) and added to 100 µl of competent cells on ice. Heat shock competent cells in 42 °C water bath for 45 seconds. Immediately put back on ice after heat shock. Wait for 5 minutes before adding 1 ml of LB into each tube of competent cells. Grow the cells at 37 °C for 30 minutes, and centrifuge the cells at 3000 rpm for 2 minutes. Discard supernant and wash cells with PBS for two times. Eventually, resuspend cells in PBS for flow cytometry.

4.2.6.3 Preparation of competent cells for electroporation

On day 1, streak out frozen glycerol stock of bacterial cells onto an LB plate. Grow plate overnight at 37 °C. On day 2, select a single colony of *E. coli* from the LB plate and inoculate a 5 ml starter culture of LB. Grow culture at 37 °C in shaker overnight. On day 3, inoculate 5 ml of LB media with 100 µl overnight culture. Grow culture at 37 °C in shaker and measure the OD_{600} every hour until OD_{600} reaches 0.2~0.3. Inoculate 5 ml of LB media with 100 µl of the

aforementioned culture and grow until OD_{600} reaches 0.2~0.3 again. Place a bottle of Millipore water on ice to keep it cold. Centrifuge down cells at 3500 rpm for 10 min. Discard supernatant and add 25-50 ml of cold Millipore H_2O. Resuspend cells and centrifuge again. Repeat washing step at least three more times to make sure all the salt is removed. At the end, resuspend cells in 1 ml of cold Millipore water. Aliquot 100 µl into sterile 1.5 ml microfuge tubes.

4.2.6.4 Electroporation

Place electroporation cuvettes on ice before use. Mix cells (100 µl) with 4 µl of annealed Fe(II) DNAzyme (Table 4.5, total amount of DNAzyme is 1 nmol) and transfer it to the cuvette. Turn on the electroporator, and increase the value on the board to 2.00 using raise button. Push TIME CONST button to see elapsed time. Place the cuvette in the instrument. Make sure that the metal ends are well connected to the metal walls of electrode. Push both red buttons together and hold until a beep is heard. Transfer the cells into clean microfuge tubes, and add LB medium to let cells recover at 37 °C for 30 minutes. Centrifuge down cells at 3000 rpm for 2 minutes and discard supernatant. Wash the cells twice with PBS and eventually resuspend cells in PBS.

Table 4.5 Annealing reaction of Fe(II) DNAzyme for electroporation.

Components	Volume
Fe2E	1.5 µl of 1 mM
Fe2S	1.5 µl of 1 mM
2 × Buffer Fe2	1.5 µl
H_2O	1.5 µl

4.2.7 Detection of Fe(II) in mammalian cells using AuNP-Fe(II) DNAzyme probe

- **REAGENTS**

Freshly prepared 100 × ammonium ferrous sulfate (10 mM and 50 mM); PBS solution; Dulbecco's modification of Eagle's medium (DMEM); Opti-MEM (Gibco®); Fetal Bovine Serum (FBS); penicillin; streptomycin; trypsin-EDTA (0.25%); Hoechst 33258 (Invitrogen®).

- **EQUIPMENT**

Zeiss LSM 710 NLO confocal microscope (IGB imaging center at UIUC)

- **METHODS**

After incubating HeLa cells with ammonium ferrous sulfate for 17 hours, cells were thoroughly washed with PBS. 2 mL of Opti-MEM containing 5 nM Fe2ES-AuNP was added to each glass-bottom dish. After 2 hours, cells were washed with PBS three times and fresh Opti-MEM was added. Cells were further stained for 20 minutes with Hoechst 33258 (Invitrogen) at a final concentration of 2.5 ng/mL. Images were obtained using a Zeiss LSM 710 NLO confocal microscope at 63x magnification equipped with a Mai-Tai Ti-Sapphire laser. Fluorescence emission was measured over 450-520 nm and 500-570 nm ranges, with excitation at 401 nm for Hoechst stain and 488 nm for Alexa488 fluorophore, respectively. The pinhole and gain settings were kept constant throughout the whole imaging process. Z-stack images were also obtained to confirm that the fluorescent signal were inside cells.

4.2.8 Flow cytometry of HeLa cells delivered with AuNP-Fe(II) DNAzyme

HeLa cells were grown with or without ammonium ferrous sulfate in culture media in a

24-well plate for 17 hours. After washing cells thoroughly with PBS for five times, Opti-MEM containing 5 nM active Fe2ES-AuNP was added to cells. After 2-hour incubation, cells were washed with PBS and detached from the culture plate by 0.25% trypsin. The suspended cell solution was centrifuged at 2,000 g for 5 min and washed with PBS three times. Flow cytometry was performed using a BD FACSCanto system under 488 nm excitation. Control cells without any treatment were used to set the gating.

4.2.9 Flow cytometry of bacterial cells delivered with Fe(II) DNAzyme

Fe(II) DNAzyme was delivered into competent cells made from wild-type *E.coli* or *E.coli* mutants, such as Fur^- or *lacZ feo tonB* mutants, by heat shock or electroporation (Section 4.2.6). After recovering in LB medium for 10 min at 37 °C, cells were centrifuged at 4,000 rpm in benchtop centrifuge, and washed thoroughly with PBS for 2 times. It is important to do this washing step, since excess fluorophore-labeled DNAzyme in solution will give high fluorescent signal in flow cytometry results too, although they are not inside cells. This would cause false positive signals. Cells were kept on ice until they were measured by flow cytometry to reduce signal dilution due to cell division. Flow cytometry was performed using a BD FACSCanto system under 488 nm excitation. Control cells without any treatment were used to set the gating.

4.3 Results and discussions

4.3.1 Activity of AuNP-Fe(II) DNAzyme probe in buffer

Fe(II) DNAzymes with different lengths of polyA linker were successfully conjugated to the surface of AuNPs following the protocol in Section 4.2.2 (Figure 4.1). To test whether these DNAzyme-AuNP conjugates maintained their activity, I tested their activity in the presence of various concentrations of Fe^{2+} in buffer. As shown in Figure 4.2, all the three conjugates showed increased fluorescence over time in the presence of Fe^{2+}, suggesting that the Fe(II) DNAzyme was still active after the functionalization step. The Fe(II) DNAzyme with a 9A linker showed relatively lower turn-on fluorescence compared with the other two constructs. 12A and 15A linker showed very similar response to Fe^{2+}. Therefore, 12A linker was chosen for further studies, since shorter construct might lead to more dense packing of DNAzymes on the surface of AuNPs and therefore more cellular uptake.

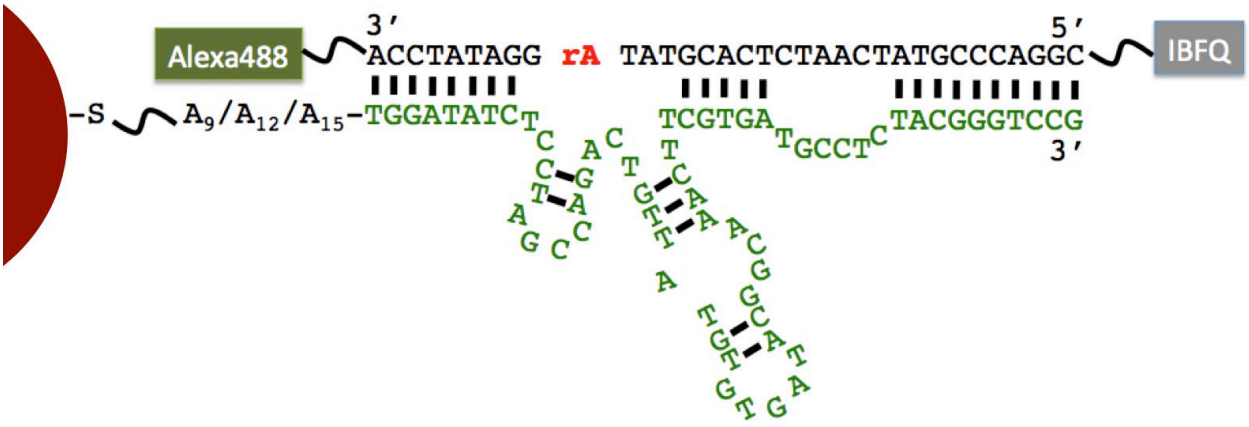

Figure 4.1 Scheme of the AuNP-Fe(II) DNAzyme probe.

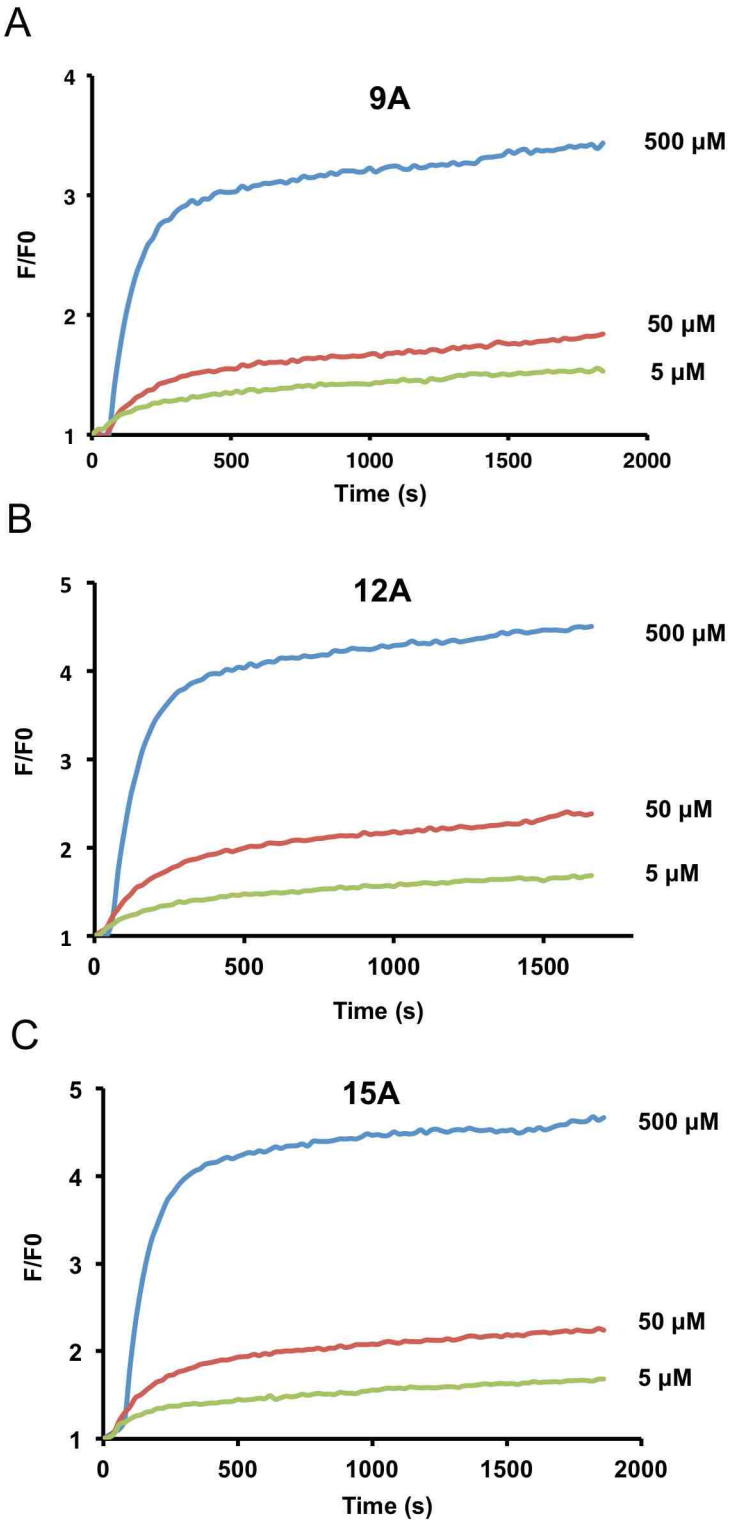

Figure 4.2 Activity of Fe(II) DNAzyme with different lengths of polyA linker (9A, 12A and 15A) conjugated to AuNPs.

Functionalization of Fe(III) DNAzyme onto AuNP surface was performed using the same protocol (Figure 4.3). However, I observed aggregation of AuNPs in the last step (centrifugation) of functionalization. Since the AuNP-Fe(III) DNAzyme conjugates could not be redispersed by pipetting, I tried using sonication to resuspend the conjugates. However, the obtained probe was not active in the presence of Fe^{3+} during activity tests. Therefore, it still needs further optimization to make an active AuNP-Fe(III) DNAzyme probe.

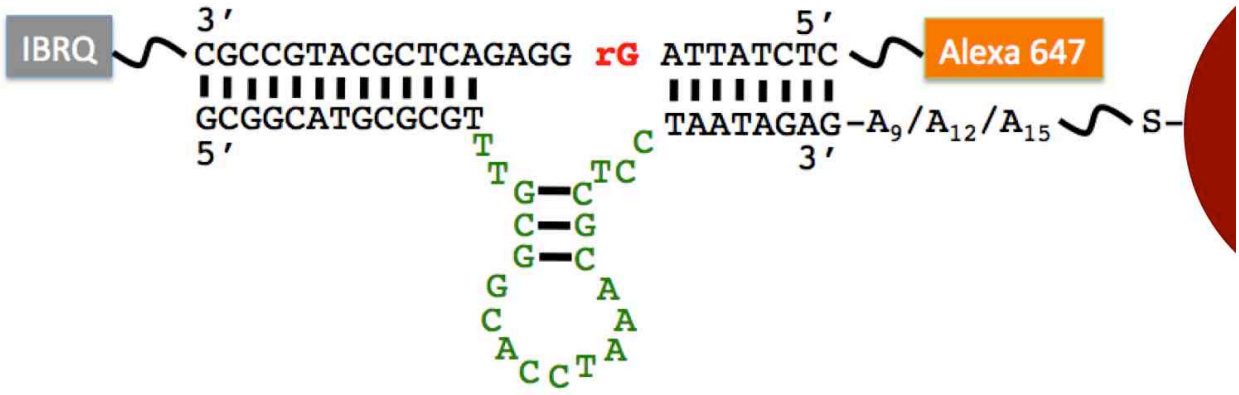

Figure 4.3 Scheme of the AuNP-Fe(III) DNAzyme probe.

4.3.2 Detection of Fe^{2+} in mammalian cells using AuNP-Fe(II) DNAzyme probe

Having demonstrated that Fe(II) DNAzyme can be conjugated to AuNPs to form an active fluorescent probe for Fe^{2+} detection, I incubated HeLa cells pre-treated with ammonium ferric sulfate (final concentrations at 100 μM, 500 μM) with the AuNP-Fe(II) DNAzyme probe. HeLa cells without pre-treatment were used as a control. From obtained fluorescent images, there was not significant difference in the FAM signal between the control and cells pretreated with 100 μM iron salt. When cells were incubated with 500 μM iron salt, the turn-on fluorescence from FAM was obvious (Figure 4.4), suggesting that the AuNP-Fe(II) DNAzyme

was likely to be active in the cellular environment. However, before we can make the final conclusion, a negative control experiment in which an inactive enzyme or non-cleavable substrate is used should be performed, in order to rule out the possibility that the turn-on signal was due to non-specific degradation of the DNAzyme inside cells.

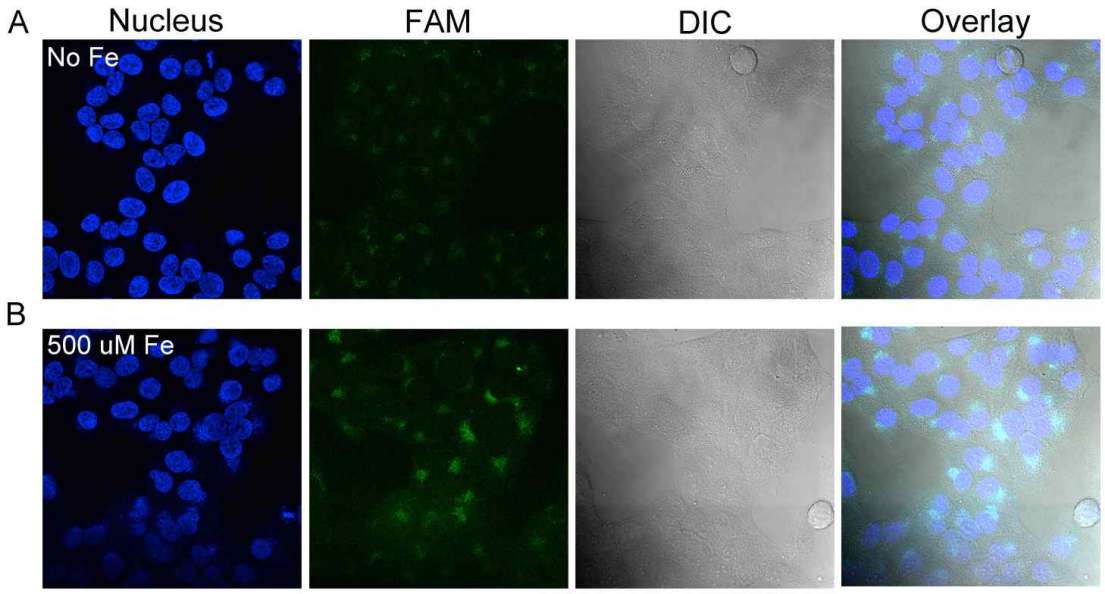

Figure 4.4 Fluorescent images of HeLa cells treated with or without 500 μM ammonium ferric sulfate and delivered with active AuNP-Fe(II) DNAzyme probes.

4.3.3 Delivery of Fe(II) and Fe(III) DNAzymes into mammalian cells using G8 polypeptide

HepG2 cell, a human liver carcinoma cell line, has been commonly used as a model cell line for testing iron sensors, since liver is known as the main organ for iron storage in human body. Therefore, I chose to test the delivery of Fe(II) and Fe(III) DNAzymes into both HepG2 and HeLa cells. In order to reduce non-specific degradation at the cleavage site during delivery, an all-DNA substrate strand modified with a FAM fluorophore was used to form complex with

the unmodified enzyme strand.

In Figure 4.5 and Figure 4.6, HepG2 cells were delivered with G8-Fe(II) DNAzyme complex. The upper panel shows nucleus stain and FAM fluorescence from DNAzyme, and the lower panel shows DIC images of cells. HelpG2 cells tend to grow in clusters, and the FAM fluorescence mainly came from cell membranes on the edge of cell clusters, suggesting that the DNAzyme did not enter cells effectively.

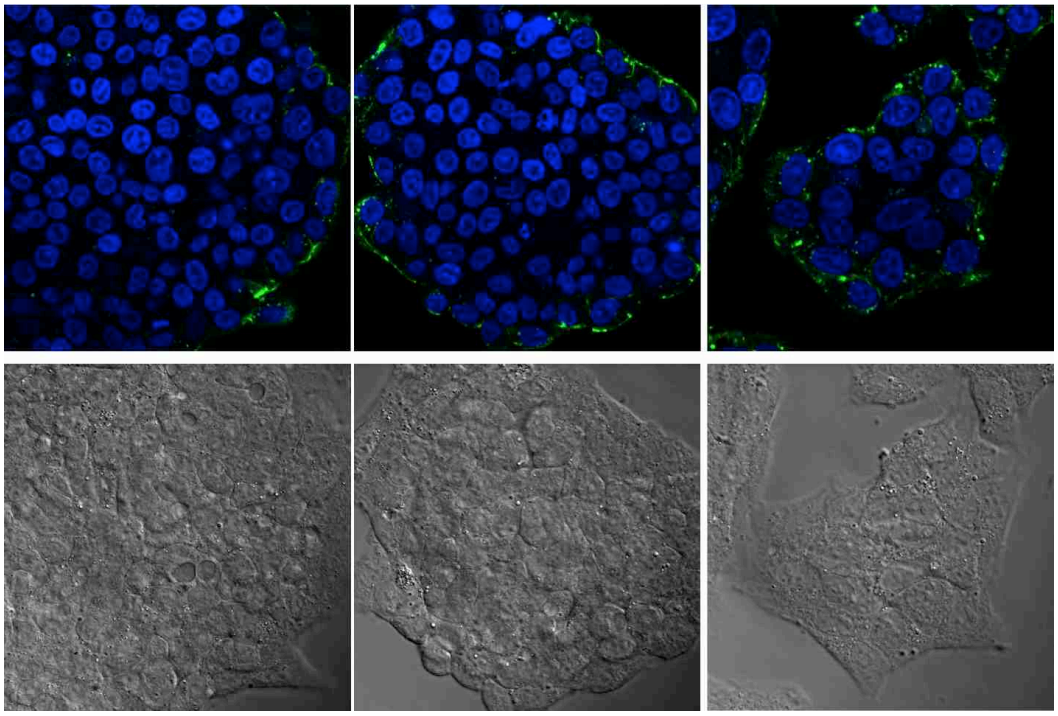

Figure 4.5 Fluorescent images of HepG2 cells delivered with Fe(II) DNAzyme (volume ratio of 20:1).

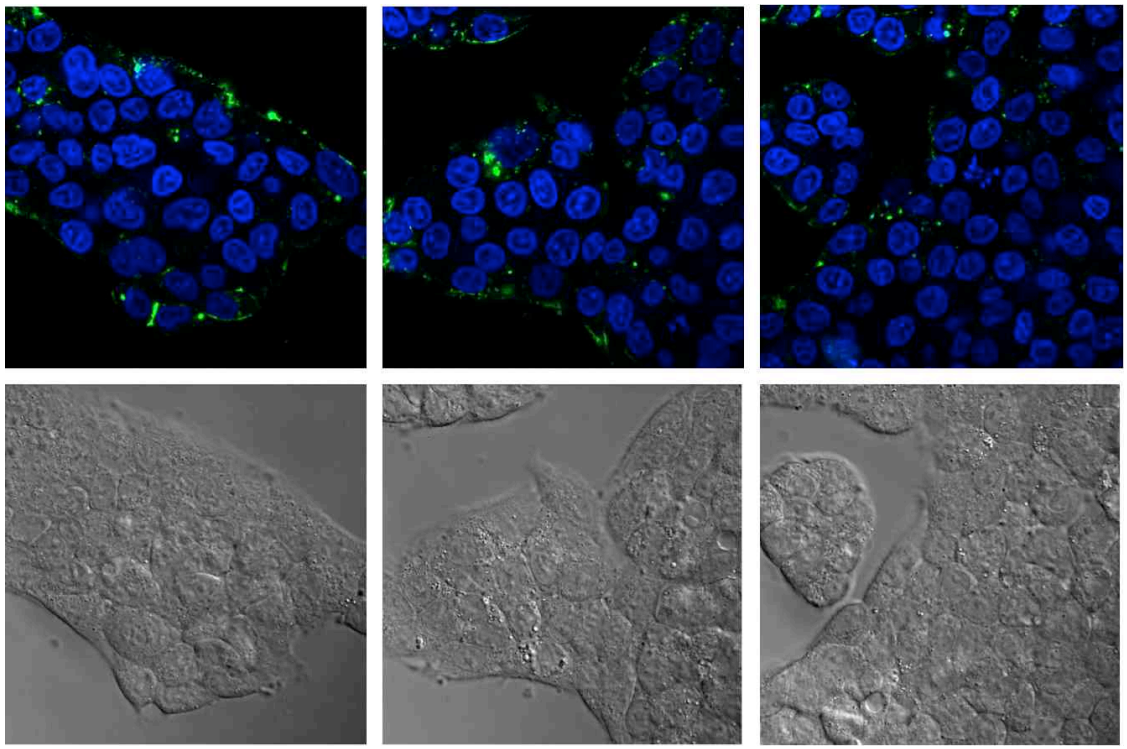

Figure 4.6 Fluorescent images of HepG2 cells delivered with Fe(II) DNAzyme (volume ratio of 30:1).

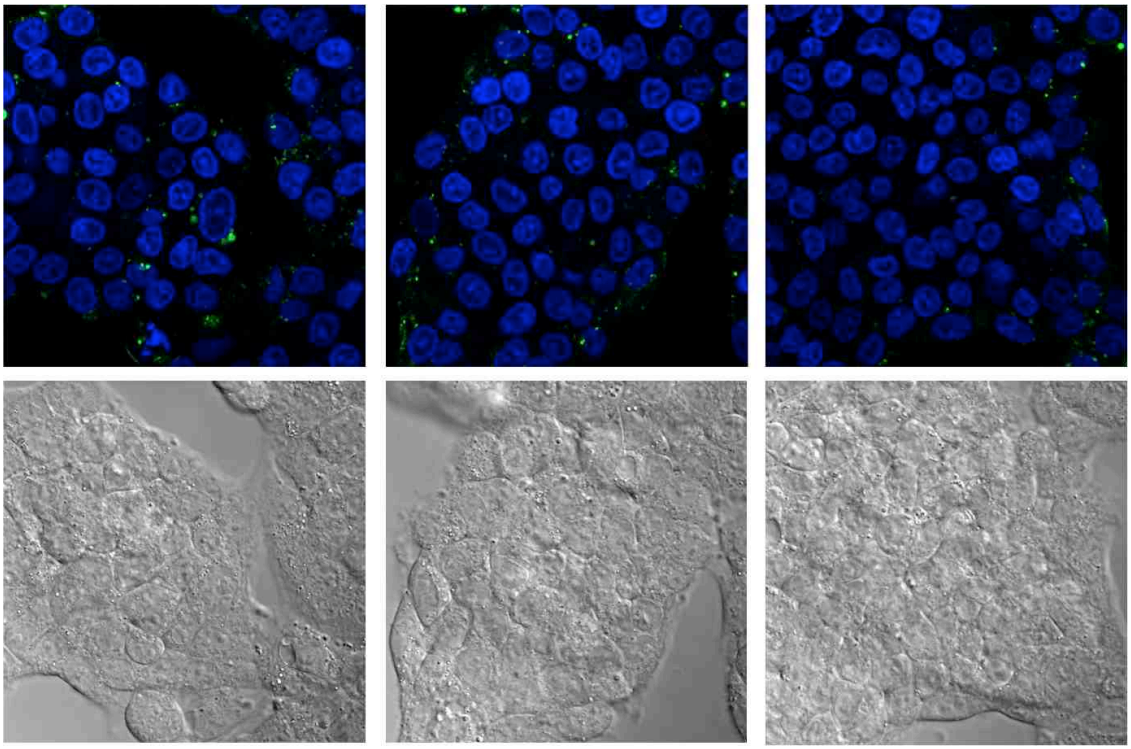

Figure 4.7 HepG2 cells delivered with complex formed by G8 polypeptide and 8-17 DNAzyme (volume ratio of 20:1)

Such low delivery efficiency was out of my expectation, since G8 has been shown to deliver 8-17 DNAzyme and Na DNAzyme with very good efficiency in HeLa cells. To see if it is because of the different cell line I used, I looked at the delivery of 8-17 DNAzyme using G8 polypeptide in HepG2 cells. As shown in Figure 4.7, even 8-17 DNAzyme was not able to enter HepG2 cells efficiently with the help of G8 polypeptide, suggesting HepG2 cell is a hard-to-transfect cell line compared with HeLa cells.

In comparison, if HeLa cells were used instead of HepG2, much better delivery efficiency was observed for all the conditions I tried (Figure 4.8). If the total amount of DNAzyme for delivery was increased, brighter FAM fluorescence was observed from cells, suggesting more uptake was achieved (Figure 4.8 A and B). Moreover, increased ratio of G8 to DNAzyme also lead to increased uptake of DNAzyme (Figure 4.8 B and C).

The delivery of Fe(III) DNAzyme by G8 was also tested in HeLa cells. By following the protocol in Section 4.2.5, good delivery was achieved as shown in Figure 4.9. Brighter FAM fluorescence was observed from cells if the total amount of DNAzyme for delivery was increased (Figure 4.9 A and B). If the ratio of G8 to DNAzyme was increased, more uptake of DNAzyme was observed (Figure 4.9 B and C).

In summary, transfection of HepG2 cells with DNAzymes using G8 polypeptide did not give efficient delivery. No obvious FAM signal was observed inside cells, and some amount of FAM signal was observed from the cell membrane at the outer layer of cell clusters. In contrast, using the same transfection conditions, both Fe(II) and Fe(III) DNAzymes were able to enter HeLa cells with large quantity, and showed cytosol localization. These results suggest that HepG2 is a hard-to-transfect cell line compared with HeLa cells, and a more potent delivery

method should be used to achieve high delivery efficiency in HepG2 cells. Therefore, HeLa cells supplemented with iron seem to be a better choice for initial tests of Fe(II)/Fe(III) DNAzyme-based sensors.

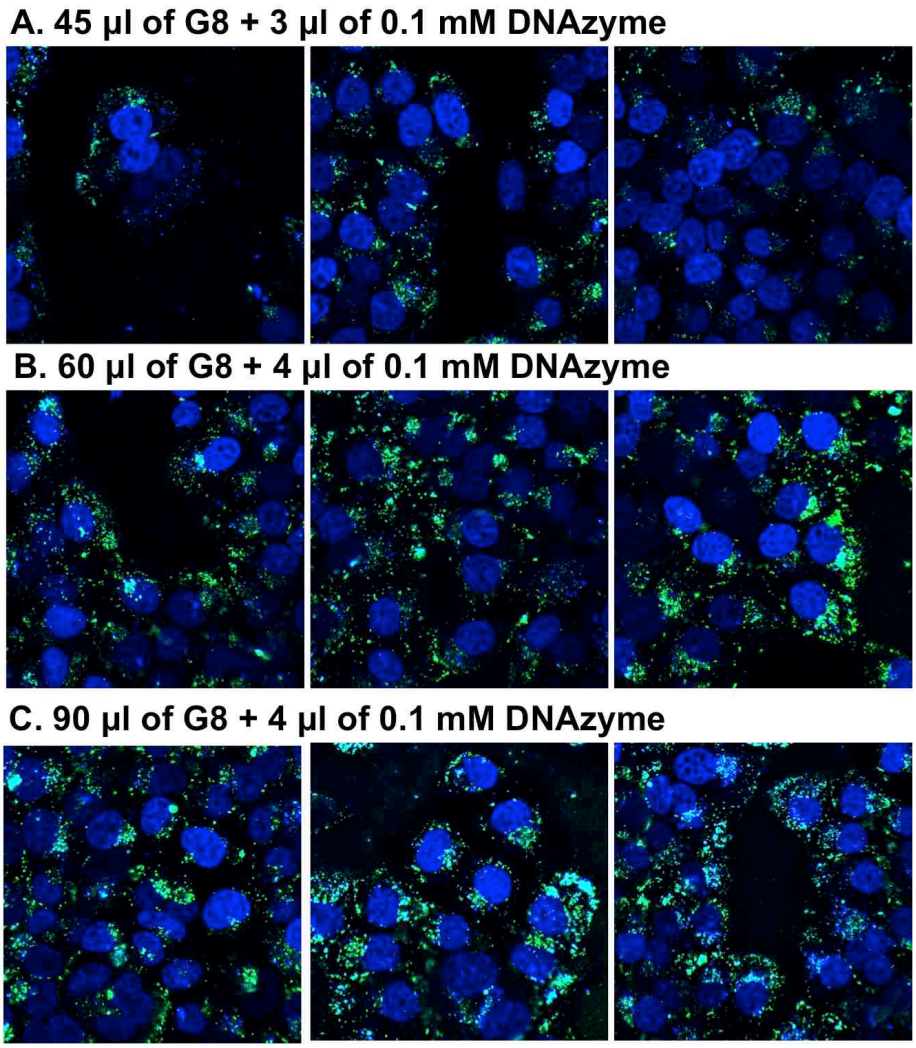

Figure 4.8 HeLa cells delivered with Fe(II) DNAzymes with different ratios of G8 polypeptide to DNAzyme.

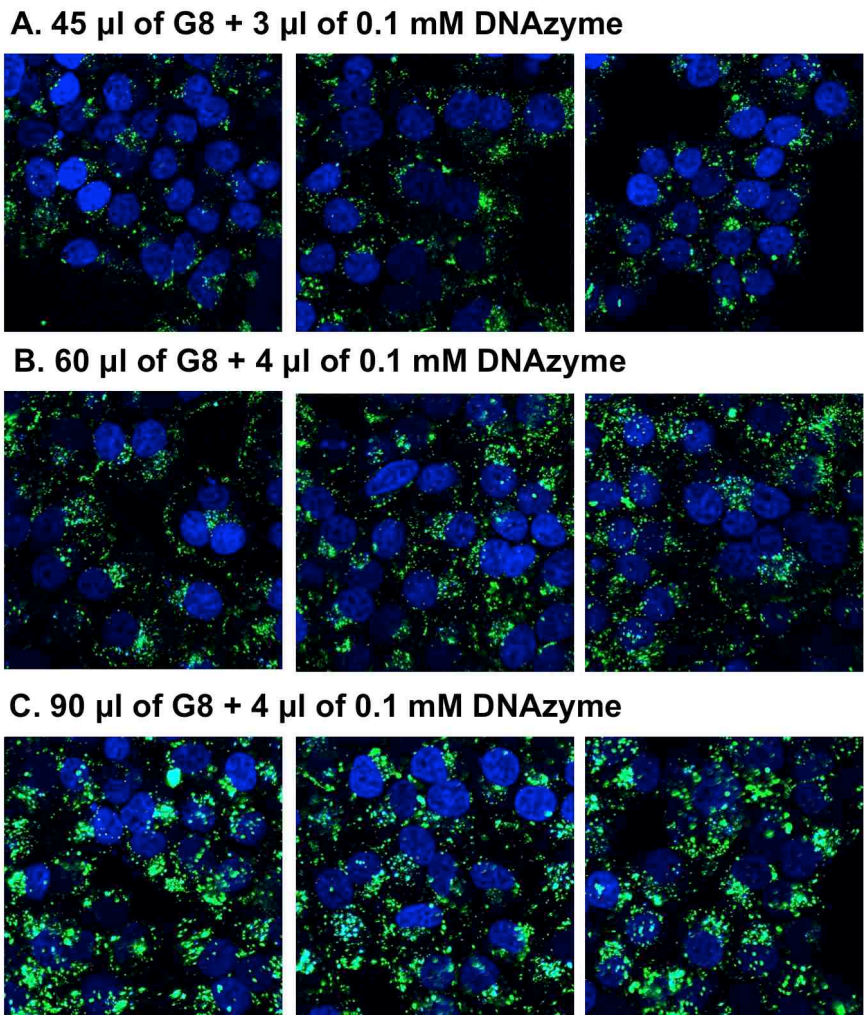

Figure 4.9 HeLa cells delivered with Fe(III) DNAzymes with different ratios of G8 polypeptide to DNAzyme.

4.3.4 Delivery of Fe(II) DNAzymes into bacterial cells

Three *E. coli* strains, a wild-type E. coli, a Fur$^-$ mutant and a *lacZ feo tonB* mutant, were kindly provide by Dr. James Imlay from Department of Microbiology at University of Illinois at Urbana-Champaign. The *E.coli* Fur$^-$ mutant lacks the global iron repressor protein Fur and constitutively imports iron, resulting in 2-5 times higher intracellular iron concentration versus

wild type *E.coli*. The *lacZ feo tonB* mutant is defective in import of ferrous iron and ferric chelates and serves as a low iron control. These mutants will allow us to evaluate the performance of our sensors over the full range of physiologically possible Fe^{2+} ranges, and will allow us to compare our results with established standard techniques (EPR after desferrioxamine treatment for Fe^{2+}, as developed by the Imlay lab).

Electroporation was first used to deliver Fe(II) DNAzyme into wild-type *E.coli* cells. Preparation of competent cells was performed by following the protocol in Section 4.2.6.1. As shown in Figure 4.10, in general, the mean of FAM fluorescence shifted toward a higher value as the amount of FAM-labeled Fe(II) DNAzyme increased from 0.05 nmol to 1 nmol. The distributions of FAM fluorescence in the cell populations showed very large variations, as reflected by the broad peaks from flow cytometry. Such a broad peak might be a potential issue for further studies, since it is harder to observe a consistent turn-on signal from a whole cell population with large variations in sensor uptake. In the mean time, uptake of Fe(III) DNAzyme was test using the wild-type *E.coli* cells too. Similar trends were observed for Fe(III) DNAzyme, and further optimization on electroporation needs to be performed for both DNAzymes to achieve a more even loading of sensor molecules and therefore a sharper peak of fluorescence from the whole population.

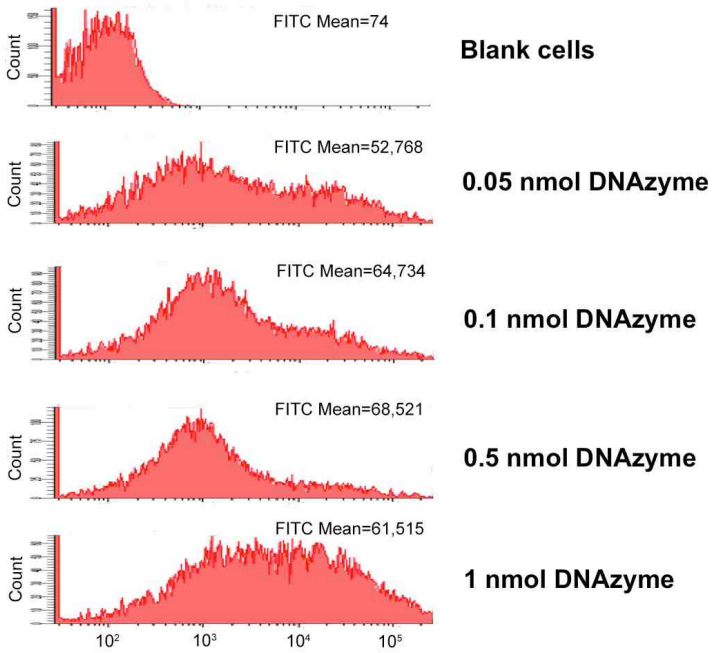

Figure 4.10 Flow cytometry measurement of wild-type *E. coli* cells delivered with different amounts of Fe(II) DNAzymes via electroporation.

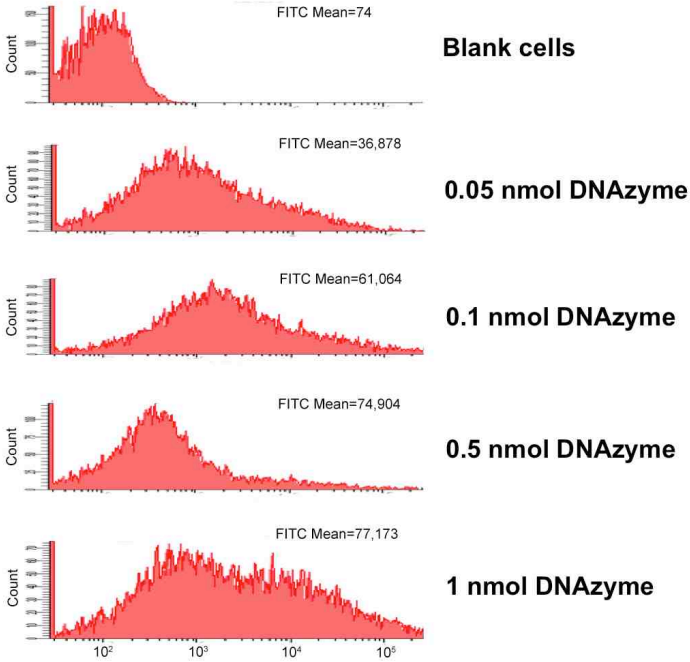

Figure 4.11 Flow cytometry measurement of wild-type *E. coli* cells delivered with different amounts of Fe(III) DNAzymes via electroporation.

One potential issue with electroporation is that it requires no metal ions in the competent cell solution in order to achieve efficient delivery. However, DNAzymes generally need mM amount of monovalent or divalent metal ions to keep the hybridization between the enzyme strand and substrate strand. Once they are added to the competent cells without ions, DNAzymes might undergo dehybridization, leading to single-stranded DNA that are less stable and inactive.

In order to circumvent this potential problem, I used heat shock as an alternative approach, since it does not require the competent cell solution to be free of metal ions. Heat shock showed more homogenous loading of DNAzymes, as reflected by sharper peaks of fluorescence associated with the whole cell populations (Figure 4.12 and Figure 4.13). Wild-type *E.coli*, Fur^- mutant and *lacZ feo tonB* mutant all showed increased fluorescence with increased amounts of DNAzymes for heat shock. It was also found that higher concentrations of DNAzyme and lower cell density normally lead to more uptake of DNAzyme per single cell. Therefore, it is recommended to use lower cell density and higher DNAzyme concentration to achieve sufficient loading of the sensor, as long as the number of cells is sufficient for later tests, such as flow cytometry and imaging.

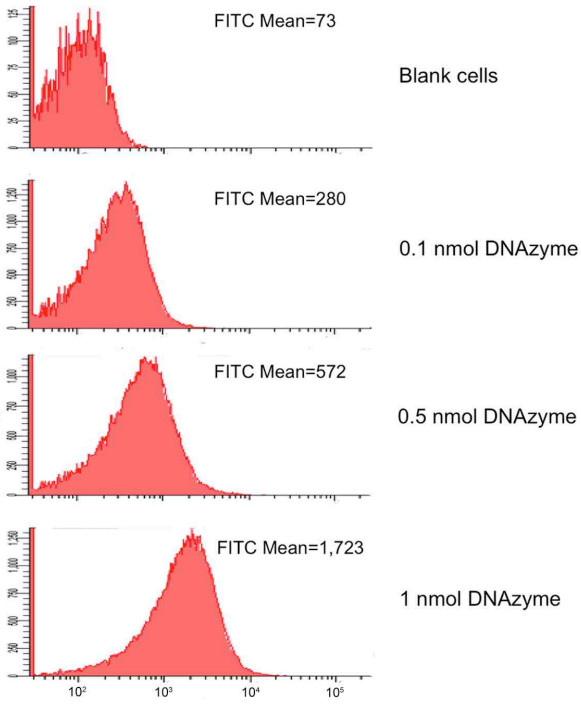

Figure 4.12 Flow cytometry measurement of *E. coli* Fur⁻ mutant delivered with different amounts of Fe(II) DNAzymes via heat shock.

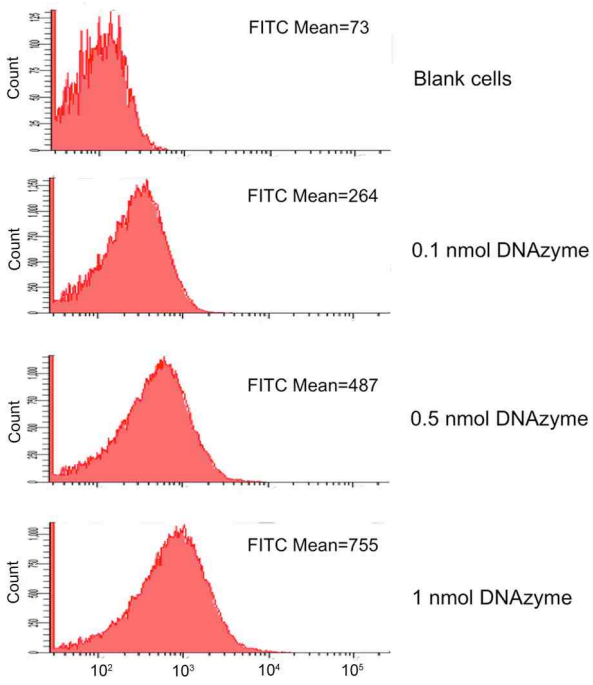

Figure 4.13 Flow cytometry measurement of *E. coli lacZ feo tonB* mutant delivered with different amounts of Fe(II) DNAzymes via heat shock.

4.3.5 Detection of labile Fe^{2+} in *E. coli* mutants using Fe(II) DNAzyme

Initial attempt to detect labile Fe^{2+} in *E. coli* was carried out using heat shock to deliver Fe(II) DNAzyme into bacterial cells. Three strains were used, including wild type *E. coli*, one high-iron mutant Fur^-, and one low-iron mutant *lacZ feo tonB*. Cells were recovered in LB medium for half an hour after heat shock, and centrifuges and washed with PBS for two times before the first flow cytometry measurement. This measurement served as the 0 time point. Cells were kept on ice for another hour, and measured by flow cytometry again. As shown in Figure 4.14, the top panel shows the fluorescence distribution at 0 time point, and the bottom panel corresponds to the one hour time point for three strains, respectively. No significant change in fluorescence was observed for any of the strains, suggesting that our sensor did not turn on under the test conditions. Many factors could contribute to the failure of this initial trial. It could be because the recovering time was too long and most of the DNAzyme had been cleaved at 0 time point. Or the DNAzyme construct was not stable inside bacteria, since bacteria are known to degrade foreign DNA quickly with different exo- or endo-nucleases. Further optimization is needed in order to find the best timing for tests and photocaged DNAzymes might need to be incorporated in order to increase the stability of DNAzymes.

4.3.6 Stability of Fe(II) DNAzyme in the presence of Fenton reactions

Since iron is known to be involved in the generation of ROS in bacteria, I tested the stability of Fe(II) DNAzyme under several conditions that mimic Fenton reactions. The enzyme strand of Fe(II) DNAzyme was radioisotope labeled, and the DNAzyme complex was also subjected to 100 μM Fe(II)-EDTA or Mn(II)-EDTA in the presence of 50 μM H_2O_2 and 100 μM ascorbate in buffer in the air. No cleavage was observed for these conditions for up to 12 hours,

indicating that our DNAzyme was stable under the conditions we will study with.

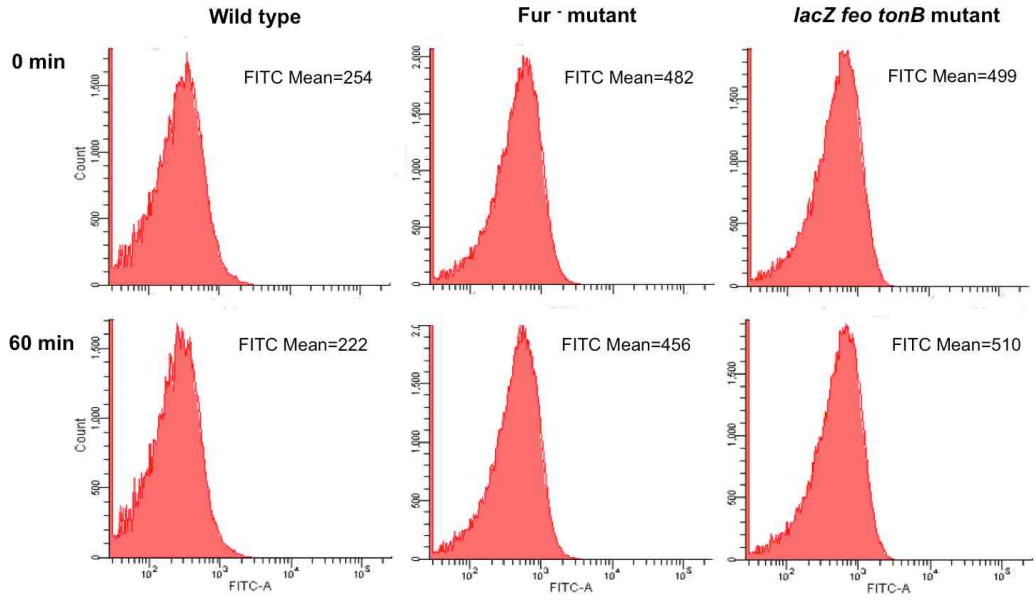

Figure 4.14 Flow cytometry measurement of *E. coli* wild type, Fur- mutant, and *lacZ feo tonB* mutant delivered with Fe(II) DNAzyme sensors at 0 min and 60 min.

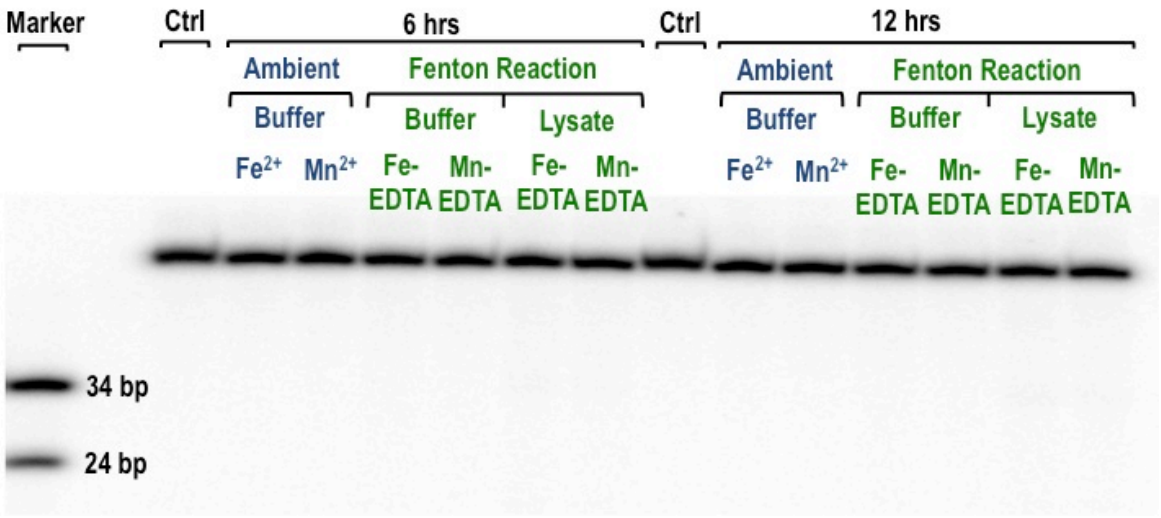

Figure 4.15 Stability of the enzyme strand of Fe(II) DNAzyme in the presence of Fenton reactions.

4.4 Conclusions

In summary, delivery of Fe(II) and Fe(III) DNAzyme into mammalian cells was carried out using both polypeptide-based method and AuNP-based method. Although HepG2 is the most commonly used cell line for iron sensors, it turned out to be a hard-to-transfect cell line compared with HeLa cell, and therefore different delivery vehicles should be chosen in order to achieve sufficient sensor loading. Activity test of AuNP-Fe(II) DNAzyme conjugates in living HeLa cells was performed with HeLa cells supplemented with 100 μM and 500 μM iron. Turn-on fluorescence was observed from the sensors in cells with 500 μM iron. This is a very encouraging result, although more control experiments with non-cleavable substrate strand or inactive enzyme strand need to be conducted before we can confirm that the signal was actually due to the activity of the DNAzyme in the presence of Fe^{2+}.

Moving to the bacteria system, different delivery strategies were chosen in order to achieve sufficient loading of the sensors. Both electroporation and heat shock were tested, and the activity of Fe(II) DNAzyme inside bacteria was initially tested in three mutants that would cover a wide range of physiologically possible concentrations of iron. However, no turn-on signal was observed for these mutants, and further optimization is still needed in order to evaluate the stability of DNAzyme inside living bacteria and the proper timing for measurements.

One potential issue of using the current Fe(III) DNAzyme for intracellular sensing might be that the DNAzyme is Bis-Tris dependent. The DNAzyme is not very active in the presence of Fe^{3+} alone, and it needs certain amount of Bis-Tris in the buffer to perform the reaction. In addition, the DNAzyme has a very narrow working range. It is most active at pH 5.5, while its activity is almost completely lost when pH increases to 6.5. This Bis-Tris dependence needs to

be better characterized in order to evaluate the possibility of utilizing this DNAzyme for intracellular application, since Bis-Tirs is not a common ligand found in the natural biological system. Otherwise, re-selection of a Fe(III) DNAzyme needs to be carried out in order to obtain a different DNAzyme that is not Bis-Tris dependent and has a working pH range close to neutral pH.

4.5 References

1. Andrews NC, Schmidt PJ, Iron homeostasis. *Annu. Rev. Physiol.* **2007** *69*, 69-85.

2. Lawen A, Lane DJ, Mammalian iron homeostasis in health and disease: uptake, storage, transport, and molecular mechanisms of action. *Antioxid. Redox Signal.* **2013** *18*, 2473-2507.

3. Pantopoulos K, Porwal SK, Tartakoff A, Devireddy L, Mechanisms of mammalian iron homeostasis. *Biochemistry* **2012** *51*, 5705-5724.

4. Crichton RR, Wilmet S, Legssyer R, Ward RJ, Molecular and cellular mechanisms of iron homeostasis and toxicity in mammalian cells. *J. Inorg. Biochem.* **2002** *91*, 9-18.

5. Rieske JS, MacLennan DH, Coleman R, Isolation and properties of an iron-protein from the (reduced coenzyme Q)-cytochrome C reductase complex of the respiratory chain. *Biochem. Biophys. Res. Commun.* **1964** *15*, 338-344.

6. Rotig A, de Lonlay P, Chretien D, Foury F, Koenig M, Sidi D, Munnich A, Rustin P, Aconitase and mitochondrial iron-sulphur protein deficiency in Friedreich ataxia. *Nat. Genet.* **1997** *17*, 215-217.

7. Dröse S, Brandt U. Molecular Mechanisms of Superoxide Production by the Mitochondrial Respiratory Chain. In: Kadenbach B, editor. Mitochondrial Oxidative Phosphorylation: Springer New York; 2012. p. 145-169.

8. Netz DJ, Stith CM, Stumpfig M, Kopf G, Vogel D, Genau HM, Stodola JL, Lill R, Burgers PM, Pierik AJ, Eukaryotic DNA polymerases require an iron-sulfur cluster for the formation of active complexes. *Nat. Chem. Biol.* **2012** *8*, 125-132.

9. Stehling O, Vashisht AA, Mascarenhas J, Jonsson ZO, Sharma T, Netz DJ, Pierik AJ, Wohlschlegel JA, Lill R, MMS19 assembles iron-sulfur proteins required for DNA metabolism and genomic integrity. *Science* **2012** *337*, 195-199.

10. Wu Y, Brosh RM, Jr., DNA helicase and helicase-nuclease enzymes with a conserved iron-sulfur cluster. *Nucleic Acids Res.* **2012** *40*, 4247-4260.

11. Pontarin G, Ferraro P, Bee L, Reichard P, Bianchi V, Mammalian ribonucleotide reductase subunit p53R2 is required for mitochondrial DNA replication and DNA repair in quiescent cells. *Proc. Natl. Acad. Sci. U. S. A.* **2012** *109*, 13302-13307.

12. Brissot P, Ropert M, Le Lan C, Loreal O, Non-transferrin bound iron: A key role in iron overload and iron toxicity. *Biochimica Et Biophysica Acta-General Subjects* **2012** *1820*, 403-410.

13. Nunez MT, Urrutia P, Mena N, Aguirre P, Tapia V, Salazar J, Iron toxicity in neurodegeneration. *BioMetals* **2012** *25*, 761-776.

14. Ray PD, Huang BW, Tsuji Y, Reactive oxygen species (ROS) homeostasis and redox regulation in cellular signaling. *Cell. Signal.* **2012** *24*, 981-990.

15. Dixon SJ, Stockwell BR, The role of iron and reactive oxygen species in cell death. *Nat. Chem. Biol.* **2014** *10*, 9-17.

16. Nathan C, Cunningham-Bussel A, Beyond oxidative stress: an immunologist's guide to reactive oxygen species. *Nat. Rev. Immunol.* **2013** *13*, 349-361.

17. Ford GC, Harrison PM, Rice DW, Smith JMA, Treffry A, White JL, Yariv J, Ferritin - Design and Formation of an Iron-Storage Molecule. *Philosophical Transactions of the Royal Society of London Series B-Biological Sciences* **1984** *304*, 551-&.

18. Harrison PM, Arosio P, The ferritins: molecular properties, iron storage function and cellular regulation. *Biochim. Biophys. Acta* **1996** *1275*, 161-203.

19. Chasteen ND, Harrison PM, Mineralization in ferritin: An efficient means of iron storage. *J. Struct. Biol.* **1999** *126*, 182-194.

20. Shi HF, Bencze KZ, Stemmler TL, Philpott CC, A cytosolic iron chaperone that delivers iron to ferritin. *Science* **2008** *320*, 1207-1210.

21. Subramanian P, Rodrigues AV, Ghimire-Rijal S, Stemmler TL, Iron chaperones for mitochondrial Fe-S cluster biosynthesis and ferritin iron storage. *Curr. Opin. Chem. Biol.* **2011** *15*, 312-318.

22. Ebrahimi KH, Bill E, Hagedoorn PL, Hagen WR, The catalytic center of ferritin regulates iron storage via Fe(II)-Fe(III) displacement. *Nat. Chem. Biol.* **2012** *8*, 941-948.

23. Carmona F, Palacios O, Galvez N, Cuesta R, Atrian S, Capdevila M, Dominguez-Vera JM, Ferritin iron uptake and release in the presence of metals and metalloproteins: Chemical implications in the brain. *Coord. Chem. Rev.* **2013** *257*, 2752-2764.

24. Finazzi D, Arosio P, Biology of ferritin in mammals: an update on iron storage, oxidative damage and neurodegeneration. *Arch. Toxicol.* **2014** *88*, 1787-1802.

25. Theil EC, The Ferritin Family of Iron Storage Proteins. *Adv. Enzymol. Relat. Areas Mol. Biol.* **1990** *63*, 421-449.

26. Connor JR, Snyder BS, Beard JL, Fine RE, Mufson EJ, Regional distribution of iron and iron-regulatory proteins in the brain in aging and Alzheimer's disease. *J. Neurosci. Res.* **1992** *31*, 327-335.

27. Cairo G, Pietrangelo A, Iron regulatory proteins in pathobiology. *Biochem. J.* **2000** *352 Pt 2*, 241-250.

28. Eisenstein RS, Iron regulatory proteins and the molecular control of mammalian iron metabolism. *Annu. Rev. Nutr.* **2000** *20*, 627-662.

29. Rouault TA, The role of iron regulatory proteins in mammalian iron homeostasis and disease. *Nat. Chem. Biol.* **2006** *2*, 406-414.

30. Rouault T, Klausner R, Regulation of iron metabolism in eukaryotes. *Curr. Top. Cell. Regul.* **1997** *35*, 1-19.

31. Eisenstein RS, Blemings KP, Iron regulatory proteins, iron responsive elements and iron homeostasis. *J. Nutr.* **1998** *128*, 2295-2298.

32. Thomson AM, Rogers JT, Leedman PJ, Iron-regulatory proteins, iron-responsive elements and ferritin mRNA translation. *Int. J. Biochem. Cell Biol.* **1999** *31*, 1139-1152.

33. Wallander ML, Leibold EA, Eisenstein RS, Molecular control of vertebrate iron homeostasis by iron regulatory proteins. *Biochim. Biophys. Acta* **2006** *1763*, 668-689.

34. Klausner RD, Rouault TA, Harford JB, Regulating the fate of mRNA: the control of cellular iron metabolism. *Cell* **1993** *72*, 19-28.

35. Pantopoulos K, Hentze MW, Nitric oxide signaling to iron-regulatory protein: direct control of ferritin mRNA translation and transferrin receptor mRNA stability in transfected fibroblasts. *Proc. Natl. Acad. Sci. U. S. A.* **1995** *92*, 1267-1271.

36. Hentze MW, Kuhn LC, Molecular control of vertebrate iron metabolism: mRNA-based regulatory circuits operated by iron, nitric oxide, and oxidative stress. *Proc. Natl. Acad. Sci. U. S. A.* **1996** *93*, 8175-8182.

37. Theil EC, Eisenstein RS, Combinatorial mRNA regulation: Iron regulatory proteins and iso-iron-responsive elements (Iso-IREs). *J. Biol. Chem.* **2000** *275*, 40659-40662.

38. Esposito BP, Breuer W, Sirankapracha P, Pootrakul P, Hershko C, Cabantchik ZI, Labile plasma iron in iron overload: redox activity and susceptibility to chelation. *Blood* **2003** *102*, 2670-2677.

39. Park CH, Valore EV, Waring AJ, Ganz T, Hepcidin, a urinary antimicrobial peptide synthesized in the liver. *J. Biol. Chem.* **2001** *276*, 7806-7810.

40. Pigeon C, Ilyin G, Courselaud B, Leroyer P, Turlin B, Brissot P, Loreal O, A new mouse liver-specific gene, encoding a protein homologous to human antimicrobial peptide hepcidin, is overexpressed during iron overload. *J. Biol. Chem.* **2001** *276*, 7811-7819.

41. Nicolas G, Chauvet C, Viatte L, Danan JL, Bigard X, Devaux I, Beaumont C, Kahn A, Vaulont S, The gene encoding the iron regulatory peptide hepcidin is regulated by anemia, hypoxia, and inflammation. *J. Clin. Invest.* **2002** *110*, 1037-1044.

42. Nicolas G, Bennoun M, Porteu A, Mativet S, Beaumont C, Grandchamp B, Sirito M, Sawadogo M, Kahn A, Vaulont S, Severe iron deficiency anemia in transgenic mice expressing liver hepcidin. *Proc. Natl. Acad. Sci. U. S. A.* **2002** *99*, 4596-4601.

43. Nemeth E, Tuttle MS, Powelson J, Vaughn MB, Donovan A, Ward DM, Ganz T, Kaplan J, Hepcidin regulates cellular iron efflux by binding to ferroportin and inducing its internalization. *Science* **2004** *306*, 2090-2093.

44. Nemeth E, Rivera S, Gabayan V, Keller C, Taudorf S, Pedersen BK, Ganz T, IL-6 mediates hypoferremia of inflammation by inducing the synthesis of the iron regulatory hormone hepcidin. *J. Clin. Invest.* **2004** *113*, 1271-1276.

45. Ganz T, Systemic iron homeostasis. *Physiol. Rev.* **2013** *93*, 1721-1741.

46. Ganz T, Nemeth E, Hepcidin and iron homeostasis. *Biochim. Biophys. Acta* **2012** *1823*, 1434-1443.

47. Bates GW, Billups C, Saltman P, The Kinetics and Mechanism of Iron(III) Exchange between Chelates and Transferrin: I. THE COMPLEXES OF CITRATE AND NITRILOTRIACETIC ACID. *J. Biol. Chem.* **1967** *242*, 2810-2815.

48. Princiotto JV, Zapolski EJ, Difference between the two iron-binding sites of transferrin. *Nature* **1975** *255*, 87-88.

49. Ponka P, Beaumont C, Richardson DR, Function and regulation of transferrin and ferritin. *Semin. Hematol.* **1998** *35*, 35-54.

50. Ohgami RS, Campagna DR, Greer EL, Antiochos B, McDonald A, Chen J, Sharp JJ, Fujiwara Y, Barker JE, Fleming MD, Identification of a ferrireductase required for efficient transferrin-dependent iron uptake in erythroid cells. *Nat. Genet.* **2005** *37*, 1264-1269.

51. Aisen P, Entry of iron into cells: a new role for the transferrin receptor in modulating iron release from transferrin. *Ann. Neurol.* **1992** *32 Suppl*, S62-68.

52. Aisen P, Transferrin receptor 1. *Int. J. Biochem. Cell Biol.* **2004** *36*, 2137-2143.

53. Trinder D, Zak O, Aisen P, Transferrin receptor-independent uptake of differic transferrin by human hepatoma cells with antisense inhibition of receptor expression. *Hepatology* **1996** *23*, 1512-1520.

54. Chua AC, Graham RM, Trinder D, Olynyk JK, The regulation of cellular iron metabolism. *Crit. Rev. Clin. Lab. Sci.* **2007** *44*, 413-459.

55. Ponka P, Lok CN, The transferrin receptor: role in health and disease. *Int. J. Biochem. Cell Biol.* **1999** *31*, 1111-1137.

56. Young SP, Bomford A, Williams R, The effect of the iron saturation of transferrin on its binding and uptake by rabbit reticulocytes. *Biochem. J.* **1984** *219*, 505-510.

57. Anderson GJ, Powell LW, Halliday JW, The endocytosis of transferrin by rat intestinal epithelial cells. *Gastroenterology* **1994** *106*, 414-422.

58. Bali PK, Zak O, Aisen P, A new role for the transferrin receptor in the release of iron from transferrin. *Biochemistry* **1991** *30*, 324-328.

59. Wright TL, Brissot P, Ma WL, Weisiger RA, Characterization of Non-Transferrin-Bound Iron Clearance by Rat-Liver. *J. Biol. Chem.* **1986** *261*, 909-914.

60. Craven CM, Alexander J, Eldridge M, Kushner JP, Bernstein S, Kaplan J, Tissue distribution and clearance kinetics of non-transferrin-bound iron in the hypotransferrinemic mouse: a rodent model for hemochromatosis. *Proc. Natl. Acad. Sci. U. S. A.* **1987** *84*, 3457-3461.

61. Hider RC, Nature of nontransferrin-bound iron. *Eur. J. Clin. Investig.* **2002** *32*, 50-54.

62. Kristiansen M, Graversen JH, Jacobsen C, Sonne O, Hoffman HJ, Law SK, Moestrup SK, Identification of the haemoglobin scavenger receptor. *Nature* **2001** *409*, 198-201.

63. Van Gorp H, Delputte PL, Nauwynck HJ, Scavenger receptor CD163, a Jack-of-all-trades and

potential target for cell-directed therapy. *Mol. Immunol.* **2010** *47*, 1650-1660.

64. Weinberg ED, Iron and Susceptibility to Infectious-Disease. *Science* **1974** *184*, 952-956.

65. Weinberg ED, Iron and Infection. *Microbiological Reviews* **1978** *42*, 45-66.

66. Chandra RK, Nutrition, immunity, and infection: present knowledge and future directions. *Lancet* **1983** *1*, 688-691.

67. Chandra RK, Nutrition and the immune system: An introduction. *Am. J. Clin. Nutr.* **1997** *66*, 460-463.

68. Oppenheimer SJ, Iron and its relation to immunity and infectious disease. *J. Nutr.* **2001** *131*, 616S-633S.

69. Skaar EP, The Battle for Iron between Bacterial Pathogens and Their Vertebrate Hosts. *PLoS Pathog.* **2010** *6*.

70. Hood MI, Skaar EP, Nutritional immunity: transition metals at the pathogen-host interface. *Nat. Rev. Microbiol.* **2012** *10*, 525-537.

71. Skaar EP, Schneewind O, Iron-regulated surface determinants (Isd) of Staphylococcus aureus: stealing iron from heme. *Microbes Infect.* **2004** *6*, 390-397.

72. Fabian M, Solomaha E, Olson JS, Maresso AW, Heme transfer to the bacterial cell envelope occurs via a secreted hemophore in the Gram-positive pathogen Bacillus anthracis. *J. Biol. Chem.* **2009** *284*, 32138-32146.

73. Wandersman C, Stojiljkovic I, Bacterial heme sources: the role of heme, hemoprotein receptors and hemophores. *Curr. Opin. Microbiol.* **2000** *3*, 215-220.

74. Mazmanian SK, Skaar EP, Gaspar AH, Humayun M, Gornicki P, Jelenska J, Joachmiak A, Missiakas DM, Schneewind O, Passage of heme-iron across the envelope of Staphylococcus aureus. *Science* **2003** *299*, 906-909.

75. Wandersman C, Delepelaire P, Bacterial iron sources: from siderophores to hemophores. *Annu. Rev. Microbiol.* **2004** *58*, 611-647.

76. Cescau S, Cwerman H, Letoffe S, Delepelaire P, Wandersman C, Biville F, Heme acquisition by hemophores. *BioMetals* **2007** *20*, 603-613.

77. Crosa JH, Genetics and molecular biology of siderophore-mediated iron transport in bacteria. *Microbiol Rev* **1989** *53*, 517-530.

78. Leong J, Neilands JB, Mechanisms of siderophore iron transport in enteric bacteria. *J. Bacteriol.* **1976** *126*, 823-830.

79. Crosa JH, Walsh CT, Genetics and assembly line enzymology of siderophore biosynthesis in bacteria. *Microbiol. Mol. Biol. Rev.* **2002** *66*, 223-249.

80. Griffin AS, West SA, Buckling A, Cooperation and competition in pathogenic bacteria. *Nature*

2004 *430*, 1024-1027.

81. Abergel RJ, Zawadzka AM, Raymond KN, Petrobactin-mediated iron transport in pathogenic bacteria: coordination chemistry of an unusual 3,4-catecholate/citrate siderophore. *J. Am. Chem. Soc.* **2008** *130*, 2124-2125.

82. Domaille DW, Que EL, Chang CJ, Synthetic fluorescent sensors for studying the cell biology of metals. *Nat. Chem. Biol.* **2008** *4*, 168-175.

83. Esposito BP, Epsztejn S, Breuer W, Cabantchik ZI, A review of fluorescence methods for assessing labile iron in cells and biological fluids. *Anal. Biochem.* **2002** *304*, 1-18.

84. Jung HJ, Singh N, Jang DO, Highly Fe(3+) selective ratiometric fluorescent probe based on imine-linked benzimidazole. *Tetrahedron Lett.* **2008** *49*, 2960-2964.

85. Hirayama T, Okuda K, Nagasawa H, A highly selective turn-on fluorescent probe for iron(II) to visualize labile iron in living cells. *Chem. Sci.* **2013** *4*, 1250-1256.

86. Li JB, Hu QH, Yu XL, Zeng Y, Cao CC, Liu XW, Guo J, Pan ZQ, A Novel Rhodamine-Benzimidazole Conjugate as a Highly Selective Turn-on Fluorescent Probe for Fe3+. *J. Fluoresc.* **2011** *21*, 2005-2013.

87. Au-Yeung HY, Chan J, Chantarojsiri T, Chang CJ, Molecular Imaging of Labile Iron(II) Pools in Living Cells with a Turn-On Fluorescent Probe. *J. Am. Chem. Soc.* **2013** *135*, 15165-15173.

5 Chapter 5 Crystallization of DNAzymes

5.1 Introduction

For centuries, bimolecular catalytic ability had been thought to be restricted to the realm of protein. Nucleic acids were considered solely as carriers of hereditary information. However, with the discovery of catalytic RNA (ribozymes) in the 1980s, it became clear that nucleic acids also have the capability of catalyzing chemical reactions.[1,2] DNA molecules entered the realm of catalytic biomolecules in 1994, when the first DNAzyme (also called deoxyribozyme or catalytic DNA) was discovered through a combinatorial process call *in vitro* selection.[3] Although no catalytic DNA has yet been identified in nature, a variety of DNAzymes have been isolated for different types of reactions since then.[4-16] RNA-cleaving DNAzymes using metal ions as their cofactors are of particular interest, due to their fast reaction rate and ease of practical application into metal ion sensors for both environmental detection[12,17-22] and intracellular monitoring of particular metal ion.[16,23,24] Despite numerous practical applications, the mechanism of metallo-DNAzymes' reaction and the role of metal ion in their structure and function are not yet fully understood. It remains unclear how DNA can carry out catalysis with simpler building blocks, fewer functional groups and less diverse structures than ribozymes and proteins. Similarly, the spatial arrangement of the DNAzyme enabling its superior selectivity for one metal ion over others also remains a mystery.

To enrich our understanding of metallo-DNAzymes, our group as well as other groups in the filed has carried out both biochemical and biophysical characterization to probe the active site inside the DNAzyme and its binding pocket for metal ions.[25] However, although these

characterizations provide us with precious information about possible mechanisms and potential folding conformations, their resolution is generally not good enough to differentiate single nucleotides. Without three-dimensional structural information at atomic resolution, we are still puzzled by how the DNAzyme can bind the metal ion selectively and carry out the reaction efficiently, and an atomic resolution structure of a DNAzyme would greatly improve our understanding about the role of metal ion and nucleotide bases in the catalysis. However, unlike the mature fields of ribozyme and protein crystallization, DNA crystallization, especially of molecules with non-canonical structures, remains very challenging.

In 1999, Joyce and co-workers reported the only known crystal structure of a DNAzyme sequence.[26] However, in the crystal, the DNAzyme adopted a four-way junction structure formed by two enzyme strands and two substrate strands, inconsistent with the known stoichiometry of the DNAzyme and indicative of an inactive form. Despite tremendous effort from researchers, a high-resolution structure of DNAzyme with correct conformation is not yet available.

Previously, our lab has obtained DNAzyme crystals based on the 8-17 DNAzyme.[27] However, the quality of the crystal was not good enough to obtain high-resolution diffraction, and we were not able to solve the structure of the crystals due to lack of phasing information. Due to the unavailability of previous structures, the structure cannot be solved from this data by molecular replacement. In order to solve the structure, anomalous diffraction experiments (MAD or SAD) must be performed. To perform these experiments, we need to obtained crystals in which one of the nucleotides is replaced with a Se or Br substituted nucleotide. By collecting the X-ray diffraction data of both native and Se or Br modified DNAzyme crystals, we might be able to solve the structure of 8-17 DNAzyme and elucidate the relationship between structure and

activity of the DNAzyme.

In this chapter, continuous efforts towards obtaining a crystal structure of DNAzyme will be covered, including introducing molecular imprinted polymer to facilitate crystallization process, introducing selenium-modified deoxyribonucleotides for anomalous diffraction experiments, and optimization of cryoprotection techniques to obtain better diffraction.

5.2 Materials and Methods

5.2.1 Sequences

Table 5.1 Sequences of 8-17 DNAzyme used for crystallization study.

Name	Sequences (5′ to 3′)
17S_CGC_D_3A	CGCGAATTCGCGAGGCG A
17E_CGC_D_3T	CGCTCCGAGCCGGTCGAACGCGAATTCGCG T
17S_CGC_D_5A	A CGCGAATTCGCGAGGCG
17E_CGC_Dickerson	CGCTCCGAGCCGGTCGAACGCGAATTCGCG

5.2.2 Purification of DNAzyme for crystallization

All the DNAzyme constructs were purified by PAGE followed by desalting by Sep-Pak column. The obtained solution was dried by speed vacuum and re-dissolved in Millipore water at concentrations as high as possible (usually around 3-4 mM). The accurate concentration was determined by UV spectroscopy. The purity of the DNAzyme was checked by Mass Spec.

5.2.3 Denature and annealing of DNAzymes

The enzyme and substrate strands were mixed together in slightly buffered solution (*e.g.,*

5 mM NaCac, 2 mM $MgCl_2$, pH 6.5) with ratio of 1:1 in PCR tubes. The final concentrations of DNAzyme complex were kept at 0.5-1 mM. The annealing process was conducted in a thermocycler, which was programmed to heat to 85 °C first and then cool to 25 °C at a rate of 0.1 °C/min.

5.2.4 Co-crystallization with Hoechst 33258

Hoeschst 33258 is a small molecule that binds to the minor groove of double-stranded DNA with a preference for sequences rich in A and T. Several DNA crystal structures have been reported with this molecule, and therefore it might facilitate the growth of DNAzyme crystals. The annealed DNAzyme solution (1 mM) was mixed with 2 mM Hoechst 33258 solution and incubated for 3-4 hours at room temperature to allow intercalation.

5.2.5 Preparation of molecularly imprinted polymers (MIPs)

The following protocol of preparing DNAzyme imprinted polymers was adapted from a recent paper, in which they reported using MIPs as a template for inducing protein crystallization.[28] to prepare DNAzyme imprinted polymers, dissolve 5.4 g of acrylamide and 600 mg of N,N′-methylenebisacrylamide in 100 ml of Millipore water. Filter solution with a 0.2 μm filter and store the solution in clean glass container at 4 °C. Add 450 μl of this solution to 50 μl of previously annealed DNAzyme solution (4 μM in 50 mM NaHEPES, 50 mM NaCl, 2 mM $MgCl_2$), and add 10 μl of a 10% (w/v) APS solution. Purged the solution with nitrogen or argon for 5 min. Once the solution was degassed, add 10 μl of a 5% (v/v) TEMED solution. Leave the solution at room temperature for at least 18 hours to let it polymerize. After polymerization, pass the gel through a 75 μm sieve (stored at Marjorie's bench). Put the crashed gel in a microfuge

tube with the help of a spatula. Extract the template DNA with 500 µl of extraction buffer by incubating for 30 min on a rocker, followed by centrifugation at 2050 rcf for 3 min. Discard the supernatant and repeat the extraction process for another two times. Finally wash the gel 5 times with 500 µl of Millipore water and stored at 4 °C.

5.2.6 The hanging drop method

To set up the crystallization drop, hanging drop approach was used since it is the most common method for macromolecule crystallization. 1 µl of the annealed DNAzyme with Hoechst 33258 was mixed with 1 µl of MIP solution and 1 µl of precipitant solution on a non-wetting silicone coated microscope cover slip, which is then placed over a small well containing 0.5-1 ml of precipitating solution. Store the crystallization boxes at 18 °C.

5.2.7 Precipitating solution conditions

Table 5.2 RJV II-Na buffer condition

Components	**Concentrations**
NaCac, pH 5.5	100 mM
$MgCl_2$	250 mM
$(NH_4)_2SO_4$	0.5 M
$Pb(OAc)_2$	1 mM
Isopropanol	5% (%v/v)

Table 5.3 RJV II-K buffer condition

Components	**Concentrations**
KCac, pH 5.5	100 mM
$MgCl_2$	250 mM
$(NH_4)_2SO_4$	0.5 M
$Pb(OAc)_2$	1 mM
Isopropanol	5% (%v/v)

Table 5.4 RJV II-Ba buffer condition

Components	**Concentrations**
NaCac, pH 5.5	100 mM
$BaCl_2$	250 mM
LiCl	0.5 M
$Pb(OAc)_2$	1 mM
Isopropanol	5% (%v/v)

Table 5.5 RJV II-Sr buffer condition

Components	**Concentrations**
NaCac, pH 5.5	100 mM
$SrCl_2$	250 mM
LiCl	0.5 M
$Pb(OAc)_2$	1 mM
Isopropanol	5% (%v/v)

Table 5.6 RJV II-K-Ba buffer condition

Components	Concentrations
KCac, pH 5.5	100 mM
$BaCl_2$	250 mM
LiCl	0.5 M
$Pb(OAc)_2$	1 mM
Isopropanol	5% (%v/v)

Table 5.7 RJV II-K-Sr buffer condition

Components	Concentrations
KCac, pH 5.5	100 mM
$SrCl_2$	250 mM
LiCl	0.5 M
$Pb(OAc)_2$	1 mM
Isopropanol	5% (%v/v)

Table 5.8 A set of precipitant screen buffer for DNAzyme crystallization.

	Buffer	Salt		Precipitant			
Li-Sr-Screen	KCac, pH5.5	MgCl2	SrCl2	Li2SO4	LiCl	Isopropanol	MPD
Precp-1	100 mM		250 mM		0.25 M	5%	
Precp-2	100 mM		250 mM		0.5 M	5%	
Precp-3	100 mM		250 mM		0.75 M	5%	
Precp-4	100 mM		250 mM		1 M	5%	
Precp-5	100 mM		250 mM		1.25 M	5%	
Precp-6	100 mM		250 mM		1.5 M	5%	
Precp-7	100 mM		250 mM		0.25 M		5%
Precp-8	100 mM		250 mM		0.5 M		5%
Precp-9	100 mM		250 mM		0.75 M		5%
Precp-10	100 mM		250 mM		1 M		5%
Precp-11	100 mM		250 mM		1.25 M		5%
Precp-12	100 mM		250 mM		1.5M		5%
Precp-13	100 mM	250mM		0.25 M		5%	
Precp-14	100 mM	250mM		0.5M		5%	
Precp-15	100 mM	250mM		0.75M		5%	
Precp-16	100 mM	250mM		1M		5%	
Precp-17	100 mM	250mM		0.25M			5%
Precp-18	100 mM	250mM		0.5M			5%
Precp-19	100 mM	250mM		0.75M			5%
Precp-20	100 mM	250mM		1M			5%

Table 5.8 (cont.)

	Buffer	Salt		Precipitant				
Li-Sr-Screen	KCac, pH5.5	MgCl2	SrCl2	U2SO4	LiCl	Isopropanol	MPD	Ethylene Glycol
Precp-21	100 mM		250 mM		0.5 M	5%		
Precp-22	100 mM		250 mM		0.5 M	10%		
Precp-23	100 mM		250 mM		0.5 M	15%		
Precp-24	100 mM		250 mM		0.5 M	20%		
Precp-25	100 mM		250 mM		0.5 M	25%		
Precp-26	100 mM		250 mM		0.5 M	30%		
Precp-27	100 mM		250 mM		0.5 M		5%	
Precp-28	100 mM		250 mM		0.5 M		10%	
Precp-29	100 mM		250 mM		0.5 M		15%	
Precp-30	100 mM		250 mM		0.5 M		20%	
Precp-31	100 mM		250 mM		0.5 M		25%	
Precp-32	100 mM		250 mM		0.5 M		30%	
Precp-33	100 mM		250 mM		0.5 M			5%
Precp-34	100 mM		250 mM		0.5 M			10%
Precp-35	100 mM		250 mM		0.5 M			15%
Precp-36	100 mM		250 mM		0.5 M			20%
Precp-37	100 mM		250 mM		0.5 M			25%
Precp-38	100 mM		250 mM		0.5 M			30%
Precp-39	100 mM	250mM		0.5M		5%		
Precp-40	100 mM	250mM		0.5M		10%		
Precp-41	100 mM	250mM		0.5M		15%		
Precp-42	100 mM	250mM		0.5M		20%		
Precp-43	100 mM	250mM		0.5M		25%		
Precp-44	100 mM	250mM		0.5M		30%		
Precp-45	100 mM	250mM		0.5M			5%	
Precp-46	100 mM	250mM		0.5M			10%	
Precp-47	100 mM	250mM		0.5M			15%	
Precp-48	100 mM	250mM		0.5M			20%	
Precp-49	100 mM	250mM		0.5M			25%	
Precp-50	100 mM	250mM		0.5M			30%	
Precp-51	100 mM	250mM		0.5M				5%
Precp-52	100 mM	250mM		0.5M				10%
Precp-53	100 mM	250mM		0.5M				15%
Precp-54	100 mM	250mM		0.5M				20%
Precp-55	100 mM	250mM		0.5M				25%
Precp-56	100 mM	250mM		0.5M				30%

Table 5.9 A set of salt screen buffer for DNAzyme crystallization.

	Buffer	Salt		Precipitant				
Li-Sr-Screen	KCac, pH5.5	MgCl2	SrCl2	Li2SO4	LiCl	Isopropanol	MPD	Ethylene Glycol
Salt-1	100 mM		150 mM		0.5 M	5%		
Salt-2	100 mM		200 mM		0.5 M	5%		
Salt-3	100 mM		250 mM		0.5 M	5%		
Salt-4	100 mM		300 mM		0.5 M	5%		
Salt-5	100 mM		350 mM		0.5 M	5%		
Salt-6	100 mM		400 mM		0.5 M	5%		
Salt-7	100 mM		150 mM		0.5 M		5%	
Salt-8	100 mM		200 mM		0.5 M		5%	
Salt-9	100 mM		250 mM		0.5 M		5%	
Salt-10	100 mM		300 mM		0.5 M		5%	
Salt-11	100 mM		350 mM		0.5 M		5%	
Salt-12	100 mM		400 mM		0.5 M		5%	
Salt-13	100 mM	150mM		0.5M		5%		
Salt-14	100 mM	200mM		0.5M		5%		
Salt-15	100 mM	250mM		0.5M		5%		
Salt-16	100 mM	300mM		0.5M		5%		
Salt-17	100 mM	350mM		0.5M		5%		
Salt-18	100 mM	400mM		0.5M		5%		
Salt-19	100 mM	150mM		0.5M			5%	
Salt-20	100 mM	200mM		0.5M			5%	
Salt-21	100 mM	250mM		0.5M			5%	
Salt-22	100 mM	300mM		0.5M			5%	
Salt-23	100 mM	350mM		0.5M			5%	
Salt-24	100 mM	400mM		0.5M			5%	
Salt-25			150 mM		0.5 M	5%		5%
Salt-26			200 mM		0.5 M	5%		5%
Salt-27			250 mM		0.5 M	5%		5%
Salt-28			300 mM		0.5 M	5%		5%
Salt-29			350 mM		0.5 M	5%		5%
Salt-30			400 mM		0.5 M	5%		5%

Table 5.10 A set of PEG screen buffer for DNAzyme crystallization.

	Buffer	Salt		Precipitant						
Li-Sr-Screen	KCac, pH5.5	MgCl2	SrCl2	Li2SO4	LiCl	PEG200	PEG400	PEG2000	PEG4000	PEG6000	PEG8000
PEG-1	100 mM		250 mM		0.5 M	5%					
PEG-2	100 mM		250 mM		0.5 M	10%					
PEG-3	100 mM		250 mM		0.5 M	15%					
PEG-4	100 mM		250 mM		0.5 M	20%					
PEG-5	100 mM		250 mM		0.5 M	25%					
PEG-6	100 mM		250 mM		0.5 M	30%					
PEG-7	100 mM		250 mM		0.5 M		5%				
PEG-8	100 mM		250 mM		0.5 M		10%				
PEG-9	100 mM		250 mM		0.5 M		15%				
PEG-10	100 mM		250 mM		0.5 M		20%				
PEG-11	100 mM		250 mM		0.5 M		25%				
PEG-12	100 mM		250 mM		0.5 M		30%				
PEG-13	100 mM		250 mM		0.5 M			5%			
PEG-14	100 mM		250 mM		0.5 M			10%			
PEG-15	100 mM		250 mM		0.5 M			15%			
PEG-16	100 mM		250 mM		0.5 M			20%			
PEG-17	100 mM		250 mM		0.5 M			25%			
PEG-18	100 mM		250 mM		0.5 M			30%			
PEG-19	100 mM		250 mM		0.5 M				5%		
PEG-20	100 mM		250 mM		0.5 M				10%		
PEG-21	100 mM		250 mM		0.5 M				15%		
PEG-22	100 mM		250 mM		0.5 M				20%		
PEG-23	100 mM		250 mM		0.5 M				25%		
PEG-24	100 mM		250 mM		0.5 M				30%		
PEG-25	100 mM		250 mM		0.5 M					5%	
PEG-26	100 mM		250 mM		0.5 M					10%	
PEG-27	100 mM		250 mM		0.5 M					15%	
PEG-28	100 mM		250 mM		0.5 M					20%	
PEG-29	100 mM		250 mM		0.5 M					25%	
PEG-30	100 mM		250 mM		0.5 M					30%	
PEG-31	100 mM		250 mM		0.5 M						5%
PEG-32	100 mM		250 mM		0.5 M						10%
PEG-33	100 mM		250 mM		0.5 M						15%
PEG-34	100 mM		250 mM		0.5 M						20%
PEG-35	100 mM		250 mM		0.5 M						25%
PEG-36	100 mM		250 mM		0.5 M						30%

Table 5.10 (cont.)

PEG-37	100 mM	250mM		0.5M		5%					
PEG-38	100 mM	250mM		0.5M		10%					
PEG-39	100 mM	250mM		0.5M		15%					
PEG-40	100 mM	250mM		0.5M		20%					
PEG-41	100 mM	250mM		0.5M		25%					
PEG-42	100 mM	250mM		0.5M		30%					
PEG-43	100 mM	250mM		0.5M			5%				
PEG-44	100 mM	250mM		0.5M			10%				
PEG-45	100 mM	250mM		0.5M			15%				
PEG-46	100 mM	250mM		0.5M			20%				
PEG-47	100 mM	250mM		0.5M			25%				
PEG-48	100 mM	250mM		0.5M			30%				
PEG-49	100 mM	250mM		0.5M				5%			
PEG-50	100 mM	250mM		0.5M				10%			
PEG-51	100 mM	250mM		0.5M				15%			
PEG-52	100 mM	250mM		0.5M				20%			
PEG-53	100 mM	250mM		0.5M				25%			
PEG-54	100 mM	250mM		0.5M				30%			
PEG-55	100 mM	250mM		0.5M					5%		
PEG-56	100 mM	250mM		0.5M					10%		
PEG-57	100 mM	250mM		0.5M					15%		
PEG-58	100 mM	250mM		0.5M					20%		
PEG-59	100 mM	250mM		0.5M					25%		
PEG-60	100 mM	250mM		0.5M					30%		
PEG-61	100 mM	250mM		0.5M						5%	
PEG-62	100 mM	250mM		0.5M						10%	
PEG-63	100 mM	250mM		0.5M						15%	
PEG-64	100 mM	250mM		0.5M						20%	
PEG-65	100 mM	250mM		0.5M						25%	
PEG-66	100 mM	250mM		0.5M						30%	
PEG-67	100 mM	250mM		0.5M							5%
PEG-68	100 mM	250mM		0.5M							10%
PEG-69	100 mM	250mM		0.5M							15%
PEG-70	100 mM	250mM		0.5M							20%
PEG-71	100 mM	250mM		0.5M							25%
PEG-72	100 mM	250mM		0.5M							30%

5.3 Results and discussions

5.3.1 Previous progress toward obtaining a crystal structure of the 8-17 DNAzyme

The construct that gave crystals contained an arm that is a Dickerson sequence and a 3′ overhang (Figure 5.1). Crystals were obtained with the RJV II-Na buffer, with or without $Pb(OAc)_2$ and MIP. It usually took 6 months to a year for the crystal to grow. A complete data set was collected for one of the native crystals at 2.7 Å at Argonne National Laboratory.

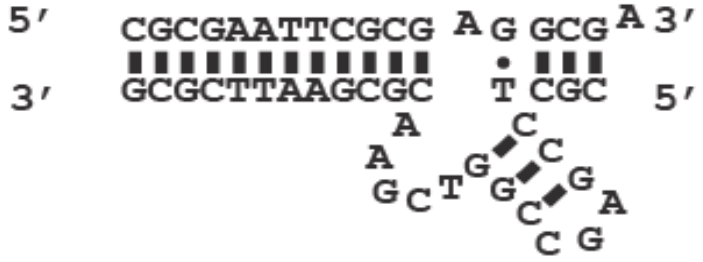

Figure 5.1 Secondary structure of the 8-17 DNAzyme that resulted in crystals.

5.3.2 Crystallization of selenium-modified 8-17 DNAzyme

In order to obtain phasing information to solve the crystal structure, we tried crystalizing selenium-modified 8-17 DNAzyme (Figure 5.2). The constructs were kindly provide by Dr. Huang Zhen's lab at Georgia State University. It turned out that sequence 1 lead to crystals under several conditions while no crystal was observed for sequences 2 (Figure 5.2).

Se modified DNA

Se modified 17S_CGC_D_3A

Sequence 1: 5′-CGCGAATTCGCGAGGCGA-3′ (sj136)
Sequence 2: 5′-CGCGAATTCGCGAGGCGA-3′ (sj137)

Where A =

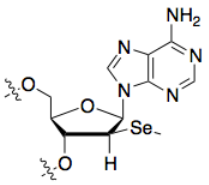

Figure 5.2 Constructs of selenium-modified substrate strand of 8-17 DNAzyme.

Needle shaped crystals from the selenium-modified DNAzyme (Sequence 1) were observed under the RJV II-K-Sr condition after three-month growth. Interestingly, these crystals had a very different shape from the native DNAzyme crystals, which had an oval shape instead. However, X-ray diffraction of these crystals did not lead to high-resolution diffraction patterns that could be used for phasing (> 10 Å).

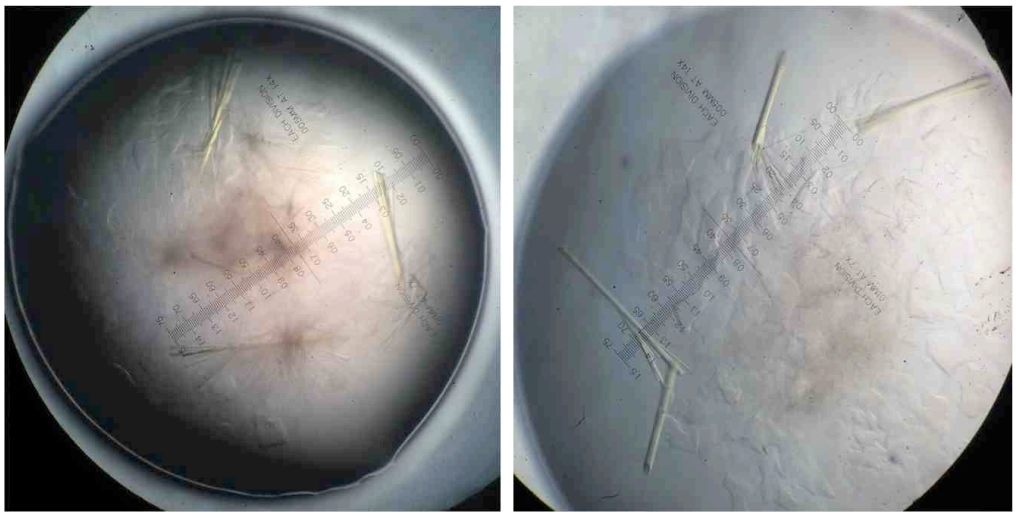

Figure 5.3 Crystals of selenium-modified 8-17 DNAzyme (Sequence 1) grown under RJV II-K-Sr condition.

5.3.3 Optimization of cryoprotection techniques for mounting crystals

It has been reported that proper cryoprotection of crystals could lead to better diffraction. To find the best cryoprotectant for our DNAzyme crystals, we prepared a series of cryoprotection solutions, and mounted several crystals under each condition. For each crystal, it was first transferred from the crystallization drop to a drop of cryoprotection solution containing 15% of the corresponding cryoprotectant. Closely observe the morphology of the crystals under microscope for half an hour to ensure that the crystal was stable in the solution. Then the crystal was transferred to the 30% cryoprotection solution and frozen by liquid nitrogen.

Table 5.11 Cryoprotection solutions with different cryoprotectants.

	Cryoprotection solutions
1.	100 mM MES, 250 mM $MgCl_2$, 0.5 M $(NH_4)_2SO_4$, 30% glycerol
2.	100 mM MES, 250 mM $MgCl_2$, 0.5 M $(NH_4)_2SO_4$, 30% glucose
3.	100 mM MES, 250 mM $MgCl_2$, 0.5 M $(NH_4)_2SO_4$, 30% sucrose
4.	100 mM MES, 250 mM $MgCl_2$, 0.5 M $(NH_4)_2SO_4$, 30% NaGluconate
5.	100 mM MES, 250 mM $MgCl_2$, 0.5 M $(NH_4)_2SO_4$, 30% ethylene glycol
6.	Paraffin oil

From the screen results, gluconate and glycerol lead to the best diffraction patterns of crystals containing selenium-modified DNAzyme (7.8 ~ 8.2 Å). Therefore, it is recommended to use these two cryoprotectants for later studies.

5.4 Conclusions

Preliminary results based on the diffraction patterns and initial modeling work all suggest that the native crystals we had was most likely not for the active DNAzyme construct. It seems that the DNA strands in the crystal are not in the form of enzyme and substrate complex. Since Dickerson sequence is a palindromic sequence, it is possible that the substrate or the enzyme strand underwent self-hybridization during the crystallization process and grew into crystals. Further careful characterization of the crystals is needed in order to confirm the component of crystals. Moreover, different sequences should be designed for future crystallization studies, with special attention on avoiding self-hybridizing sequences. Protein-mediated crystallization could be considered as an alternative approach for DNAzyme crystallization. Based on some successful trials of using proteins for DNA crystallization, flexible DNA strands were found to be restrained and stabilized in the protein matrix, resulting in high-quality crystals and high resolution structures. Protein-assisted DNA crystallization could also shorten the time of crystallization process, and thus it would be extremely helpful for initial screening of crystallization conditions.

5.5 References

1. Kruger K, Grabowski PJ, Zaug AJ, Sands J, Gottschling DE, Cech TR, Self-splicing RNA: autoexcision and autocyclization of the ribosomal RNA intervening sequence of Tetrahymena. *Cell* **1982** *31*, 147-157.

2. Guerrier-Takada C, Gardiner K, Marsh T, Pace N, Altman S, The RNA moiety of ribonuclease P is the catalytic subunit of the enzyme. *Cell 35*, 849-857.

3. Breaker RR, Joyce GF, A DNA enzyme that cleaves RNA. *Chem. Biol.* **1994** *1*, 223-229.

4. Breaker RR, Joyce GF, A DNA enzyme with Mg2+-dependent RNA phosphoesterase activity. *Chem. Biol.* **1995** *2*, 655-660.

5. Cuenoud B, Szostak JW, A DNA Metalloenzyme with DNA-Ligase Activity. *Nature* **1995** *375*, 611-614.

6. Li YF, Sen D, A catalytic DNA for porphyrin metallation. *Nat. Struct. Biol.* **1996** *3*, 743-747.

7. Burmeister J, vonKiedrowski G, Ellington AD, Cofactor-assisted self-cleavage in DNA libraries with a 3'-5'-phosphoramidate bond. *Angew. Chem., Int. Ed.* **1997** *36*, 1321-1324.

8. Santoro SW, Joyce GF, A general purpose RNA-cleaving DNA enzyme. *Proc. Natl. Acad. Sci. U. S. A.* **1997** *94*, 4262-4266.

9. Zhan ZYJ, Lynn DG, DNA catalyzed reductive amination. *Abstr. Pap. Am. Chem. Soc.* **1997** *213*, 363-ORGN.

10. Carmi N, Balkhi SR, Breaker RR, Cleaving DNA with DNA. *Proc. Natl. Acad. Sci. U. S. A.* **1998** *95*, 2233-2237.

11. Li YF, Breaker RR, Phosphorylating DNA with DNA. *Proc. Natl. Acad. Sci. U. S. A.* **1999** *96*, 2746-2751.

12. Li J, Lu Y, A highly sensitive and selective catalytic DNA biosensor for lead ions. *J. Am. Chem. Soc.* **2000** *122*, 10466-10467.

13. Sheppard TL, Ordoukhanian P, Joyce GF, A DNA enzyme with N-glycosylase activity. *Proc. Natl. Acad. Sci. U. S. A.* **2000** *97*, 7802-7807.

14. Flynn-Charlebois A, Prior TK, Hoadley KA, Silverman SK, In vitro evolution of an RNA-cleaving DNA enzyme into an RNA ligase switches the selectivity from 3 '-5 ' to 2 '-5 '. *J. Am. Chem. Soc.* **2003** *125*, 5346-5350.

15. Liu J, Brown AK, Meng X, Cropek DM, Istok JD, Watson DB, Lu Y, A catalytic beacon sensor for uranium with parts-per-trillion sensitivity and millionfold selectivity. *Proc. Natl. Acad. Sci. U. S. A.* **2007** *104*, 2056-2061.

16. Torabi S-F, Wu P, McGhee CE, Chen L, Hwang K, Zheng N, Cheng J, Lu Y, In vitro selection of a sodium-specific DNAzyme and its application in intracellular sensing. *Proc. Natl. Acad. Sci. U. S. A.*

2015 *112*, 5903-5908.

17. Liu JW, Lu Y, A colorimetric lead biosensor using DNAzyme-directed assembly of gold nanoparticles. *J. Am. Chem. Soc.* **2003** *125*, 6642-6643.

18. Liu J, Lu Y, Accelerated color change of gold nanoparticles assembled by DNAzymes for simple and fast colorimetric Pb2+ detection. *J. Am. Chem. Soc.* **2004** *126*, 12298-12305.

19. Liu JW, Lu Y, Optimization of a Pb2+-directed gold nanoparticle/DNAzyme assembly and its application as a colorimetric biosensor for Pb2+. *Chem. Mater.* **2004** *16*, 3231-3238.

20. Liu J, Lu Y, A DNAzyme catalytic beacon sensor for paramagnetic Cu2+ ions in aqueous solution with high sensitivity and selectivity. *J. Am. Chem. Soc.* **2007** *129*, 9838-9839.

21. Liu J, Lu Y, Rational design of "Turn-On" allosteric DNAzyme catalytic beacons for aqueous mercury ions with ultrahigh sensitivity and selectivity. *Angew. Chem., Int. Ed.* **2007** *46*, 7587-7590.

22. Liu JW, Brown AK, Meng XL, Cropek DM, Istok JD, Watson DB, Lu Y, A catalytic beacon sensor for uranium with parts-per-trillion sensitivity and millionfold selectivity. *Proc. Natl. Acad. Sci. U. S. A.* **2007** *104*, 2056-2061.

23. Wu P, Hwang K, Lan T, Lu Y, A DNAzyme-gold nanoparticle probe for uranyl ion in living cells. *J. Am. Chem. Soc.* **2013** *135*, 5254-5257.

24. Hwang K, Wu P, Kim T, Lei L, Tian S, Wang Y, Lu Y, Photocaged DNAzymes as a General Method for Sensing Metal Ions in Living Cells. *Angew. Chem., Int. Ed.* **2014** *53*, 13798-13802.

25. Kim HK, Rasnik I, Liu J, Ha T, Lu Y, Dissecting metal ion-dependent folding and catalysis of a single DNAzyme. *Nat. Chem. Biol.* **2007** *3*, 763-768.

26. Nowakowski J, Shim PJ, Prasad GS, Stout CD, Joyce GF, Crystal structure of an 82-nucleotide RNA-DNA complex formed by the 10-23 DNA enzyme. *Nat. Struct. Biol.* **1999** *6*, 151-156.

27. Lan T. I. In vitro selection of aptamers for perchlorate and melamine; II. Towards crystallization of DNAzymes; III. A highly selective lead sensor based on a classic lead DNAzyme: University of Illinois at Urbana-Champaign; 2012.

28. Saridakis E, Khurshid S, Govada L, Phan Q, Hawkins D, Crichlow GV, Lolis E, Reddy SM, Chayen NE, Protein crystallization facilitated by molecularly imprinted polymers. *Proc. Natl. Acad. Sci. U. S. A.* **2011** *108*, 11081-11086.